TECHNISCHE UNIVERSITÄT MÜNCHEN

Lehrstuhl für Entwicklungsgenetik

Identification and analysis of the *cis*-regulatory element for the AID-mediated somatic hypermutation and application of this process for the artificial protein evolution in chicken B-cell line DT40

Vera Batrak

Vollständiger Abdruck der von der Fakultät Wissenschaftszentrum Weihenstephan für Ernährung, Landnutzung und Umwelt der Technischen Universität München zur Erlangung des akademischen Grades eines

Doktors der Naturwissenschaften

genehmigten Dissertation.

Vorsitzender: Univ.- Prof. Dr. S. Scherer

Prüfer der Dissertation:

1. Univ.- Prof. Dr. W. Wurst
2. Univ.- Prof. Dr. M. J. Atkinson

Die Dissertation wurde am 23.06.2009 bei der Technischen Universität München eingereicht und durch die Fakultät Wissenschaftszentrum Weihenstephan für Ernährung, Landnutzung und Umwelt am 27.10.2009 angenommen.

SUMMARY

Somatic hypermutation (SHM) is one of three mechanisms of immunoglobulin *(Ig)* gene diversification at the post-*V(D)J*-recombination stage. Depending on species SHM is responsible for antibody repertoire production and/or affinity maturation of germinal centre B lymphocytes. The diversification process involves introducing non-template mutations into the *Ig* gene at a rate which is 10^6 higher than the spontaneous mutation rate in somatic cells. SHM is initiated by activation-induced cytidine deaminase (AID), an enzyme that deaminates cytosine residues in transcription-dependent manner and completed by error-prone repair of the resulted uracils.

SHM is specific for the *Ig* locus; other transcribed genes of B-cells do not undergo mutations at such a high rate. When mistargeted, hypermutation represents a threat to genome integrity and was shown to be associated with a number of B-cell lymphomas. Although there have been identified a number of factors including *cis*- and *trans*- regulatory elements which seem to play a role in recruiting of the SHM to the *Ig* locus, unambiguous element responsible for the SHM targeting has not been identified and mechanisms of this process remain unclear.

The present study describes the generation of a reporter for somatic hypermutation which allowed deletion analysis of the *Ig* light chain (*IgL*) locus of the DT40 B-cell line in order to identify a *cis*-regulatory element responsible for activation of the hypermutation. Deletion of this element, extending for 9.8 kb from the *IgL* transcription start site towards the next downstream locus, named *DIVAC* for diversification activator, abolished hypermutation. It was also shown that *DIVAC* is able to act over a distance in both directions, which allowed suggesting of a model for the action of this element.

Also the study describes the generation of a second type of a hypermutation vector which allowed biotechnological exploitation of the somatic hypermutation. Use of this vector and the DT40 cell line allowed the specific and efficient mutation of a transgene placed within the *Ig* locus. This strategy permits optimization of *in situ* directed protein evolution based on hypermutation. This artificial evolution system has a number of advantages compared to the known methods of *in vitro* and *in situ* directed evolution and can be applied for optimization of any gene whose phenotype can be screened in DT40 cells. Using the described system it was possible to optimize both green and red fluorescent proteins and generate variants with higher fluorescent intensity and spectrally shifted emissions.

ZUSAMENFASSUNG

Die Somatische Hypermutation (SHM) ist einer von drei Mechanismen des Rearrangements der Immunoglobulin(*Ig*)-Gene, die im Anschluss an die *V(D)J* Rekombination stattfindet und, je nach Spezies, entweder für das Antikörperrepertoire und/oder für Reifung von Antikörper-Affinität verantwortlich ist. Durch die SHM werden Zufallsmutationen in das *Ig* Gen eingeführt, wobei die Mutationshäufigkeit um bis zu 10^6-fach höher ist als die spontane Mutationsrate in somatischen Zellen. SHM wird während der Transkription durch Deaminierung von Cytosin durch das Enzym Aktivierungsinduzierte Cytidin Deaminase (AID) ausgelöst und durch eine fehlerhafte DNA-Reparatur des daraus resultierenden Uracils abgeschlossen.

SHM ist spezifisch für den *Ig* Locus, während andere transkribierte Gene in B-Zellen nicht eine solche hohe Mutationshäufigkeit zeigen. Bei fehlerhafter unspezifischer Aktivität von AID stellt die SHM aber eine Gefahr für die Integrität des Genoms und wird mit verschiedenen B-Zell Lymphomen in Zusammenhang gebracht. Es ist noch weitgehend unklar, welche Mechanismen dazu führen, dass SHM auf den *Ig*-locus beschränkt ist.

In dieser Arbeit ist die Entwicklung eines Reporterkonstrukts zum Nachweis der SHM beschrieben, das erlaubte eine Deletionsanalyse des *Ig*-Leichtkettenlocus der DT40 B-Zelllinie durchzuführen. Dabei wurde das *cis*-regulatorisches Element (*DIVAC*, Diversification Activator) entdeckt, das für die Auslösung von SHM verantwortlich ist. Bei Deletion von *DIVAC* konnte keine SHM mehr nachgewiesen werden. Des weiteren wurde auch bestimmt, über welche genomischen Distanzen *DIVAC* seine Funktion entfalten kann. Diese Ergebnisse erlaubten die Erstellung eines Modells zur Funktionsweise von *DIVAC* während der SHM.

Darüberhinaus wird in dieser Arbeit auch die Entwicklung eines Vektors beschrieben, der eine biotechnologische Anwendung der SHM möglich macht. Der Vektor ist für die Zellinie DT40 konstruiert und ermöglicht ein beliebiges Transgen spezifisch und effizient im *Ig* Locus durch SHM zu mutieren. Das daraus resultierende System der künstlichen *in situ* Proteinevolution hat eine Reihe von Vorteilen zu bereits etablierten Methoden, Proteine *in vitro* oder *in situ* artifiziel zu verändern. SHM kann zur Optimierung eines jeden Proteins angewendet werden, dessen Phänotyp in der DT40 Zellinie erkennbar ist. Im Rahmen dieser Arbeit war es daher möglich, grün und rot fluoreszierende Proteine zu optimieren, wobei sowohl Varianten mit erhöhter Fluoreszensintensität als auch mit Verschiebung des Emissionsspektrums entwickelt wurden.

ABBREVIATIONS

AID Activation Induced Cytidine Deaminase
APOBEC-1 Apolipoprotein B RNA Editing Catalytic Polypeptide 1
BDT Big Dye Terminator
BSR Blasticidine S Resistance gene
C region Immunoglobulin Constant region
CIP Calf Intestine Phosphatase
CSR Class Switch Recombination
D region Immunoglobulin Diversity region
DMSO Dimethyl Sulfoxide
dNTP Deoxynucleotide Triple Phosphate
DSB Double Strand Break
EDTA Ethylene di-Amine Tetra Acetic Acid
EF Elongation Factor
FACS Fluorescence Activated Cell Sorting
FBS Fetal Bovine Serum
FRET Fluorescence Resonance Energy Transfer
FSC Forward Scatter
EtBr Ethidium Bromide
GC Gene Conversion
GFP Green Fluorescent Protein
GPT Guanine Phosphoribosyl Transferase
4-HT 4-Hydroxy Tamoxifen
Ig Immunoglobulin
IgL Immunoglobulin Light Chain
IRES Internal Ribosome Entry Site
J region Immunoglobulin Joining region
LB Luria Broth
MAR Matrix Attachment Region
MMR Mismatch Repair
NHEJ Nonhomologues End Joining
PBS Phosphate Buffer Saline
PCR Polymerase Chain Reaction
pKS (+) pBluescript vector
Pol Polymerase
Puro Puromycin
RFP Red Fluorescent Protein
RSV Rous Sarcoma Virus
S region Switch region
SDS Sodium Dodecyl Sulphate
SHM Somatic Hypermutation
sIgM Surface Immunoglobulin M
SSB Single Strand Break
TAE Tris Acetic Acid ETDA
TE Tris EDTA
TLS Trans Lesion Synthesis
UNG Uracil DNA Glycosylase
V region Immunoglobulin Variable region
2YT 2 x Yeast Extract Tryptone

TABLE OF CONTENTS

RESULTS

DISCUSSION

INTRODUCTION

I. Evolution of the immune system

The major part of the earth biomass consists of microorganisms, many of which are pathogens capable of causing life-threating infections to other organisms. The first host response to infection is innate immunity, which is based on the recognition of specific pathogen-associated molecular patterns (PAMPs) by germ-line encoded Toll-like receptors [1]. Some of the innate immunity pathways are conserved between plants and animals that are divided by billions of years of evolution [2].

In addition to the PAMPs-recognition system, vertebrates have evolved an adaptive immunity which is triggered by innate defense mechanisms and mediated primarily by specialized white blood cells (lymphocytes). There are two classes of lymphocytes: T-cells, responsible for the cell-mediated immune response, and B-cells which mediate humoral immunity. Lymphocytes perform antigen-specific recognition using receptors expressed on their surface, T-cell receptors (TCRs) and B-cell receptors (BCRs, antibodies or immunoglobulins (Igs)). All receptors produced by an individual lymphocyte have the same antigen-biding site recognizing a specific epitope of the antigen [3]. The recognition is achieved in different manner: while BCRs are capable to interact with antigens directly, TCRs recognize a processed form of antigen, presented on the surface of the specialized cells by Major Histocompatibility Complex (MHC)-encoded proteins.

While the T-cell receptor has a dimeric configuration, the immunoglobulin is a tetramer of two light and two heavy polypeptide chains encoded by different loci: light chains fall into the *lambda* (λ) and *kappa* (κ) families and heavy chains form a single family. Each Ig or TCR polypeptide consists of a terminal variable region contributing to the antigen recognition and a constant region that serves structural, signaling and effector functions. Antigen receptor genes exist in the germline in a "split" configuration and are assembled somatically during B- and T-lymphocytes development by site-specific recombination. Multiple *C* regions, each with specialized effector function, are encoded in the heavy chain locus. The *Variable (V)* region is encoded by *Variable* (*V*), *Joining* (*J*) (in heavy chain also *Diversity* (*D*)) gene segments which are assembled by *V(D)J* recombination, a process, which can be found in all jawed vertebrates (*gnathostomata*), beginning with cartilaginous fish [4-7]. Evolutionary appearance of RAG1 and RAG2 recombinases coincides with *V(D)J* rearrangements [8, 9]. As these recombinases are able to catalyze transposition, it was suggested that during evolution the diversification of germ-line antigen receptors may have

developed by germline insertion of a transposable element into an ancestral receptor gene, probably containing an *Ig*-like *V*-domain [10, 11] soon after the evolutionary divergence of jawed and jawless vertebrates [12-14].

As BCRs and TCRs possess sequence conservation and use the same recombination machinery, it is speculated that they may have derived from a common "primordial" receptor [15, 16]. While configuration and diversification mechanisms of TCRs have been maintained during evolution, those for BCRs underwent significant changes [16-18]. While all TCRs described to date have a translocon configuration (each cluster containing individual *V*, (*D*), *J*, and *C* as the repeating unit) (Figure 1), *Ig* genes have either cluster configuration (repeating unit contains all the gene segments necessary for expression of the receptor) as in cartilaginous fish, or translocon configuration as in mammals and amphibians, or a combination of the two as in bony fish. In addition to the functional *V*-segments, the *Ig* loci of farm animals and birds were shown to contain non-functional *pseudo* (ψ)-genes. Birds represent an extreme in the evolution of the translocon configuration: while both light and heavy chain loci contain multiple *V* regions, all but one of them is a pseudo-gene (Figure 1).

Conflicting with the theory linking the appearance of adaptive immunity to the RAG – transposon invasion [18] is a recent study of lamprey and hagfish, the only survived groups of jawless vertebrates (*agnatha*). This investigation revealed that these animals lacking RAG1/2 are nevertheless capable of an adaptive immune response using a recombinatorial mechanism of receptor gene generation. This process uses a previously unknown class of non-*Ig* receptor molecules called variable lymphocyte receptors, VLRs [19, 20].

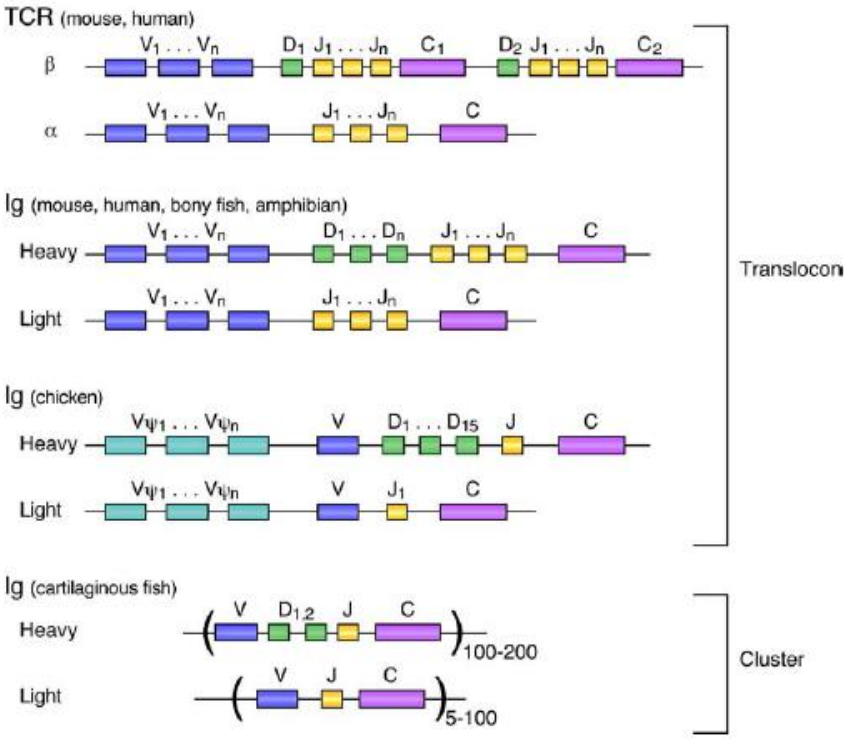

Figure 1. The organization of antigen receptor genes depicted using rectangles to indicate the individual variable region gene segments (blue, *V*, green, *D*; and yellow, *J*) or the constant region genes (violet). Pseudo-genes of chicken are depicted in light blue. Taken from [18].

As only lamprey, hagfish and jawed vertebrates survived from the early vertebrate radiation, it is not clear whether the *agnathan* VLRs were the precursors of vertebrate immune receptors or if the rearranging VLRs and Igs/TCRs developed independently from "primordial" receptors during convergent evolution [15, 20].

Unlike TCRs, B-cell receptors undergo additional diversification following *V(D)J* recombination, including gene conversion, somatic hypermutation and class switch recombination. It is known that somatic hypermutation was found already in cartilaginous fish (sharks) [15, 16, 21-23], class switch recombination appears in a primitive form in amphibians [24, 25]. Dogfish (cartilaginous fish) was found also to have a structural and functional homolog of the protein AID (Activation Induced Deaminase), necessary for initiation of the post-*V(D)J*-recombination diversification processes (Section V) [26].

II. Immunoglobulin repertoire generation in *gnathostomata*

Diversification of the *Ig* receptor gene allowed jawed vertebrates to generate a lymphocyte receptor repertoire of sufficient diversity for recognition the antigenic component of many potential pathogens or toxins.

In the mice and humans the primary *Ig* repertoire is achieved by *V(D)J* recombination within the light and heavy chains separately while in farm animals and birds primary diversity is mediated by post-*V(D)J* remodeling that includs gene conversion and somatic hypermutation. After antigen stimulation, the affinity maturation of *Ig* gene in most species is achieved by somatic hypermutation (in rare cases accompanied by gene conversion) and the effector function of immunoglobulin can be changed by class switch recombination.

II.1. *V(D)J* recombination

In order to assemble the complete receptor molecule early in lymphocyte development (Section III) germline-encoded segments of the *Ig* gene are somatically recombined in different permutations within individual lymphocytes (Figure 2) [4, 5, 27]. *V(D)J* recombination is mediated by lymphocyte–specific recombinases RAG1 and RAG2 using special signal sequences flanking the individual segments [8]. This recombinatorial joining of

the segments uses non-homologous end-joining (NHEJ) DNA-repair complexes in order to join the double strand breaks (DSBs) [28].

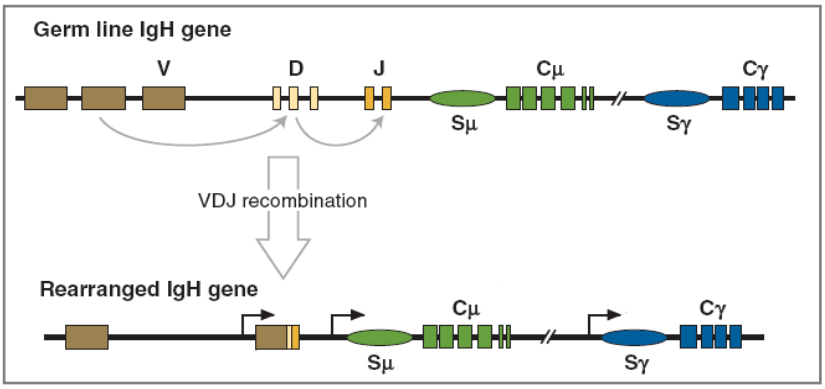

Figure 2. *V(D)J* rearrangement. The genomic organization of the murine germline *IgH* locus is shown. One diversity (*D*) segment (yellow rectangles) and one joining segment (orange rectangles) rearrange to form *DJ* segment that subsequently recombines with a variable (*V*) segment (brown rectangles) to form a *VDJ* (*V*) region (bottom diagram). Taken from [29].

II.2. Post-*V(D)J* remodeling of the immunoglobulin gene

II.2.a. Gene conversion

As rabbit, cattle, swine, sheep, horse and birds have only a limited number of germline *V*, *D* and *J* segments (only one in birds), the rearranged variable (*V*) regions of their *Ig* genes have minimal diversity [30-32]. The required level of diversity of the primary *Ig* repertoire in these species is achieved mainly by gene conversion (well described in chicken) and accompanied to different extents by SHM [33-37].

Ig gene conversion (GC) is a form of diversification that involves "copy and paste" insertion of donor sequences derived from *cis*-located pseudo-genes into the rearranged *V* region (Figure 4) with the approximate frequency of 0.05-0.1 conversions per cell generation [38, 39]. Reciprocal transfer of the donor fragment does not take place and there is no change to the sequence of the ψV [40]. Pseudo-genes have high homology to the target sequence and differ by about 10 to 20% from the *V*-segment [34, 38]. The actual donor sequences range from 8 to 200 bp [34]. There are 25 pseudo-genes located in the light chain of chicken *Ig* locus and 80 - in the heavy chain [38, 41], each of these are transcriptionally silent and characterized by the absence of the *V(D)J*-recombination signals [42].

There is no clear data on mechanisms for the activation of gene conversion, but as it is known that it starts right after lymphocytes enter the developmental microenvironment (Peyer's patches, bursa of Fabricius (Section III)), it is likely that the activation is mediated by external cytokines or cell interactions specific for the microenvironments. It has not been tested whether transcription of the *Ig* locus itself is required for the initiation of gene

conversion. However, GC is dependent on the activity of AID [43, 44] which only works on transcribed genes (Section V) and, as was recently shown in the chicken light chain locus, on the presence of a *cis*-element containing the *Ig* enhancer [45, 46]. While the initial DNA change leading to GC is not yet known (likely to be a single strand break (SSB) if it is related to AID editing model), it is clear that the further processing is mediated by the homologous recombination pathway [33].

II.2.b. Somatic hypermutation

Binding of the immunoglobulin to the inducing antigen epitope during the primary response is of low affinity (in fact one epitope can be recognized by a number of different primary antibodies). Affinity is improved during the secondary response by Somatic Hypermutation (SHM) which, depending on the species, can be accompanied by gene conversion (Section III). SHM is a process of introducing non-templated point mutations into the rearranged variable region of the *Ig* gene at a high rate (10^{-5} to 10^{-3} mutation per base pair per cell division, which is 10^6-fold higher than the spontaneous rate in somatic cells) [47, 48]. Improvement in the ability to bind antigen is known as affinity maturation [49] which results in the clonal expansion of lymphocytes expressing highly specific immunoglobulins (Section III). SHM is targeted to the rearranged *V* region [39, 50] beginning approximately 150-200 bp downstream of the *Ig* promoter and extending for a further 1-1.5 kb downstream [51-53] (Figure 3), leaving the promoter and the terminal constant region unaffected [54].

Although mutations can occur throughout the rearranged *V* region, the majority of them are preferentially targeted to deoxycytidines within the hotspot motive WRCY (W = A or T, R = purin, Y = pyrimidin) [50, 55]. These were shown to correspond to the complementarity-determining regions (CDRs) of the immunoglobulin molecule that are most implicated in contact with antigen [29, 56, 57]. In the *V* region some potential hot spots are targeted by SHM while others are not, suggesting that an additional influence on the selection of mutation targets is mediated by higher-order structures [58, 59], or is inherent to the structure of the DNA binding proteins mediating SHM [60]. Transition mutations (exchange of a purin for a purin or pyrimidine for a pyrimidine) arise more frequently than transversions (C to A or G; G to C or T) [61].

Initiation of SHM (of either the *Ig* locus or an artificial substrate) requires transcription [62-64] and the activity of AID which was shown in mouse [60, 65], human [66] and chicken [67] models. Transcription alone though is not sufficient, as sequence analysis of transcribed non-*Ig* genes in B-cells revealed either no or infrequent mutations compared to the

Ig genes [68-70]. SHM activity was also shown to be influenced by the presence of murine *Ig* enhancers and their flanking regions [71-73].

It is unclear if SHM is initiated and/or associated with a break of DNA and if so, it is unknown if it is a single DNA strand break (SSB) [74] or a double strand DNA break [35, 75-77] or both [78], because later DSBs were shown to arise independently of AID [75, 79].

Mutations in SHM are produced by Base Excision Repair (BER), error-prone repair processing (translesion synthesis) or Mismatch Repair System (described in Section V).

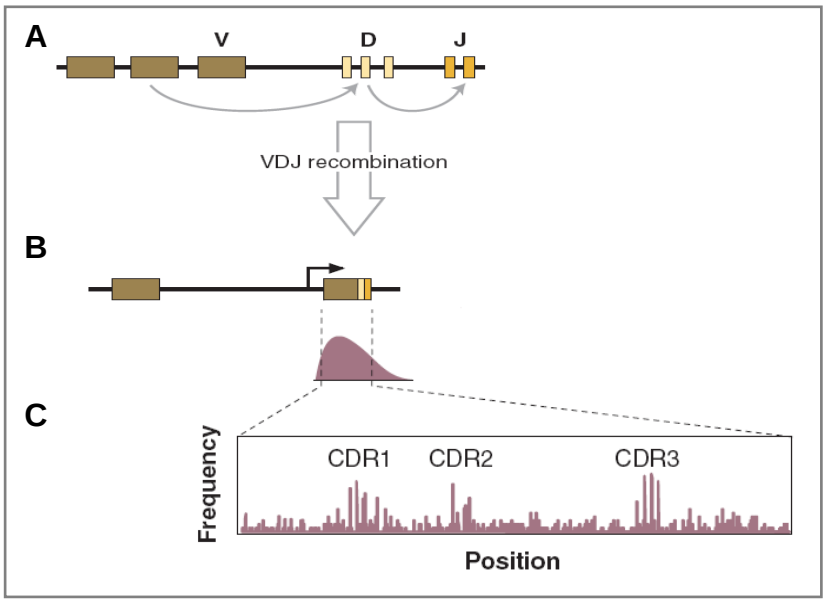

Figure 3. *V(D)J* rearrangement and somatic hypermutation of antibody of a heavy chain. (A) A scheme of a germline heavy chain. (B) Rearranged *Ig* gene. (C) Distribution of mutations. The *VDJ* region was expanded as a histogram to illustrate the existence of intrinsic mutational hot spots. Consistency of hot spots with CDRs are shown. Taken from [29].

II.2.c. Class switch recombination

Ig isotype (or class), defining the antibody effector function, is determined by the constant region of the heavy chain (C_H). The first naive cells in the B-cell lineage use the $C\mu$ constant *Ig* region and express only IgM. During affinity maturation the Ig isotype can be changed by Class Switch Recombination (CSR) which allows expression of antibodies that retain the same antigen specifity but have different to naive B-cells function. CSR occurs between switch sequences (*S*-regions) [80] located upstream of the C_H regions and results in the joining of a variable region with a different C_H, followed by excision of the intervening sequence (Figure 3) [81].

Activation of B-cells by antigen or signaling from T-cells and/or macrophages initiates selection of a target *S*-region [82] and induction of the class-switch recombination [65, 83].

Initiation of CSR requires AID [65, 83-85] and germline transcription (through the recombining *S*-regions) [86] which is probably important for the recruitment of the AID [87].

There are several lines of evidence indicating that CSR uses a DNA double-stranded-break intermediate [81, 86, 88]. The rejoining processes in CSR are mediated by the non-homologous end-joining repair pathway [59, 83, 89].

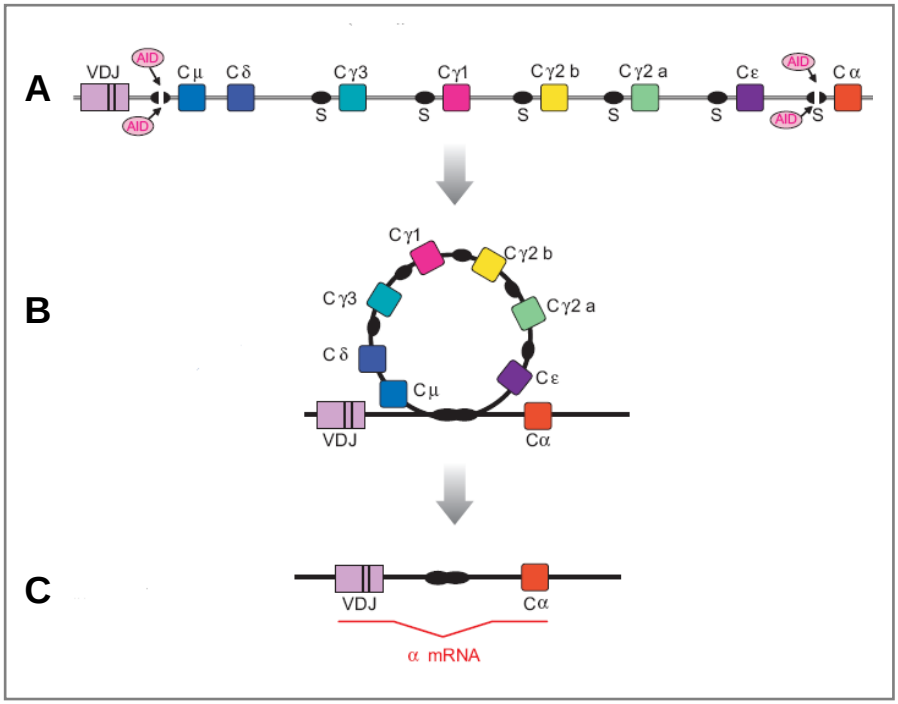

Figure 3. Scheme of class switch recombination of murine primary Ig type M (*Cμ* constant region) to the IgA. (A) Heavy chain locus in B-cells expressing IgM. During CSR, AID deaminates dC residues in the transcriptionally active *S*-regions (*Sμ* and *Sα*), initiating a process that results in double-strand DNA breaks in both *S*-regions and CSR by intrachromosomal deletion (B). (C) Heavy chain locus after switch to IgA. Splicing of the *Igα* transcript is shown. Taken from [90].

	GC	SHM	CSR
Function: 1. Before antigen stimulation	In birds, rabbit, cattle, swine, horse, sheep: primary Ig repertoire	In birds, rabbit, cattle, swine, horse participates in primary Ig repertoir formation	None
2. After antigen stimulation	Secondary Ig repertoire formation	Affinity maturation	Change of Ig isotype
Target	*V*-region of the *Ig* gene	Rearranged *Ig* locus	Switch (*S*) regions
Activation	Probably by factors of microenvironment (not shown)	Antigen (for affinity maturation)	Cytokines of activated T-cells and/or macrophages or antigen
Initiation: transcription AID Ig enhancer	 Not shown Required Required	 Required Required Required	 Required (germline transcription) Required Not shown
DNA cleavage	likely SSB (?) DSB?	SSB(?) DSB (?)	DSB
Repair of DNA strand	Homologous recombination	Base-excision repair Translesion synthesis Mismatch repair (?)	NHEJ, non-homologous end joining

Table 1. Compared characteristics of immunoglobulin gene conversion (GC), somatic hypermutation (SHM) and class switch recombination (CSR).

III. B-lymphocytes development

III.1 Mouse and human

The diverse repertoire of BCRs and TCRs is generated during lymphopoiesis of the B and T-cells from common lymphoid progenitors. This takes place in specialized lymphoid tissues (in mouse and human - in bone marrow for adults and in liver for fetus) [91]. After the antigen specificity of an individual lymphocyte has been determined by *V(D)J* recombination and immunoglobulin is expressed on the cell surface [92], the primary antibody repertoire is tested for ability to recognize self-antigens. This is followed by negative selection of those cells that recognize self-antigens present in the innate environment [93]. The surviving lymphocytes migrate to the peripheral lymphoid tissues, and after undergoing further maturation circulate between lymph, blood and lymphoid tissues at a relatively constant number in the absence of infection [94]. Following antigen recognition by the T-cells the B-

cells begin to proliferate and migrate to primary lymphoid follicles where they form germinal centers where rapid proliferation and differentiation takes place [95, 96]. This is accompanied by activation of SHM [97] and CSR [98] to increase the affinity to the antigen. Negative selection of those cells whose affinity is reduced due to diversification also occurs [99]. Recently, it has been shown in mice that CSR is actually activated prior to germinal center formation [100, 101]. Cells demonstrating improved ability to bind antigen are expanded and then differentiated into either antibody-secreting plasma cells or memory cells. Therefore, in mice and human the polyclonal migration of antigen-activated B-cells into germinal centers results in oligoclonal expansion, i.e. clonal selection of antibody specifity [99, 102, 103].

III.2 *Gallus gallus* and other species with post-*V(D)J*-*Ig* repertoire formation

In birds, rabbit, cattle, swine, horse and sheep after *V(D)J* recombination the primary *Ig* repertoire is developed by gene conversion and somatic hypermutation that takes place in special microenvironments. In sheep, cattle and horse – in ileal Peyer's patches [35, 104, 105]. In rabbit and chicken it is in gut-associated appendix [106] and the bursa of Fabricius, respectively [107].

Chicken prebursal stem cells are derived from hematopoietic precursors in the dorsal aorta. Primary lymphocytes with completed *V(D)J* recombination can be found in spleen, thymus, blood and even in nonlymphoid organs [108, 109]. These progenitor populations expand and diversify only in the bursa of Fabricius and decline with time at the other sites [107, 110, 111]. The mature bursa of Fabricius contains approximately 10000 lymphoid follicles, each of which is seeded by oligoclonal B-stem cells [33] in which *Ig* is diversified by gene conversion even in the absence of antigen stimulation [33, 112] and to a minor extent – by somatic hypermutation [113]. Therefore, opposite to mouse and human, in spite of the oligoclonal initialization each follicle in the bursa of Fabricius develops a highly diverse repertoire.

Starting at about the time of hatching, B-cells migrate from the bursa to populate peripheral organs. Upon antigen stimulation activated lymphocytes form germinal centers in the spleen. At the early stage of the germinal centers *Ig* is diversified by both GC and SHM [114]; at later stages gene conversion is downregulated and most of subsequent modifications are created by SHM [115].

IV. Chicken B-cell line DT40

IV.1. Unique characteristic of DT40

DT40 is an avian leucosis virus (ALV)-induced chicken lymphoma developmentally arrested at the stage of the B-lymphocytes from the bursa of Fabricius [116] with ALV-induced downregulation of *p53* and overexpression of *Myc* gene [117-121]. DT40 contains one *V(D)J* rearranged and one germline allele at the *Ig* light chain locus and expresses surface IgM [34, 118, 122]. DT40 was shown to continue the process of diversification of the rearranged *Ig* gene allele during *in vitro* culture by the process of gene conversion [118, 122]. While gene conversion in bursal B-lymphocytes occurs on average once every 10-20 divisions (Section II.2.a), in DT40 one GC event occurs once per 40 cell cycles [122]. Although most DT40 cells express surface IgM receptor, IgM-negative clones with frameshifts in the *V*-region, most likely deriving from non-functional recombination events, can be detected. It was shown that on-going gene conversion resulted in repair of these frameshifts leading to the appearance of the cells reexpressing surface IgM (Ig reversion assay, Figure 4) [122].

The unique characteristic of DT40 is its ability to maintain a high frequency of targeted integration into virtually any locus, including those not transcribed, unlike transfection in mammalian or murine cell lines which results in random genome integrations [123, 124]. Such an endogenous high efficiency of targeted integration is not present in murine and human B-cell lines, nor in chicken non-B-cell lines, which suggests that this unique property of DT40 might be related to the diversification of the *Ig* locus by gene conversion [125]. The high efficiency of targeted integration in DT40 makes it a powerful tool for testing the function of candidate genes by gene knockout [126, 127].

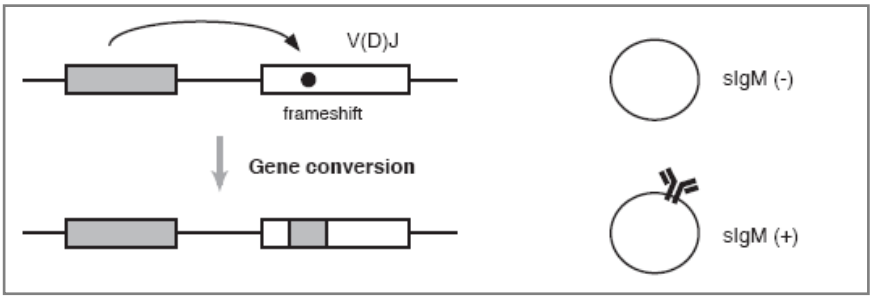

Figure 4. *Ig* reversion assay. One of the pseudo-genes is depicted in grey. Surface IgM-negative cells and cells reexpressing Ig molecule are shown on the right side. Taken from [128].

Besides efficient targeted integration, DT40 possess such advantageous properties as karyotype and phenotype stability even during extended periods of culture, rapid growth rate

with a doubling time of approximately 8-10h facilitating colony-formation essays, nearly 100% cloning efficiency of wild-type cells which results in efficient stable transfection and subcloning. The absence of functional apoptosis-inducing p53 makes it possible to isolate clones with a targeted disruption of genes responsible for genome instability [129]. Taken together the properties of DT40 make it convenient for reverse genetics studies [121].

IV.2. Elimination of gene conversion in DT40. Cross talk between gene conversion and somatic hypermutation

Although a few single nucleotide substitutions were found in the *IgL VJ* region of wild-type DT40 cells [118, 122], it is difficult to classify these mutations as non-templated because the sequence of the ψV genes used in this strain is not available [128]. The first evidence for hypermutation in DT40 appeared after disruption of the genes responsible for homologous recombination which suppresses gene conversion and later by the deletion of the pseudo-gene templates.

Among numerous reverse genetic experiments in DT40, the data on disruption of three particular gene groups is important for understanding the mechanism of the *Ig* gene conversion and somatic hypermutation, and their cross talk in this cell line: 1) *Aid*, 2) *Rad51* paralogues responsible for the homology search and strand invasion in the homology recombination [130] and proteins *Brac2* [131] and *Brac1* [132] which are though to regulate *Rad51*, 3) *Rad54* which is suggested to contribute to late stages of homologous recombination [133] and its counterpart *Nbs1* [134].

DT40 cells with either disrupted *Rad54* or *Nbs1* have 100-fold decreased ratios of targeted integration and also reduced gene conversion activity [135].

DT40 mutants of each of 5 paralogues of *Rad51* in vertebrates have reduced targeted integration frequencies and double strand break repair deficiencies [136]. The disruption of either one of three *Rad51*-paralogues (*Xrcc2*, *Xrcc3* and *Rad51b)* caused the appearance of single non-templated mutations within the *V*-region at a high rate of 0.4×10^{4} per bp per generation (similar to the rate previously calculated for the human Ramos lymphoma cell line) [78] whereas only a few gene conversion events were detected [137].

The hypermutation activity associated with *Rad51*-paralogues mutants was measured by quantifying the frequency of surface IgM-negative cells, which presumably had appeared due to introduction of the deleterious mutations in the rearranged *Ig* light and heavy alleles (Ig loss assay, similar to the Ig reversion assay used for measurement of the gene conversion) [137].

The deletion of the upstream *ψV* genes resulted in the abolition of gene conversion together with an upregulation of AID-dependent somatic hypermutation. The mutation rate observed using both FACS analysis of Ig loss and sequencing of the *VJ* region was approximately 2.5 times higher than that observed for the *Xrcc3*-mutant [67].

The characteristics of the mutations observed in both assays, using disruption of the *Rad51*-paralogues or deletion of the *ψV* genes, had features typical for the somatic hypermutation in mammalian B-cell lines [60, 138, 139]: namely *Ig* locus specificity with the typical distribution downstream of the promoter with preference for the hotspots, dependence on AID and occurrence by way of transversions of G to C and C to G bases and absence of mutations at A/T pairs observed for the germinal centers in mouse and human.

These experiments suggested a model of initiation and regulation of gene conversion and somatic hypermutation pathways (Figure 5). As AID disruption blocks GC completely but does not produce a DNA repair defect, the first step of *Ig* GC is most likely AID-dependent DNA modification, which leads to the recruitment of a series of cofactors that result in a DNA lesion within the *V* region (detailed in Section V). Processing of this lesion in the absence of the nearby *ψV* donors or factors of homologous recombination (RAD51-paralogues) leads to a single nucleotide substitution (Figure 5, right side). However, if the donor sequences are available, processing of the AID-induced lesion can be divided into two stages, before and after strand invasion, with and without a possibility of shifting to a somatic hypermutation, respectively. As the first stage requires the involvement of the RAD51-paralogues, the second stage involves more downstream recombination factors, such as RAD54. This model explains why the disruption of *Rad51*-paralogues or pseudo-genes not only abolishes gene conversion but also induces hypermutation while disruption of *Rad54* alone only decreases GC. DT40 mutants for *Brca1* [7] and *Brca2* [132] behave like the *Rad51*-paralogues mutants, whereas mutants of the *Nbs1* gene [134] or of members of the Faconi anemia pathway [140] show phenotypes similar to the *Rad54* mutant, indicating that encoded proteins participate either in first or the second stage of gene conversion, respectively. The model also predicts that low homologous recombination activity in the B-cell prevents *Ig* gene conversion, even when conversion donor pseudo-genes are present [128]. Such a low homologous recombination activity might be the reason why chicken germinal center B-cells have shifted the balance from *Ig* gene conversion to *Ig* hypermutation [115] and also why human and murine B-cells never diversify *Ig* by gene conversion despite the presence of nearby candidate donors in the form of unrearranged *V* segments.

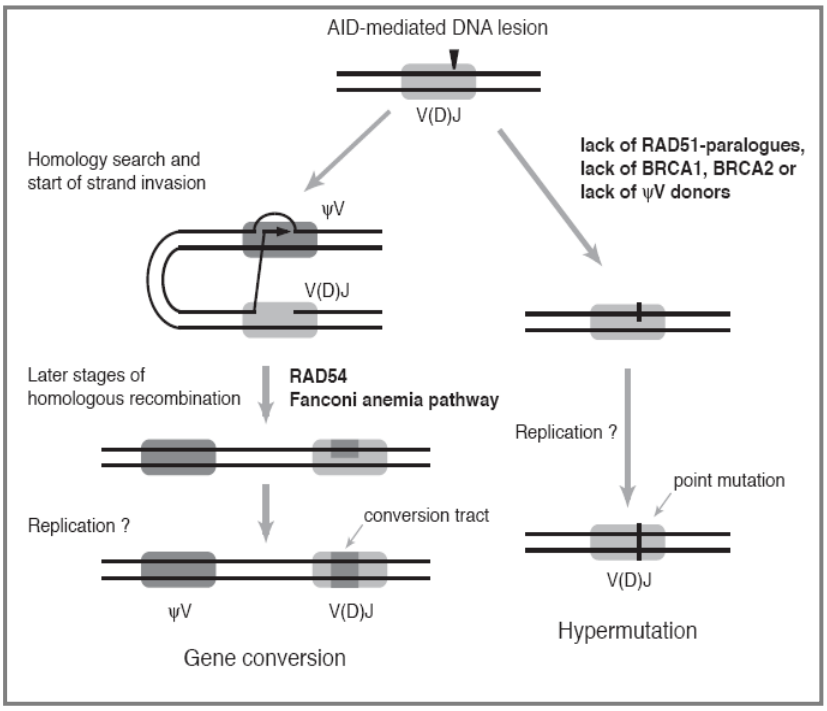

Figure 5. Cross talk of gene conversion and somatic hypermutation in DT40. Taken from [128].

V. Molecular mechanisms of somatic hypermutation

V. 1. First phase: cytidine deamination by AID

All three processes known to be involved in the post-*V(D)J* recombination, SHM, GC and CSR, require AID, activation induced deaminase, that is specifically expressed in activated B-cells [141]. The role of AID as the initiating factor for SHM and CSR became evident after the generation of *Aid*-deficient mice [65] and the finding that the human hyper-IgM syndrome (HIGM-2), characterized by a lack of CSR and SHM, is caused by inactivating mutations in the *AID* gene [66]. Later it was shown that disruption of the *Aid* gene in DT40 completely blocks *Ig* gene conversion, and in the absence of the pseudo-gene donors, SHM [43, 44, 67].

After its identification AID was suggested to be an RNA-editing enzyme because of strong homology with APOBEC-1, a protein editing the mRNA of the *apoB* gene [141, 142]. However, numerous *in vitro* studies have established that purified AID acts specifically on single-stranded DNA (ssDNA) [143-146] by deamination of deoxicytidine residues, producing U:G mismatches [147, 148] and does not deaminate RNA [149, 150]. Since transcription is thought to have a key role in opening double strand DNA to provide ssDNA, the single stranded specificity can explain the fact that AID action depends on transcription [87, 144, 151, 152].

An ssDNA-binding Replication Protein A (RPA), involved in replication, recombination and repair, may play a role in the control of AID activity as it was shown to determine AID targeting to ssDNA-transcribed substrates *in vitro.* This was by direct interaction with AID that is phosphorylated by Protein Kinase A (PKA) [153-155]. One model suggests that *in vivo* the small regions of ssDNA produced during transcription are bound by RPA, which in turn facilitates activity of AID at the *V*- and *S*-regions [153, 156].

Although AID is specifically expressed in the B-lymphocytes, overexpression of this enzyme in bacteria, fibroblasts and hybridomas results in the induction of SHM in multiple highly expressed genes [60, 64, 87]. Aberrant expression of AID in the mouse caused T-cell lymphoma that is associated with hypermutation in *Tcr* and *Myc* genes [143, 157]. Deregulation of AID may, through its mutagenic activity, lead to malignancy *in vivo.* All this data suggest that the B-cell and *Ig* specificity of SHM is probably maintained by specific factors of B lymphocytes.

Mutation of the N-terminal domain of AID diminishes SHM but does not influence CSR whereas C-terminal region is absolutely required for CSR but seems to be dispensable for both SHM and GC in eukaryotic cells [158-160]. These results raise the possibility that different cofactors for SHM and CSR interact with the N- and C-terminal regions of AID, respectively.

As might be expected for an enzyme that mutates DNA, the access of AID to the nucleus is regulated. The major fraction of AID is found in the cytoplasm. The C-terminal domain contains a strong nuclear export signal (NES), removal of which causes the accumulation of the AID in the nucleus. However, a putative nuclear localization signal in the N terminus does not appear to be functional [161-164]. Together, these results suggest that AID passively diffuses into the nucleus but that it is actively transported out of the nucleus by an NES-mediated mechanism.

Studies showing increased nuclear AID content after induced DNA lesions do not show increased SHM [161]. Therefore AID alone is not sufficient for SHM and factors in addition to AID are involved in regulation of this process [159, 161, 163].

V.2. Processing the AID-generated mismatches

There are different possible ways of processing the U:G mismatch generated by the AID-catalyzed deoxycytidine deamination within the *Ig* locus. If the mismatch is not repaired before the onset of DNA replication then DNA polymerases will insert an A opposite the U nucleotide creating both C to T (C→T) and G→A transition mutations (Figure 7). All other types of nucleotide substitutions (transversions at G:C and all kinds of substitutions at A:T

pairs) require recognition of the U:G lesion by factors of the base excision repair or mismatch repair pathways.

V.2.a. Uracil excision by UNG

After they have been generated by AID, the U:G lesions are most commonly removed by the Base Excision Repair pathway (BER), leading to the transversion mutations at G:C pairs [165]. BER is initiated by one of the four uracil-DNA-glycosylases described in vertebrates, UNG [166], which excises uracils from the DNA deoxyribose-phosphate backbone and thereby generates abasic sites [167].

The involvement of uracil glycosylase in SHM became apparent before the evidence for the presence of AID-created uracils in the *Ig* locus *in vivo* [168]. Expression of Uracil Glycosylase Inhibitor (UGI) in hypermutating cells revealed that the spectrum of mutations shifted from the more usual transversions to the transitions C→T and G→A. [147]. This could be explained by UGI-mediated inhibition of the removal of the AID-induced uracils by uracil glycosylases, leading to pairing of the unexcised uracils with adenines during the next round of replication. As transfection of the *Ugi* transgene to the wild type DT40 reduced the rate of gene conversion, it was suggested that excision of uracils is also required for this type of *Ig* diversification [169]. In human, deficiency of UNG leads to a decrease in CSR and perturbation of SHM [170]. These observations were confirmed by knock-out of the *Ung* gene: a similar shift in the mutation spectrum to transitions at G:C pairs, together with inhibition of the CSR, was observed for $Ung^{-/-}$ mice [171]; $Ung^{-/-}$ DT40 also possessed dramatically reduced gene conversion; at the same time the SHM rate was 7 times higher than that in the cell line with deleted ψV genes. Due to a lack of abasic sites 98% of the SHM substitutions were transitions C→T or G→A [172]. Relatively frequent conversion of uracils into mutations (one in seven, if it is assumed that the transition mutations of the $Ung^{-/-}$ reflect the total number of the induced uracils) support the error-prone repair pathway.

It was shown using DT40 and mice that *in vivo* none of the other uracil-DNA glycosylases of vertebrates act as a backup for UNG in SHM and CSR [164, 173-175]. However, in the absence of UNG other uracil glycosylases are able to process the U:G lesion. Overexpressed uracil glycosylase SMUG1 partially substitutes for UNG to assist SHM and restores isotype switching in $Msh2^{-/-}Ung^{-/-}$ mice [174]. In contrast to endogenous UNG, the overexpression of SMUG1 in mice diminishes the frequency of *Ig* diversification [174], probably because SMUG1 favors conventional non-mutagenic repair of U:G lesion [176].

The involvement of UNG in immunoglobulin diversification may be regulated through interaction with other proteins [174, 177, 178]. It was shown that UNG is able to form a

complex with PCNA and RPA in replication foci at defined cell cycle stages [178]. Regulation of UNG expression timing could be crucial in deciding the competition between BER and mismatch repair pathway for these factors and error-prone polymerases [48].

V.2.b. Mismatch repair

Mismatch Repair (MMR) is a complex process of maintaining the fidelity of DNA replication by removing errors from newly synthesized DNA. Genetic inactivation of the MMR system elevates spontaneous mutability 50-1000-fold and predisposes to cancer [179].

In eukaryotes MMR is initiated by the recognition of DNA mismatches by the heterodimeric protein MSH2-MSH6 (bacterial MMR protein MutSα homolog). Via the recruitment of a number of additional proteins it introduces a ssDNA nick near the mismatch through exonuclease Exo1 [48, 180]. After excision of the mismatch, high-fidelity polymerases resynthesize the excised DNA strand and the ends are ligated. It is known that MMR requires several other factors, most of which are also involved in transcription and replication, including PCNA (Section V.2.d), RFC (Replication Factor C) and RPA [48].

During SHM the U:G mismatch, in addition to recruitment of UNG-dependent BER, can activate the mismatch repair machinery. This is thought to result in mutations at A:T pairs near the initiating lesion, probably through an error-prone repair process [181-183].

Experiments using knock-out of *Msh2* and/or *Msh6* in mice showed that MMR influences the pattern of hypermutation [184, 185]; in the absence of these proteins a considerable bias for mutations at G:C pairs was observed while the global frequency of the SHM did not change. Consequently, the frequency of mutations at A:T pairs was considerably decreased [175, 181, 186, 187]. Among the models explaining this phenomenon [188] it has been suggested that a two-step mutation mechanism is supported by a number of studies. The first step of this model suggests introduction of mutations at G:C targets whereas during the second phase (for which recognition of the mismatch by MSH2-MSH6 heterodimer is required) error-prone translesion repair introduces secondary nucleotide substitutions at A:T pairs near the initiating lesion [182, 183] (Figure 7; Section V.2.c).

According to this mechanism, MMR might be responsible for creating the ssDNA breaks during SHM, GC and CSR [74, 189-191]. In *Exo1*$^{-/-}$ mice the activity of CSR is decreased and the SHM spectrum is similar to that observed for the *Msh2*$^{-/-}$ mutant [181]. In the case of CSR, two opposing strands mismatches in the *S*-region could result in the formation of double-stranded breaks. If the process of repair of the single- or double-stranded DNA break is through homologous recombination, then gene conversion would occur (Figure 6).

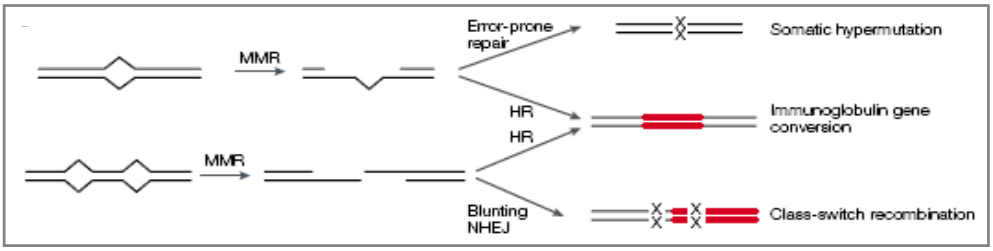

Figure 6. MMR resulting in SHM, GC or CSR. Taken from [189].

It was also shown that the A:T mutations can be created via short-patch DNA repair by both MSH2–MSH6-mediated and also by UNG-mediated recognition of the U:G. The inactivation of both pathways (*Ung* and either *Msh2* or *Msh6)* leads to a loss of practically all mutations at A:T bases in the *V* regions and a profound loss of CSR [175, 192]. However, analysis of *Msh2*$^{-/-}$ and *Msh6*$^{-/-}$ mice suggests that MSH2–MSH6-mediated recognition is the major pathway [181, 193].

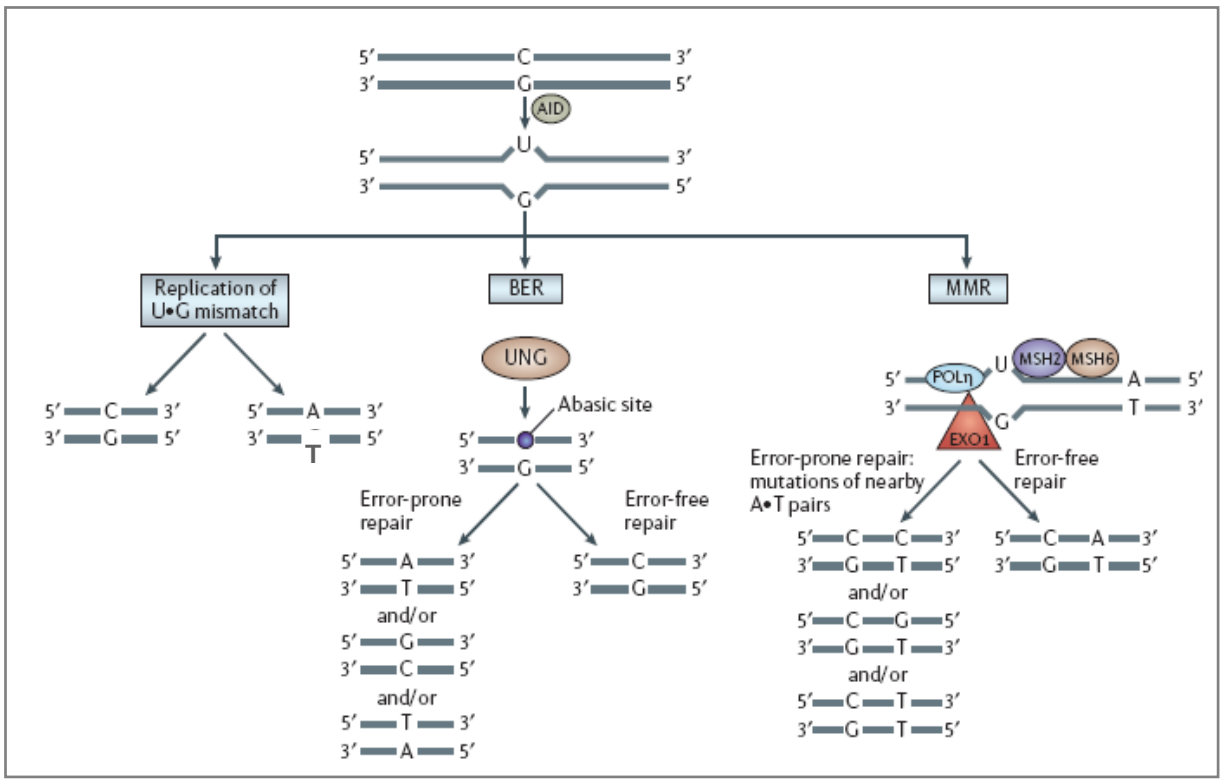

Figure 7. Activation-induced-cytidine-deaminase-dependent lesion repair. Taken from [156].

V.2.c. Translesion synthesis

In contrast to high fidelity replicative DNA polymerases which are usually stalled by encountering a damaged nucleotide, translesion synthesis (TLS) polymerases are able to synthesize through lesions, with a high processivity, albeit at the cost of high error rates [194, 195].

During normal cell growth uracils are frequently incorporated into DNA at the time of synthesis. This is independent of AID activity [177] and is repaired predominantly through BER by error-free polymerases. In the *Ig* locus, however, AID-induced uracils are repaired in an error-prone manner resulting in SHM [156, 196, 197].

In general, translesion synthesis produces mutations at the following pairs: 1) C:G while bypassing UNG-mediated abasic sites; 2) at C:G and A:T while extending past these abasic sites and 3) at C:G and A:T while copying undamaged DNA template during patch DNA synthesis in MMR or BER. In fact the mismatches introduced by TLS polymerases could trigger a new round of MMR, resulting in the amplification of the original mutations (Figure 7 and 8).

During SHM Pol η, Rev1 and pol ζ act together. Due to their low processivity pol η and Rev1 perform mispair insertion while pol ζ extends the DNA strand ignoring mispairs previously inserted by pol η or Rev1 [198] (Figure 8).

Pol η is supposed to play a key role in introducing mutations at A:T pairs since there is a lack of such substitutions in the mutation spectrum seen in *Xeroderma pigmentosum* variant (XP-V) patients, who are pol η deficient, and in pol η-deficient mice [199-201]. As deficiency of pol ι, a paralog of pol η, causes in mice slight reduction in overall mutation spectrum only when combined with *Pol η* disruption, this polymerase seems to play only a minor role in SHM [202, 203].

Rev1 is responsible for introducing most of the C→G and G→C transversions at abasic sites, as seen in DT40 and *Rev1*-deficient mice [204-206].

Pol θ is the first DNA polymerase recognized that can bypass efficiently an abasic site by functioning as both a mismatch inserter and a mismatch extender [207]. P*ol* $\theta^{-/-}$ mice had decreased overall frequency of mutations at C:G and A:T [208]. This polymerase is though to contribute to the residual mutation activity at A:T found in the η-deficient mice [57, 198, 200, 201].

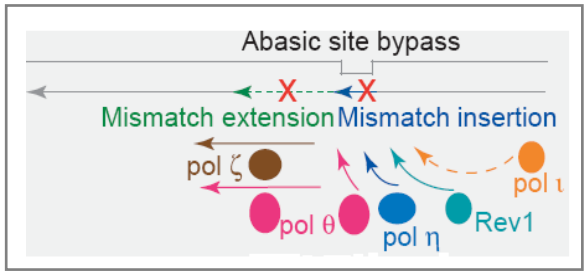

Figure 8. Recruitment of different error-prone polymerases into repair of abasic site within *Ig* locus. While Pol η, Rev1 and pol ι perform mispair insertion, pol ζ extends DNA strand past mispair. Pol θ is involved in both mismatch insertion and strand extension. Taken from [209].

Biochemical studies indicate that TSL polymerases are recruited at the sites of DNA lesion through interactions with repair factors as part of a TSL complex including RPA, proteins of MMR and BER and PCNA.

V.2.d Triggering of the translesion synthesis by PCNA

Proliferating Cell Nuclear Antigen (PCNA) is a polymerase processivity factor involved in replication and repair regulation, acting as a "docking station" for proteins by creating a homotrimeric PCNA clamp around DNA [210]. From studies in yeast and human it is known that stalling of the replication machinery at DNA lesion results in the mono-ubiquitination of PCNA at an evolutionary conserved residue K164. In the mono-ubiquitinated form PCNA promotes access of TLS polymerases to the replication fork [196, 197, 211, 212] and enhances the efficiency of these polymerases [194, 207, 213, 214].

In particular, it was shown that PCNA dramatically stimulates the ability of yeast pol η to insert a nucleotide opposite the lesion [215] and facilitates TLS synthesis of UV-damaged or abasic site-containing DNA by pol ζ [213]. In DT40 knock-in of *Pcna* with the conserved K164 replaced by arginine increases sensitivity of cells to DNA-damaging agents and strongly reduced the hypermutation rate in the *IgL* locus, especially transversions G→C and the C→G, suggesting a role of PCNA mono-ubiquitination in the recruitment of REV1 in SHM [205]. The PCNA-ubiquitination pathway for SHM was confirmed in a *Pcna(K164R)* knock-in mouse [216], however the spectrum of mutations was different: significantly decreased substitutions at A:T pairs were compensated by an increase of mutations at C and G bases. This study indicates that in mice pol η is the main polymerase recruited by ubiquitinated PCNA, whereas polymerases responsible for mutations at C and G bases acted independently of PCNA-ubiquitination at K164.

Although RAD6-RAD18 is the only ubiquitin-ligase for PCNA mono-ubiquitination in yeast, in *Rad18*-knock-out DT40 cells PCNA ubiquitination was decreased but not completely abolished [205] rising the possibility that there must be an alternative ubiquitin-ligase able to ubiquitinate PCNA at K164 in vertebrate cells. This is consistent with experiments on disruption of *Rad18* in DT40 possessing more modest decrease of SHM compared to the *Pcna(K164R)* mutant [205, 217]. PCNA also contributes to enhancing the mismatch-binding specificity during MMR [218-220] and probably recruits TLS polymerases into MMR since it was shown to facilitate the interaction between pol η and Msh2–Msh6 [183].

VI. *Ig* locus specificity of somatic hypermutation

Unregulated somatic hypermutation represents a threat to genome integrity and has been suggested to play a role in the development of cell lymphomas when inappropriately activated [68, 221]. Only *Ig* genes undergo hypermutation at a high rate, and this seems to be precisely targeted as sequence analysis of neighboring to the *IgL* locus genes in DT40 revealed no diversity [222]. However, some non-*Ig* genes, including *BCL6, FAS, CD79A* and *CD95B* were found to undergo SHM in normal B-cells, albeit at lower frequencies compared to the *Ig* locus [68, 223-225]. In human B-cell tumours several other loci, such as *BCL6, MYC, PIM1, RHOH* and *PAX5* were demonstrated to be targeted by SHM [221, 225].

Since a retroviral reporter construct was shown to undergo AID-mediated SHM in mice when introduced at different genomic sites [226, 227] and sequence analysis indicated that AID of B-cells from Peyer's patch acts broadly on the genome [70], the term "targeting of SHM" implicates not only recruitment of AID (which still might be important for high rates of hypermutation) but also mechanisms for the enlistment of error-prone BER and MMR factors to the *Ig* locus. Recent determination of the human MSH2-MSH6 complex crystal structure around various types of mismatches demonstrated that confirmation of this dimer does not depend on the type of the DNA lesion indicating that nature of the U:G mismatch itself is unlikely to play a role in recruitment of error-prone repair [228]. Although an unambiguous factor responsible for targeting of SHM has not been found, numerous studies suggest that this process could be driven by a complex of factors including *cis*- and *trans*-elements binding to the *Ig* locus. These may well act in a temporal manner, corresponding to cell cycle restriction, specific nuclear localization of SHM and accessibility of the *V*-region due to the transcription activity, a high density of mutational hotspots or epigenetic pattern which is discussed in following chapters.

VI.1. *Cis*-acting DNA elements

Recent evidence indicated that the coding sequence of the *V* region does not itself contain the sequences necessary for targeting of SHM, since replacement of the *V* and *J* segment by heterologous DNA fragments does not affect the rates of hypermutation [156, 229].

Correlation between transcriptional activity and SHM indicates the involvement of *cis*-regulatory transcriptional elements in the recruitment of factors specific for SHM, including AID as well as proteins of BER, MMR and translesion synthesis. The observation that non-*Ig* promoters are able to promote SHM of the *Ig* genes [62, 71, 230-233] further suggests that the *Ig* promoter itself also lacks the sequences responsible for the recruitment of the SHM.

A number of studies on transgenic and knock-in mice have indicated that some of the enhancers identified within light and heavy chains of the *Ig* locus influence targeting of the SHM to the *V*-region. This is consistent with the key role of transcription in the recruitment of AID-mediated deamination (Section V.1). However, these results were not unequivocal due to the interference of the mutation rate with the transcription level. Moreover, some of these observations have been disproved by deletion analysis within the endogenous *Ig* locus. For example, both enhancers identified within murine *κ* light chain locus (intronic iEκ and 3'Eκ) were shown to be required for the SHM in the context of *Igκ* transgene [71, 234] and to be sufficient for targeting of SHM to the non-*Ig* transgene in Ramos cell line [76]. However, both of these *cis*-elements turned out to be dispensable for SHM in the endogenous murine *κ* locus [235, 236]. The same contradiction was observed when comparing the transgenic and endogenous contexts for testing various parts of the 3' regulatory region of the murine *IgH* [237, 238].

A recent study using an AID-expressing hybridoma cell line suggests that the effect of the *cis*-regulatory elements on SHM is not exclusively positive, but can also be negative. This observation is based on results showing that the *IgH* intronic core enhancer Eμ is required for SHM of the endogenous *V* region if the flanking matrix attachment region (MAR) was present. If both core Eμ and MAR were deleted, SHM was reduced back to the level of the wild-type [239]. Deletion analysis of the Eμ enhancer in the Ramos cell line resulted in a change of the SHM pattern [240] denoting the possible involvement of this *cis*-regulatory element in recruitment of the error-prone BER and MMR.

In DT40 the deletion of the only known *IgL* enhancer did not affect gene conversion activity [229]. However, the deletion of a sequence including the enhancer together with its flanking regions prevented gene conversion and non-template mutations within the *V* region [46]. As the locus containing *ψV*-genes was shown to be dispensable for SHM in DT40 [67], it is likely that the *cis*-regulatory element for targeting of the SHM is included in the 9.8 kb fragment starting from the *IgL* transcriptional start site until the border of the neighboring locus.

Although it was shown that insertion of the binding sites for a number of particular B-cell *trans*-factors, such as E2A, PU.1 and NF-EM5 increases the rate of SHM *in vivo* [73, 241], these *cis*-sequences are unlikely to be the main regulators of SHM as they are common to many other loci that are not influenced by SHM.

SsDNA structures represent a class of *cis*-elements which might play a role in targeting of the SHM, such as the G-loops observed in the transcribed switch-regions which

could serve as targets for AID binding [48, 242]. An experiment using cross-linking of proteins to DNA revealed the prevalence of ssDNA patches in genes undergoing SHM compared to other highly transcribed genes which are not targeted by hypermutation [243]. While SHM, unlike CSR, does not seem to target specialized RNA or DNA secondary structures, the mutability was found to correlate with the density of the SHM hotspots within the given sequence [230].

VI.2. *Trans*-acting factors

Consistent with a possible role of enhancers in targeting of SHM, it is likely that enhancer-binding transcription factors might be involved in the recruitment of components of hypermutation. This hypothesis was confirmed for the study of the elongation factor E2A, where overexpression of one of the alternatively spliced forms of *E2a* caused an increase in gene conversion in DT40 [45] and disruption of the *E2a* gene in DT40 with deleted ψV-genes resulted in a 3-fold decrease in SHM [244].

The inactivating mutations in AID [158, 159] and the importance of AID phosphorylation [153-155], both indicate that AID is accompanied by cofactors which might be responsible for targeting of this protein to the *Ig* locus. RNA Polymerase II is thought to be one such cofactor, as it was found to co-immunoprecipitate with AID [245] and RNA Polymerase II promoters were shown to support SHM [71, 230]. The possible preference of AID to bind the elongation, but not the initiation form of this polymerase, may explain why the 5' boundary of the SHM is located 150 bp downstream of the *Ig* gene transcription start site [246]. Among other cofactors which were shown to associate with AID are RPA, PKA, DNA PKs and ubiquitin ligase 3; however all these proteins are encoded by house-keeping genes or genes important for the B-cell development, therefore it is difficult to determine their specific role in SHM.

A recent study showed that AID purified from insect B-cells can associate with endogenous ssRNA and that degradation of this RNA is required for the AID deamination activity [149]. This is consistent with the possibility that in B-cells the association of AID with RNA has a negative regulatory role and interferes with the targeting of SHM.

VI.3. Chromatin structure

Regulation of transcription, replication and repair is often associated with changes in the epigenetic pattern, such as DNA methylation and post-transcriptional modifications of histones, associated with reduced transcription activity or silencing and increased accessibility to the trans-factors, respectively [48, 247]. It was suggested that these modifications could

also be involved in the targeting of SHM factors to the *Ig* locus by facilitating accessibility of the *V* and *S*-regions.

A role of methylation in targeting of SHM was indicated by the finding that an unmethylated allele of the κ light chain was modified ten-fold more frequently by SHM than the unmethylated locus in transgenic mice [248]. However, the mechanism of this regulation is not clear as it was shown earlier that the presence of methylated CpG in DNA does not influence AID deamination at nearby cytosines [249].

A number of studies suggested the involvement of histone acetylation in the control of SHM locus specificity: firstly, hyperacetylation was observed for AID-targeted *S*-regions undergoing CSR [90, 245, 250, 251] and for gene segments during *V(D)J* recombination [252], secondly, it was shown that the histones of the *IgH V* region of the hypermutation-inducible B-cell line BL2 are hyperacetylated while the following *C* region lacks acetylation [253], a finding later confirmed in mice [254]. Treatment of BL2 with an inhibitor of the histone deacetylase resulted in the acetylation of the *C* region followed by an increase in the SHM of this-region [253]. However, this result has no bearing in the specific targeting of SHM. Curiously, no difference in the acetylation pattern was observed *in vivo* for the *Ig*λ *V* and *C* regions which could be explained by closer colocalization between these regions in the light chain compared to the *IgH* locus and possible transcriptional activity of the *Ig*λ *C* region, which is also known to be accompanied by acetylation [254].

Another modification possibly involved in targeting of SHM is phosphorylation of histone H2B at S14 which was found to be associated with *V* regions of the light and heavy chains *in vivo* as opposed to the following *C* regions and correlate with both SHM and CSR [254]. As histone phosphorylation at S14 was found to be dependent on AID, it is unlikely that this modification is involved in initial targeting of this protein. However it might play a role in the subsequent recruitment of the error-prone BER and MMR factors. This is supported by the finding that phosphorylation of the histones at S14 that occurs at sites of DNA damage provides the requirement of the repair factors [255, 256] and also known to participate in the response to induced DSBs [257].

VI.4. Cell cycle restriction

While error-prone repair is important for SHM, error-free repair is required for DNA replication during S phase of the cell cycle. There might be a possibility that these two processes are temporally restricted, i.e. SHM may happen only during the non-replicative phase of the cycle. This hypothesis is supported by several studies, including finding that SHM can only be detected within the *V*-region of BL2 cell line during G_1 and G_2 phases but

not at S phase [139] and that during CSR the *IgH V* gene is colocalized with proteins involved in NHEJ exclusively in the G_1 phase [258]. Immunohistochemical and immunofluorescent staining techniques indicated that colocalisation of AID and other molecules involved in *Ig* diversification, including UNG and RAD51, depends on the cell cycle stage in rabbit [259, 260].

VI.5. Subcellular localization

Taking in account that the *Ig* loci contain MAR elements [45, 72, 261] and that transcription and *V(D)J* recombination is presumed to be regulated by the subnuclear positioning [262] it is possible that a defined localization of the *Ig* locus within the nucleus might be important for regulation of the SHM. Therefore, the weak hypermutation observed in non-*Ig* genes could be explained by the proximity of these genes to the *Ig* locus within the nucleus. Recently it was demonstrated that *IgH* and *IgL* genes are colocalized with *Myc* within the "transcription factories" in primary B-cells [263]. Although colocalization of these genes during SHM or CSR remains to be determined, this raises the possibility that SHM could be regulated by factors recruited by the colocalized genes.

VII. Application of the somatic hypermutation and gene conversion for biotechnology

A powerful tool for the development and optimization of new proteins is directed protein evolution. One of the most common technologies for this artificial evolution is random DNA mutagenesis *in vitro*, followed by a selection for desirable protein phenotypes. However, screening for advantageous mutations and analysis of the new phenotypes require routine methods, including expression of diverse gene libraries in bacteria, phage or translation systems followed by transfer into eukaryotic cells or organisms for analysis [264-267]. *In vivo* random mutagenesis strategies avoid the repetitive transfection and re-isolation of genes. However, randomizing mutations of genome often leads to the deleterious instead of the desired mutations [268]. In this respect hypermutation and gene conversion of the transgene combined with the appropriate selection of phenotypes carrying beneficial mutations, could become a powerful tool for artificial evolution due to the high rate of mutation and precise targeting of the diversification. Fluorescent proteins are convenient objects for establishing and validation of such a system as screening of the new phenotypes can be easily managed by Fluorescence Activated Cell Sorting (FACS).

VII.1. Green and red fluorescent proteins as objects for the directed protein evolution *in vitro*

The most popular fluorescent proteins used as reporters in cell and molecular biology [269] are mutants of the Green Fluorescent Protein (GFP) initially purified from the jellyfish *Aequorea victoria* [270, 271]. These mutants were generated using different methods of genetic engineering including random and site-directed mutagenesis [272-274]. These methods also allowed the development of GFP-derived proteins with new colors, such as yellow, cyan and blue fluorescent proteins [275]. The fluorescence of GFP-like proteins and GFP-derived mutants now cover almost the whole visible spectrum [276]. So far several GFP variants with high fluorescent intensity including eGFP [277] and Emerald [278] have been developed.

Proteins that emit red and especially far-red light are of particular interest for both basic and applied science as they are important for multicolor imaging and applications based on fluorescence resonance energy transfer (FRET) [276]. Far-red fluorescence photons cause less damage to proteins and DNA because of their lower energy, which makes far-red fluorescent proteins (RFPs) to be in high demand for labeling of tissues and whole-organisms [280, 281].

The favorable 'optical window' for the visualization in living tissues is approximately 650–1,100 nm as the water in tissues absorb photons and wavelengths longer than 1,100 nm [282]. Additionally, the light-scattering intensity drops off as the wavelength increases [281]. Recently, far-red fluorescent variants, with the reaching the 650 nm barrier, such as HcRed, mPlum and AQ143, have been derived from the DsRed or its homologs [283-285]. These proteins, however, are either characterized by weak brightness or their emission peaks are of a too short wave to reach the optical window.

Recently, the groups of S. Lukyanov and J. Wiedenmann independently purified from the sea anemone *Entacmaea quadricolor* red fluorescent proteins eqFP578 and eqFP611 encoded by the paralogous genes. These became competitive compared to the earlier RFPs due to their high fluorescent brightness (eqFP578 was 1.5 fold times brighter than DsRed), complete chromophore maturation and a reduced tendency to oligomerize [286, 287]. Brought together, these characteristics made *Entacmaea quadricolor* – derived fluorescent proteins an attractive starting point for the generation of the bright far-red fluorescent proteins. Up to 2007 the group of S. Lukyanov published a number of bright far-red proteins with different advantageous characteristics such as TurboRFP and Katyushka and their monomer forms

TagRFP and mKate, respectively (summarized in Figure 9) [281, 286]. EqFP611 and mKate were successfully crystallized, and their crystal structures have been determined [288, 289].

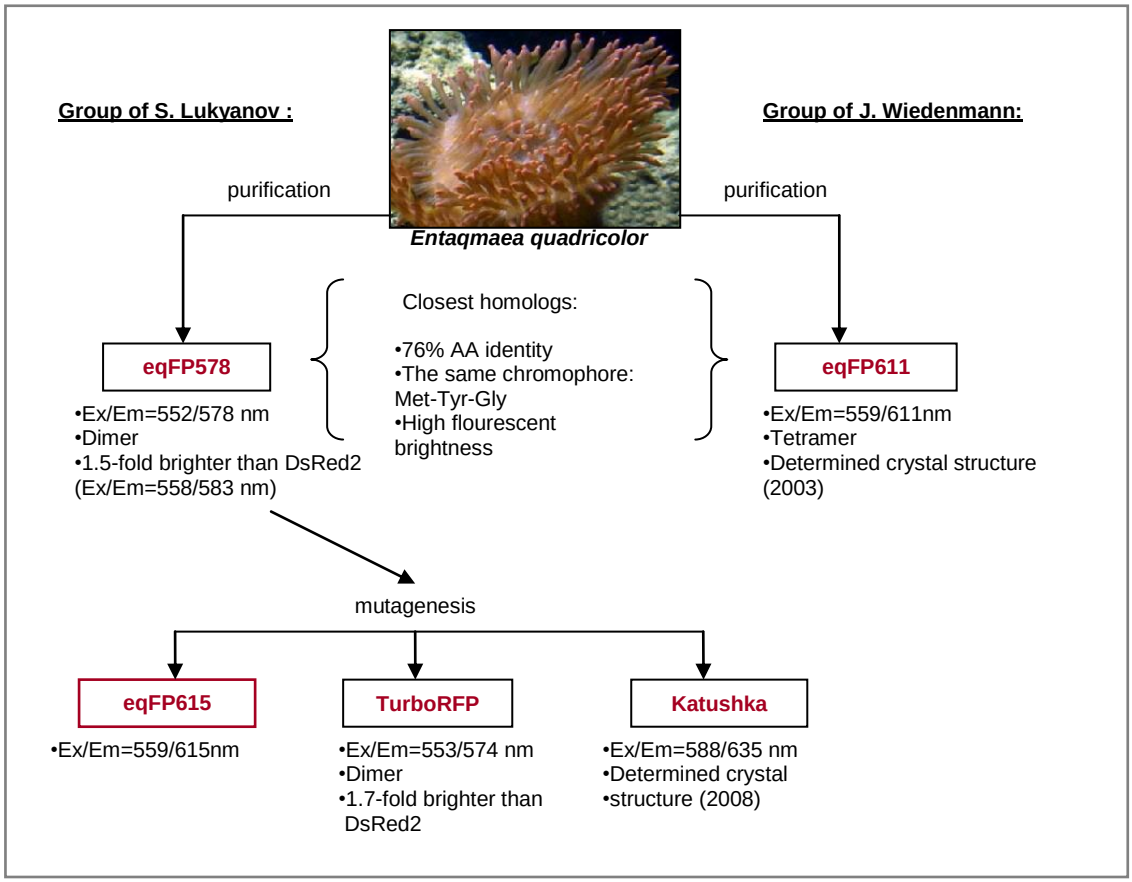

Figure 9. A scheme of the proteins and their mutants derived from the *Entacmaea quadricolor*.

VII.2. Using of *in situ* directed protein evolution based on hypermutation

Recently the AID-dependent hypermutation properties of the B-cell lines 18-81, 70Z/3 and MPC-11 have been applied to the *GFP* gene within a retroviral construct for the generation of new mutants with increased fluorescent intensity [279]. It was recently reported that retrovirus-mediated insertion of the red fluorescent protein gene into the hypermutating Ramos B-cell line, followed by selection for red-shifted fluorescence, allowed the isolation of the most far red-shifted fluorescent protein known to date, mPlum [285].

However, in the experiments using B-cell line-based mutagenesis it has proven difficult to control the targeted integration of the transgene and, therefore, the levels and efficiency of its hypermutation. In this respect it is convenient to use the DT40 cell line that is characterized by easy targeted integration and which also offers the unique advantage of using the gene conversion as an additional tool for diversification of the transgene.

DT40-based directed evolution has been used by various groups for the generation and selection of antigen-specific antibodies using *Ig* gene conversion enhanced by the histone deacetylase inhibitor TSA (trichostatin A) [290], optimization of the antigen specificity of

antibodies to independent test antigens using gene conversion and hypermutation in *RAD51* [291], converting the fluorescence of BFP to green using the GFP gene as a donor for gene conversion [292].

In our laboratory the hypermutation process of the DT40 cell line without gene conversion activity was applied to the eGFP protein (eGFP has mutations F64L and S65T enhancing its brightness compared to the GFP) [293]. The concept of an artificial evolution system was based on the assumption that a target transgene placed into the *IgL* locus of DT40 cell line can be hypermutated in an AID-dependent manner. Compared to the present *in situ* specific mutagenesis this system had certain advantages: 1) single copy insertion of a target gene into defined locus, 2) high rates of hypermutation, 3) mutation activity can be switched on/off by the presence of *Aid* (an *Aid*-conditional knockout DT40 clone AID^{R1}, which had a possibility to shut down the expression of *Aid*, was used [294]), 4) *in situ* selection of the better phenotypes. *EGFP* was inserted between the *IgL* promoter and the leader exon of the *V* region using the construct *pHypermut1* (Figure 10). FACS analysis of the transfectants $AID^{R1}IgL^{eGFP}$ revealed populations of transfectants with either increased (GFP^{high}) or decreased (GFP^{low}) GFP fluorescence (Figure 11A). Mutation activity of $AID^{R1}IgL^{eGFP}$ was dependent on AID as transfectants $AID^{-/-}IgL^{eGFP}$ did not produce mutations (Figure 11A).

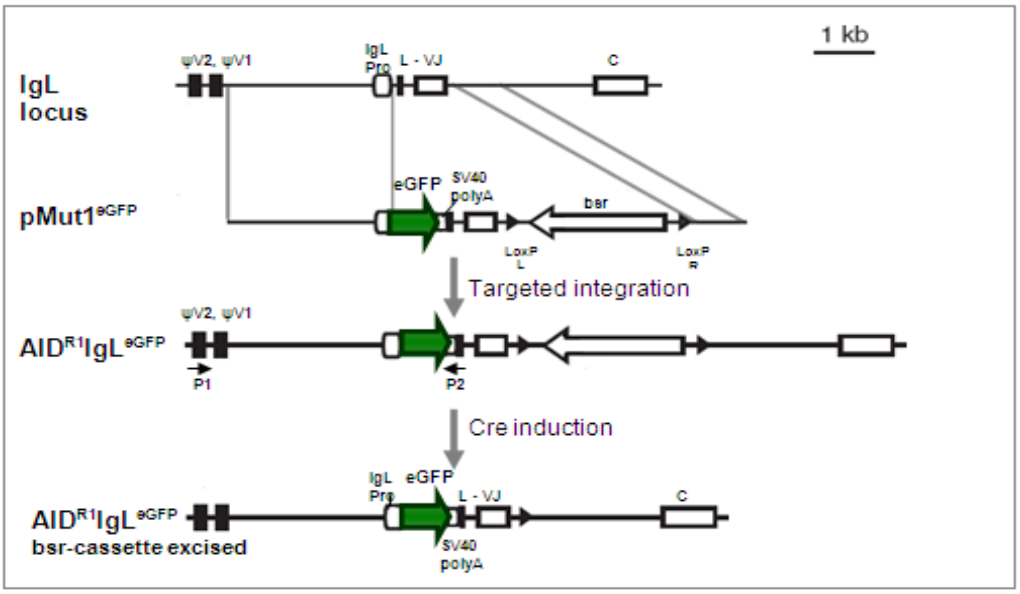

Figure 10. A scheme of the chicken rearranged *IgL* locus containing two pseudo-genes *ψV1* and *2*, Ig promoter (IgL Pro), *V*-region with leader (*L*) and *VJ* exons and constant region (*C*), targeting construct $pMut1^{eGFP}$ carrying *eGFP* gene and *bsr* gene, surrounded by *LoxP* sites for Cre-recombination, and *IgL* locus after the targeted integration and excision of the *bsr*-cassette. Primers used for target screening (P1 and P2) are shown by arrows.

In order to enrich the cells with the increased brightness, GFP^{high} were sorted from the $AID^{R1}IgL^{eGFP}$ clone (sort I) (Figure 11B). After this two subsequent sorts of the populations with the increased fluorescent brightness were done and each time the cells, expanded after the sort, demonstrated superior brightness compared to the cells from the previous sort.

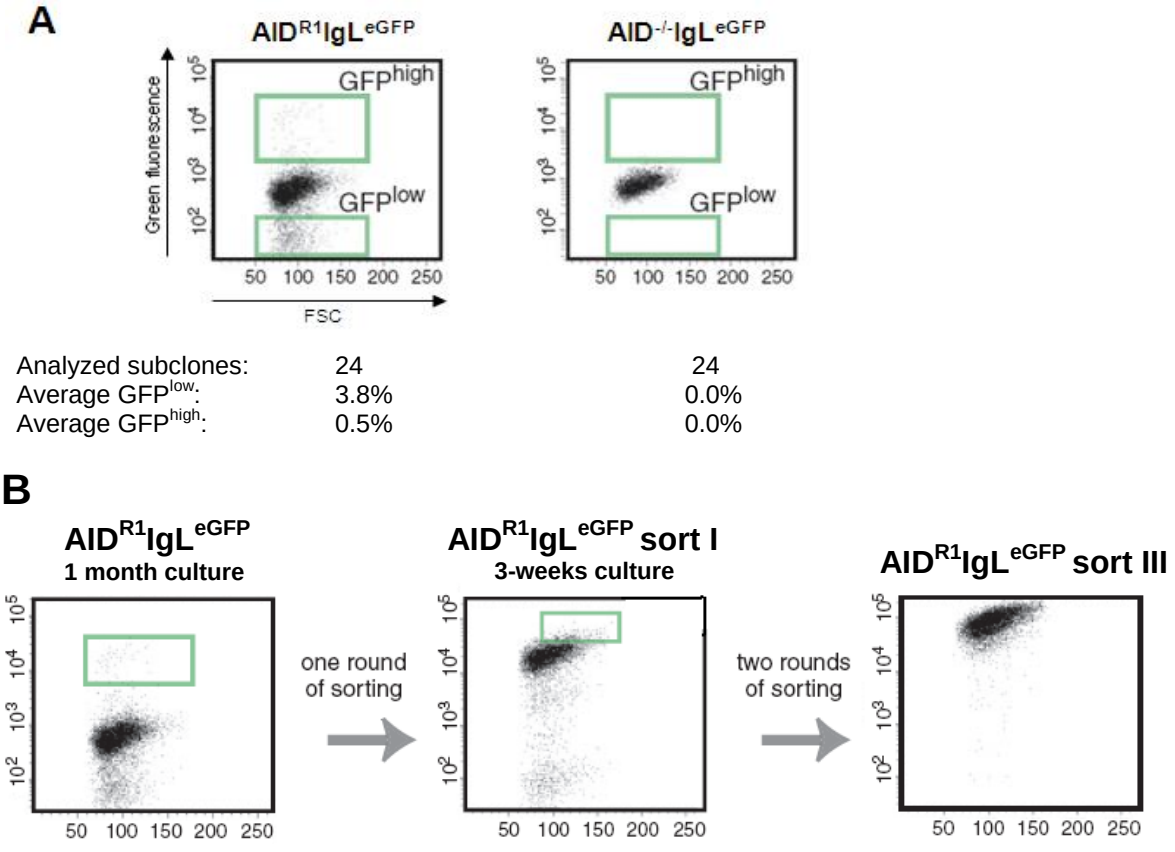

Figure 11. (A) FACS profiles of the $AID^{R1}IgL^{eGFP}$ and $AID^{-/-}IgL^{eGFP}$ clones. Average percentages of events falling into GFP^{high} and GFP^{low} gates based on the measurement of 24 subclones are shown. (B) Sorting strategy of highly bright GFP population. The gate I population was sorted from three subclones of the $AID^{R1}IgL^{eGFP}$ after 1 month of culture (sort I). After three weeks of culture of this sorted population, the gate II population was enriched by two rounds of sorts (sort III).

OBJECTIVES

The first goal of the present study was to confirm and analyze new GFP phenotypes generated using the artificial protein evolution system created in our laboratory ("Introduction", VII.2) and combine the different optimizations created using this method through site-directed mutagenesis.

Despite a number of advantages compared to the known *in situ* mutation systems, the artificial protein evolution system created in our laboratory is not efficient, due to the disadvantage that the transgene cannot be mutated specifically. Thus, the second objective of the present work was to design a vector which would allow diversification of the transgene specifically and therefore increase the efficiency of the artificial evolution system. In order to validate the new system, it was applied to the optimization of the red fluorescent protein.

It was previously shown that somatic hypermutation at the *IgL* locus is dependent on AID and requires transcription, but it remains unclear why this diversification process is targeted only to the immunoglobulin (*Ig*) genes, as other transcribed genes of B-cells do not undergo mutations at such a high rate. The final objective of the study was to find and characterize the *cis*-DNA element responsible for activation and regulation of the somatic hypermutation within the *Ig* locus of the DT40 cell line.

MATERIALS AND METHODS

I. Materials

I.1. Equipment

- Automatic Micropipettes [Eppendorf GmbH, Germany]
- Laminar Flow: HERA safe [Kendro lab. Products, Germany]
- Nitrogen tank: LS6000 [Taylor-Wharton Laboratory Systems, US]
- PCR machines: GeneAmp PCR System 9700 [Applied Biosystems, USA]
- Centrifuges: Heraeus [Kendro Lab. Products, Germany]
- Electrophoresis chambers: Horizontal [Bio-Rad Lab., USA]
- Gel Visualization: Gel Doc 2000™ [Bio-Rad Lab., USA]
- Spectrophotometer: BioPhotometer [Eppendorf GmbH, Germany]
- Incubators: Heraeus [Kendro Lab. Products, Germany]
- Culture Shaker: Innova 4430 [New Brunswick Scientific, Germany]
- Electronic balance [KERN, Germany]
- Electroporator: Gene Pulse Xcell™ [Bio-Rad Lab., USA]
- Vacuum Pump [Vacuubrand GmbH, Germany]
- Vacuum Manifold [Millipore GmbH, Germany]
- Analytical FACS: BD™ LSRII Flow Cytometer [Becton Dickinson, USA]
- Quantitative FACS: MoFlo™ Cell Sorter [Dako Colorado Inc., USA]
- Quantitative FACS: BD FACSAria Cell Sorter [Becton Dickinson, USA]
- Light Microscope: Axiovert 25 [Zeiss, Germany]
- Cell Viability Analyzer: Vi-Cell™ [Beckman Coulter GmbH, Germany]
- Luminescence Spectrometer: LS50B [Perkin Elmer, USA]
- DNA Sequencer: ABI 3730 DNA Analyzer [Applied Biosystems & Hitachi; Hitachi High Tech. Corp., Japan].

I.2. Experimental kits

- PCR Purification: Kit [Qiagen GmbH, Germany]
- Gel Extraction: Kit [Qiagen GmbH, Germany]
- DNA Ligation: Kit Version 2.1 [Takara Bio Inc., Japan]
- Plasmid Isolation (Mini): [Qiagen GmbH, Germany]
- Plasmid Isolation (Maxi): [Qiagen GmbH, Germany]
- First strand cDNA Synthesis: Super Script III™ [Invitrogen GmbH, Germany]

I.3. Enzymes

- DNA Polymerases:
  Pfu Ultra Hotstart [Stratagene, USA]
  Expand Long System [Roche Diagnostics GmbH, Germany]
  GC-rich PCR System [Roche Applied Science, USA]
- Restriction Enzymes [New England Biolabs GmbH, Germany]
- Calf Intestinal Phosphatase [New England Biolabs GmbH, Germany]
- Proteinase K [Qiagen, Germany]
- RNaseA [Qiagen, Germany]

I.4. DNA size marker

A DNA marker which was prepared from phage φX174 DNA (*Hae*III digest) and phage λ DNA (*Hin*dIII digest) was used in the present study [New England Biolabs GmbH, Germany].

I.5. Plasmids

As a backbone for the vectors, prepared for the study, *pBluescript II KS (+) (pKS)* vector [Stratagene, USA] was used. It contains *AmpR* gene for selection of transformed bacteria and *lacZα* gene for blue/white selection of successful ligations.

I.6. Bacterial strain

A DH5α strain of *E. coli* was used as a source of competent cells for transformation.

I.7. Mammalian cell line

The chicken B-cell line DT40 was used as a source of mammalian cells for transfections.

I.8. Media

Molecular Biology:

- **2YT Broth:**

Mix: Bacto tryptone 16 g, Yeast extract 10 g, NaCl 5 g, 10N NaOH 250 μl, distilled water 1000 ml. The mixture was autoclaved and if needed, ampicillin was added (to final concentration 50-100 mg/ml).

- **Agar Luria Broth (LB) Media for agar plates:**

Mix: LB Broth Base 20 g, Bacto^{TM}Agar 15 g, distilled water 1000 ml.

The mixture was autoclaved. Before pouring onto Petri plates, 1 ml of ampicillin (to final concentration 50-100 mg/ml) and 1 ml 4% X-gal was added to the mixture.

- **SOB Broth:**

Mix: Bacto tryptone 16 g, Yeast extract 10 g, NaCl 5 g, KCl 0.l86 g, 10N NaOH 250 μl, distilled water 1000 ml, $MgCl_2$ to the final concentration 10 mM, $MgSO_4$ to the final concentration 10 mM ($MgCl_2$ and $MgSO_4$ were added after autoclave of mixture).

- **FTB**:

Mix: 0,5 M PIPES 20 ml, $CaCl_2 \cdot 2H_2O$ 2.2 g, distilled water 1000 ml, KCl 18.64 g, $MnCl_2 \cdot 4H_2O$ 10,88 g. The pH was adjusted to 6.7 after KCl and $MnCl_2 \cdot 4H_2O$ treatments, respectively.

Cell culture:

- **Mixes** for cell culture media preparation:

RPMI [Invitrogen, USA]; DMEM [Invitrogen, USA]; FBS, Fetum Bovine Serum [Biochrom AG, Germany]

- **Chicken Medium:**

RPMI 500 ml, FBS 50 ml, penicillin / streptomycin (10.000 units of penicillin G sodium and 10.000 μg/ml of streptomycin sulfate) 10ml, 200mM L-glutamine 5ml, chicken serum 5 ml, 1 M β-mercaptoethanol 50 μl (RPMI could be also substituted by DMEM medium).

- **Freezing Medium:** RPMI 70 ml, FBS 20 ml, DMSO 10 ml.

I.9. Oligonucleotides

The oligonucleotides (5' to 3') [Invitrogene GmbH, Germany] are enumerated according to the genes, fragments and plasmids to which they were applied.

I.9.a. <u>Primers for Section I of the "Results":</u>

- **Plasmid *pHypermut2***

Outside primer for the targeting screening
P1: GGGACTAGTAAAATGATGCATAACCTTTTGCACA
Inside primer for the targeting screening
P2: CCCACCGACTCTAGAGGATCATAATCAGCC

- *eGFP* and *GFP* variants amplification for cloning into the *pHypermut2*

P3: GAACCTAGGGCCACCATGGTGAGCAAGGGCGAGGA
P4: GAACCTAGGACTTGTACAGCTCGTCCATGCCG

- Checking of the orientation and sequencing of the *GFP* variants within *pHypermut2*

P4: CCTAGCTCGATACAATAAACGCCATTTGAC
P5: TGGCTTCGGTCGGAGCCATGGAGATC

- Site-directed mutagenesis for development of the *GFP* chimeras:

P6: AACGGCATCAAGGcGAACTTCAAGATC
P7: GATCTTGAAGTTCgCCTTATGCCGTT
P8: CCCGACCACATGAAGgAGCACGACTTCTTC
P9: GAAGAAGTCGTGCTcCTTCATGTGGTCGGG
P10: GATCACATGGTCCTGgTGGAGTTCGTGACC
P11: GGTCACGAACTCCAcCAGGACCATGTGATC
P12: GCCGACCACTACCAGgAGAACACCCCCATC
P13: GATGGGGGTGTTCTcCTGGTAGTGGTCGGC
P14: CTGAgCACCCAGTCCaCCCTGAgCAAAGAC
P15: GTCTTTGcTCAGGGtGGACTGGGTGcTCAG
P16: ATCCTGGGGCACAAGgTGGAGTACAACT
P17: AGTTGTACTCCAcCTTGTGCCCCAGGAT

I.9.b. <u>Primers for Section II of the "Results":</u>

- **Plasmid *pIgL*^{GFP2}**

5'-arm forward: GGGGTCGACATATGATACACAGACCTGACATCTC
5'-arm reverse: GGGGGATCCACTAGTATCACATAATCACCAAGGTTGGAAA
3'-arm forward: GGGGGATCCTTCCGCCATGGCCTGGGCTCCTCTC

3’-arm reverse: GGGGCTAGCCCTCTCAGCTTTTTCAGCAGAATAA
Outside primer for the targeting screening: **P1** (Section I.9.a)
Inside primer for the targeting screening: **P2** (Section I.9.a)

- **Plasmids *pIgL$^{-,GFP2}$*, *pIgL^{W,GFP2}***

5’-arm forward: GGGCTCGAGGGTACTGCGTTTTCCACAAAATTCTCACAG
5’-arm reverse: GGGAGATCTCTGCACTCTGGCACCGTTAAGCACCATCAC
3’-arm forward: GGGTGATCAAGATCTGCTAGCACTAGTGGATCCGTCGA
3’-arm reverse: GGGGAAAAGCGGCCGCCACTGGAAGGAGCTGAAGGCCAC
Outside primer for the targeting screening: AGCTTGGAATTTAACCTCTCCTGTAAA
Inside primer for the targeting screening: **P2** (Section I.9.a)

- **Plasmid *p+26IgL^{GFP2}***

5’-arm forward: GGGATCGATTTCCCTGGTGTGGGTTTTTTTGGGT
5’-arm reverse: GGGATCGATTTGAGAAAGCTCACGCTCCTTCCAA
3’-arm forward: GGGACTAGTCATCTCAGCGGTGCTTATGAATGAC
3’-arm reverse: GGGACTAGTACCCCAAAAAGCAGCCGAGCATTTC
Outside primer for the targeting screening: GCTGCTCACCTTCCTTACCCTGCTGCTCCT
Inside primer for the targeting screening: **P2** (Section I.9.a)

- **Plasmid *p-15IgL^{GFP2}***

5’-arm forward: TTTATCGATGGAGAAGTGAGCGGCAGAGGGAAAT
5’-arm reverse: TTTATCGATTCAGCAGGGCAATGGGCACACACTG
3’-arm forward: TTTACTAGTGCGCAGCAGAGCGCACCAACCACAG
3’-arm reverse: GGGACTAGTTCGACAGCGAGTGCAAAATCATCTT
Outside primer for the targeting screening: GGACCGGGGGTGCTCACAGCACGGCTTT
Inside primer for the targeting screening: **P2** (Section I.9.a)

- **Plasmid *p+52IgL^{GFP2}***

Arms forward: GGGACTAGT TGCCCTTTTGCTTGCAGCCAGCCT
Arms reverse: GGGCTCGAGAATCTCAACAGCTGTGAAGTTTCGA
Outside primer for the targeting screening: GGGGAAACAGTGAGCATGGGGATTCCCT
Inside primer for the targeting screening: **P2** (Section I.9.a)

- **Plasmid *p-135IgL^{GFP2}***

Arms forward: GGGTCTAGAAGTAGTCCAACCAACCTATGCAGT
Arms reverse: GGGCTCGAGTCTGAAGCCTGAAATCACACAGCA
Outside primer for the targeting screening: CTTTCTATCCGTGCTTAGTCTGGTT
Inside primer for the targeting screening: **P2** (Section I.9.a)

- ***IRES*-*bsr*-cassette:**

Forward: AAATGATCACCCCTCTCCCTCCCCCCCCCCTAACGTTACT
Reverse: GGGTGATCAGGATCCGATCCAGACATGATAAGATACATTG

- ***VJ* interveining sequence of unrearranged *IgL* locus:**

Forward (VJi1): GGGGGATCCAGATCTGTGACCGGTGCAAGTGATAGAAAACT
Reverse(VJi2):TACAAAAACCTCCTGCCACTGCAAGGAGCGAGCTGATGGTTTTTAC
TGTCT

- ***GFP* RT-PCR:**

Forward: GGGTCTAGAGCCATCATGGTGAGCAAGGGCGAGGAGCTGT
Reverse: TGCGGTTCACCAGGGTGTCGCCCTCGAACT

- ***Ef1α* RT-PCR:**

Forward: GGGAAGCTTCGGAAGAAAGAAGCTAAAGACCATC
Reverse: GGGACTAGTAGAAGAGCGTGCTCACGGGTCTGCC

II. Methods

II.1. Polymerase chain reaction (PCR)

For the amplification of DNA different pairs of primers were used; their nucleotide sequences are enumerated in "Materials", I.9. For the amplification of genomic DNA with the Expand Long System, a hot start was preferred in order to prevent unspecific bands. For this reason, upper and lower mixes were prepared separately and upper mix was added onto lower mix at 80^{o}C after pre-incubation on the machine. In case of high fidelity polymerases, one common mix was prepared.

Lower Mix:	Upper Mix:
DNA 1 – 100 ng	Expand System 0.5 U
Primer forward 5 pmol	10x Expand buffer
Primer reverse 5 pmol	10xCrezol Red 1 µl
dNTP mix 0.2 mM	MiliQ water rest
10x Expand buffer	Total 5 µl
MiliQ water rest	
Total 5 µl	

Amplifications were done by using Long-range PCR protocol as following:

1 cycle:	93^{o}C, 2 min (pre-denaturation)
35 cycles:	93^{o}C, 10 sec (denaturation)
	65^{o}C, 30 sec (annealing)
	68^{o}C, 5 min (20 sec. increase after each cycle) (extension)
1 cycle:	68^{o}C, 7 min (final extension)

II.2. Analysis of DNA by electrophoresis

0.8% to 2% agarose gel (for long and short DNA fragments, respectively) which contains 0.1 µg/ml EtBr was used to visualize DNA by Gel Doc 2000^{TM} [Bio-Rad Lab., USA]. DNA samples were run at 120 V.

II.3. Restriction enzyme digestion

In general 1-5 U of enzyme was enough to digest 1µg of DNA in 1 h.

For *analytical restriction* 0.5 µg of DNA was mixed with Enzyme, 10x Buffer, 100x BSA and water up to the total volume10-20 µl was added.

For *preparative restriction* 3-5 µg of DNA was mixed with the same components of analytical restriction mix; total volume of reaction was 30-40 µl. Samples were incubated with enzyme at appropriate temperature for at least 3 h.

II.4. Purification and gel purification of DNA

After PCR or restriction enzyme digestion, DNA was purified by Qiagen PCR Purification Kit (see "Methods, I.1) according to the manufacturer's instructions.

II.5. DNA ligation

Ligation was done by using a DNA Ligation Kit (see "Methods, I.1) according to manufacturer's instructions. In principle, 1 volume of DNA (ratio of vector to insert was approximately 1:9) and 1 volume of Ligation Solution were used.

II.6. Culture of *E.coli*

For culture of *E.coli* LB agar plates and 2YT Broth medium were used. The plates with *E.coli* were stored at 4°C for about 1 month. For longer *E.coli* maintenance storage glycerol stocks were prepared as follows: (2 volumes of cells + 1 volume of 50% glycerol). Stocks were frozen at -80°C freezer.

II.7. *E.coli* DH5α competent cells preparation

1) A streak of bacterial strain DH5α was made on a LB agar plate without antibiotics for single colony isolation. The plate was incubated overnight at 37^{o}C. 2) A single colony was picked and was cultured in 5 ml of L Broth or SOB broth medium at 37^{o}C over night. 3) 2.5 ml of the overnight culture was transferred into 500 ml of SOB Broth which had been kept at 25^{o}C, and bacteria were cultured at 25^{o}C. 4) OD600 was measured every 30 min or every 1 h (background of SOB Broth was measured in advance). 5) As soon as the OD600 reached 0.4, the bacterial culture was cooled down immediately on ice and then was kept on ice for 10 min. 6) The culture was transferred into the large centrifuge tubes and was centrifuged at 3000 rpm for 10 min at 4^{o}C. 7) Supernatant was discarded and the pellet was resuspended in 330 ml of ice-cold FTB. (Vortex should not be used during this step). 8) The culture was kept on ice for 10 min, and was centrifuged at 3000 rpm at 4^{o}C for 10 min. 9) Supernatant was discarded and the pellet was resuspended in 50 ml of ice-cold FTB. (Vortex should not be used). 3.5 ml of DMSO was added, mixed gently. 10) 400 µl of aliquots was dispensed into 1.5 ml tubes. Tubes were frozen immediately by liquid nitrogen and the competent cells were kept at -80^{o}C. 11) The efficiency of competent cells was tested by using 1 ng of *pKS* plasmid for transformation to one competent cell tube (400 µl). After heat shock, 600 ml of L Broth was added to the tube. Before spreading, 10 µl (1/100) and 100 µl (1/10) of bacterial liquid was taken onto agar plates. The left (89/100) was centrifuged for 1 min at 13000 rpm. Then, the bacteria were spread by a loop. 13) The number of colonies was counted, and the titer of competent cells was calculated.

II.8. Transformation

A heat shock protocol was performed during transformation of plasmids into bacterial cells:

1) The plasmid (1-5ng) was added into 50-400 µl of thawed competent cells (the quantity of cells depended on their efficiency titer).

2) The tube was incubated on ice for 20 min and then heat shocked at 42^{o}C for 40 sec on a heat block and put on ice for 2 min.

3) 2YT Broth was added into tube until the mixture reached 1 ml and the tube was incubated at 37^{o}C for at least 10 min.

4) After mixing, 100 µl (1/10) was taken from the bacterial liquid and was put onto half of LB agar plate. The rest (9 /10) was centrifuged at 8000 rpm for 30 sec, the supernatant was discarded and the pellet (~50 µl) was put onto another half of the plate.

7) The plates were incubated overnight at 37^{o}C.

II.9. Colony PCR

At first the successful ligations of DNA were checked by colony PCR. Single bacterial colonies were resuspended in 20 µl of 2YT Broth into U-Bottom 96 well plates. 1µl of suspension was used as a DNA template for PCR.

PCR Mix:	PCR Programme:	
Bacteria suspension 1 µl	1 cycle:	94^{o}C, 1 min
Primer forward 5 pmol	30 cycles:	94^{o}C, 20 sec
Primer reverse 5 pmol		55^{o}C, 1 min
10x Expand buffer 1 µl		72^{o}C, 2 min
dNTP mix 0.2 mM	1 cycle:	72^{o}C, 6 min
Expand Long System 0.5 U		
10x Crezol red 1 µl		
MiliQ water rest		
Total 10 µl		

II.10. Plasmid preparation

Plasmid extraction from the *E.coli* culture was made using a Plasmid Isolation Kit (Mini) ("Methods, I.1) according to the manufacturer's protocol. After the constructs were checked by enzyme digest, a maxi-prep was made.

II.11. Determination of DNA and RNA concentration

The purity and the concentration of the DNA were checked by a spectrophotometer (see "Methods, I.1). Generally, the intensity of absorbance at the wavelength 260 nm was used for calculation of concentration and the ratio of 260/280 nm was used to estimate the purity of DNA. For pure DNA samples this value should be between 1.8 and 2.0.

II.12. Basic cell culture techniques

The culture conditions for DT40 cells were 41°C with 5% CO_2 according to the ATCC (American Type Culture Collection) standards. Chicken Medium ("Materials", I.8) was used for culture of DT40 cells and Freezing Medium ("Materials", I.8) was used for freezing down the cell.

II.13. Thawing of DT40 cells

1) The tube with the cells was transferred from a liquid nitrogen storage tank to 41°C and, after the cell suspension melted, the tube was centrifuged at 1.500 rpm for 5 min.

2) The supernatant was discarded; the pellet was resuspended in the Chicken Medium and transferred to a flask or plate.

II.14. Freezing down of DT40 cells

The cells were centrifuged at 1.500 rpm for 5 min. The supernatant was discarded, and the cells were resuspended in Freezing Medium ("Methods", I.8); the suspension was transferred to the cryotubes. At first the tubes were kept at - 80°C overnight and then transferred to the nitrogen tank.

II.15. Transfection

Plasmid Preparation:

1) The plasmid DNA was linearized outside of the genes of interest by an appropriate restriction enzyme. Overnight digestion was preferred. The quality of DNA and its digestion was checked by electrophoresis.

2) The DNA was prepared by phenol/chloroform purification and following isopropanol precipitation.

3) The pellet was dried up sterile inside the laminar flow and resuspended in distilled water for final concentration 1 μg/ml.

Electroporation:

1) The concentration of the cells was determined (10 million cells were used per electroporation). Calculated amount was transferred into a 50 ml tube and centrifuged for 5 min at 1500 rpm, 4^oC.

2) The supernatant was removed; the pellet was resuspended in 800 μl of Chicken Medium and transferred into the electroporation cuvette, where 40 μl of linearized DNA had been transferred in advance.

3) Electroporation was done using 25 μF and 700 V.

4) The mixture was put into the tube containing 9.5 ml of Chicken Medium and the solution was distributed on a flat-bottom microtiter plates (100μl each well).

5) The following day (12-24 h after electroporation), 100 µl of selective medium (containing twice the final concentration of the drug) was added to each well.

6) The plates were left for about seven to ten days in the incubator without changing the medium. Drug resistant colonies were identified at this stage.

II.16. Identifying targeted events by PCR

7-10 days after of electroporation, the visible colonies were picked up into 300 µl of Chicken Medium in flat-bottom 96-well plates and incubated for 3 days.

1) *Crude extract preparation:*

The cells were transferred to 96 well PCR plate, washed with PBS and centrifuged for 5 min at 1500 rpm. The supernatant was discarded; the pellet was resuspended in 10 µl of K buffer [1 x PCR buffer, 0.1 mg/ml proteinase K and 0.5% Tween 20] for proteolysis. The cells were incubated for 45 min at 56°C and then for 10 min at 95°C for inactivation of proteinase K.

2) 1 µl of the crude extract was used for PCR analysis.

II.17. Subcloning of DT40 cells

1) Viability and concentration of the cells were counted using Cell Viability Analyzer ("Methods", I.1).

2) Four wells of a six well plate were prepared to contain 300, 100 , 30 and 10 viable cells/ml (in 5 ml of chicken medium in each well).

3) The cell suspension in each well was mixed and distributed on the 96 well flat bottom microtiter plate (100 µl into each well) for final concentration 30, 10, 3 and 1 cells / well.

4) After incubation for 7-8 days (without changing the medium) subclones became visible as defined round colonies.

5) In general 24 colonies from the lowest dilutions were picked up into 1 ml of chicken medium in 24-well flat-bottom plates.

II.18. Drug resistance marker recycling

1) Around 10^5 cells were cultured with fresh chicken medium containing 0.01 mM 4-hydroxi- tamoxifen (1 day for partial and 2 days for complete excision).

2) The cells were subcloned by limiting dilution for final concentration of 0.3, 1, 3 and 10 cells / well in 96-well flat-bottom plates.

3) 7 – 8 days after subcloning, 10 µl of the visible subclones were transferred into 1 ml of chicken medium.

4) In order to test the excision of the drug-resistance genes, the aliquots of cells were incubated with drug-containing mediums. Retained samples of cells deficient for markers were selected for further studies.

II.19. Flow cytometry

In order to quantify the intensity of green (or red) fluorescence or percentage of cells expressing proteins with decreased fluorescence intensity, FACS analysis was done. 200 µl of cell culture was transferred into round-bottom 96-well plates, washed 2 times with PBS and analyzed by analytical flow cytometer ("Methods", I.1).

II.20. Fluorescence-Activated Cell Sorting (FACS)

Cells were washed in sterile conditions and collected in 1-2 ml of sterile PBS in concentration of 0.5-1x10^6 cells/ml. 2x$10^7$of the viable cells were used for each sort. This number was a reasonable estimate, as using less cells might exclude rarely occurring mutations and using more cells would lengthen the time of the sort. During every sort (excluding the sorts for the sequencing of the defined populations) approximately 0.2% of the population, i.e. 4x10^3 cells were collected. According to the cell division rate of the DT40 we should have had sufficient amount of cells for the next sort within 6 days of culture of the sorted population. However, in practice about 10-14 days was needed as the procedure of sorting was in fact damaging for cells. After each sort the results have been evaluated by comparison of the re-grown sorted population with the culture of the previous sort by FACS analysis. Sorting was done on Quantitative FACS ("Methods", I.1). Sorted cells were collected into receiver tubes containing 50% chicken medium and 50% FBS.

II.21. Genomic DNA isolation

1) 50 ml of cells (~ 50x10^6 cells) in good condition were centrifuged at 1500 rpm for 5 min. The supernatant was discarded, the pellet was washed with 1-2 ml 1x PBS and again was centrifuged at 1500 rpm for 5 min.

2) The supernatant was discarded, the pellet was resuspended in 500µl proteinase K Buffer (5 M NaCl 2 ml, 1 M Tris-HCl (pH 8.0), 1 ml 0.5 M EDTA 5 ml, MiliQ water 92 ml) containing 0.1 mg/ml of proteinase K. The mixture was transferred into a 2 ml tube and 12.5 µl of SDS (20%) was added, mixed by inverting and spinned down shortly. Protein degradation was carried out overnight at 56^{o}C.

3) The next day, 1 volume of phenol was added to the DNA extract and mixed carefully. After this the tube was centrifuged at 13000 rpm for 5 min.

4) The upper phase was transferred into a new tube and 1 volume of phenol/ chloroform was added. After mixing the tube was centrifuged at 13000 rpm for 5 min.

5) The upper phase was transferred to a new tube and 1 volume of chloroform was added. After mixing the tube was centrifuged again at 13.000 rpm for 5 min.

6) The upper phase was transferred to a new tube and 2 µl of RNAseA (100mg/ml) was added for digesting of RNA. After this tube was it was incubated for 2 h at 37^{o}C.

7) DNA was transferred into dialysis membrane and the ends were closed with clamps. The membrane was put into a glass of cold 1x TE and kept at 4^{o}C for 2 h. (Alternatively, the reaction can be stopped by adding 50µl of 0,5M EDTA pH 8.0). TE was changed at least three times with 2-4 h intervals.

8) DNA was transferred to a new tube and the concentration was measured.

II.22. Total RNA isolation

1) 20 ml cells (~ 20x10^{6} cells) were centrifuged at 1500 rpm for 5 min.

2) The supernatant was discarded and the pellet was resuspended in 1.5 ml of TRIzol reagent. After that it was transferred into a 2 ml Eppendorf tube and was incubated for 5 min at room temperature to permit the complete dissociation of nucleoprotein complexes.

3) 0.3 ml of chloroform was added into the tube. The tube was mixed for 15 sec and incubated for 3 min at room temperature, then centrifuged at 13000 rpm, 4^{o}C for 15 min.

5) The upper phase was transferred into a new 2 ml Eppendorf tube; 750 µl of propanol was added and centrifuged at 13000 rpm, 4^{o}C for 10 min.

6) RNA pellet was washed with 1 ml of 75% ethanol, and centrifuged at 13000 rpm for 5 min. The supernatant was discarded, the sample was air dried for ~10 min and dissolved in 100 µl of DEPC water. The quality was checked using 1% agarose gel after 50 min run.

II.23. First strand cDNA synthesis

Super Script III (Invitrogen, USA) was used to synthesize first strand cDNA according to the manufacturer's instructions.

II.24. Fluorescent spectra analysis

1 ml of cell suspension was used for analysis of excitation and emission spectra of the fluorescent proteins on Luminescence Spectrometer ("Methods, I.1) according to the manufacturer's instructions.

RESULTS

I. Application of somatic hypermutation for artificial protein evolution

The present study describes the development of a new vector, *pHypermut2*, which allowed diversification of a transgene specifically and efficiently when it is placed into the *IgL* locus of the DT40 cell line. *PHypermut2* proved to be a convenient tool for the efficient artificial evolution of proteins and was applied for the optimization of the fluorescent proteins. *PHypermut2* formed the basis of a research project studying the activation and regulation of the somatic hypermutation process.

I.1. Improvement of the artificial evolution system and application for optimization of the GFP proteins

I.1.a. Analysis of the mutations responsible for the increase of the GFP brightness

Although previously the *pHypermut1* vector allowed the developing of brighter variants of eGFP ("Introduction", VII.2), the system had a disadvantage: not only the *GFP* coding sequence but also its downstream sequences, including splice donor, could potentially undergo mutation. In order to analyze the mutations responsible for the increase of the GFP brightness, the coding sequence of the *eGFP* gene was PCR-amplified from the cells after the first and the third sorts, cloned into a plasmid and sequenced. Surprisingly, only a few mutations were found in the *eGFP* coding sequence of the cells after the first sort (Table 2). Extension of the sequence analysis to the region downstream of the *eGFP* coding sequence by primer walking revealed that most of mutations were concentrated at the splice donor site of the *Ig* light chain leader intron (*polyA-L* in the Table 2). Apparently inhibition of splicing increased the mRNA stability which leads to a brighter GFP phenotype.

In contrast, most of the sequences after the third sort revealed mutations in the *eGFP* coding sequence (221 mutations/85 seq) (Table 2). Many of the observed amino acid changes were not shared among independent sorts, and their functional significance remained uncertain. However, a number of codon changes occurred independently in different subclones suggesting that they were related to the increased fluorescence of the expressed proteins. The *GFP* variants, whose altered sequences were found more than once, were selected and named as *GFPv 1 – 9*.

Cell source		Gene	Mutations	Number of sequences	Mutations/ sequence	Mutations at			
						C	G	A	T
$AID^{-/-}IgLe^{GFP1}$	6-week culture	eGFP (723 bp)	1	26	0.04	0	0	1	0
$AID^{R1}IgL^{eGFP1}$	6-week culture	eGFP (723 bp)	13	39	0.33	5	8	0	0
$AID^{R1}IgL^{eGFP1}$	Sort I	eGFP (723 bp)[a]	15	95	0.16	8	6	1	0
$AID^{R1}IgL^{eGFP1}$	Sort I	polyA-L (300 bp)[a]	88	95	0.93	1	87	0	0
$AID^{R1}IgL^{eGFP1}$	Sort III	eGFP (723 bp)	221	85	2.60	130	93	6	4

Table 2. Analysis of the mutation profile of the *eGFP* and its splice donor (*polyA-L*) after three rounds of the sorts for increased intensity of the green fluorescence.

As our main interest was to improve GFP by mutations in its coding sequence rather than mutations in the splicing signal, which could interfere with the amount of transcripts, it was decided to design a new vector *pHypermut2* for improvement of the artificial evolution system.

I.1.b. Construction of a vector *pHypermut2* for improvement of the artificial evolution system

PHypermut2 was generated by five cloning steps using three plasmids, developed earlier in our laboratory: *pIgPromKoArms*, *pRSVExpress* and *pLoxPuro*. *pIgPromKoArms* was based on the *pKS* plasmid and contained target arms for homologous recombination with the *IgL* locus. For the 3' target arm the *LVJ* fragment of the *IgL* locus was used, and for the 5' arm a 2.5 kb fragment downstream of the *ψV* – gene 2. Targeted integration of the vector would result in the replacement of the *IgL* promoter with sequences contained between the target arms (Figure 12). A cassette for the cloning of the target gene for artificial evolution was amplified and inserted into the *pIgPromKoArms* from the *pRSVExpress*. The coding sequence of the target gene can be cloned into the multiple cloning sites of *pRSVExpress* (*Nhe*I, *Eco*RV and *Bgl*II sites) allowing transcription to be driven by the strong *RSV* (Rous sarcoma virus) promoter. The coding sequence is followed by the *SV40* polyadenylation signal (*SV40 polyA*). For selection of stable transfectants of *pHypermut2* a puromycin resistance (*puroR*) gene driven by the *β–actin* promoter was amplified from the *pLoxPuro* vector and inserted into *pHypermut2* downstream of the cassette for the cloning of the reporter gene coding sequence. The *puroR*–cassette from *pLoxPuro* is flanked by *loxP* sites which allowed excision by *Cre* recombinase following stable integration of the construct. As this cassette was located downstream of the reporter gene, it was unlikely that it would interfere with the transcription or mutagenesis of the reporter gene. For this reason the possibility of excising the drug-resistance cassette was retained in *pHypermut2* but was not used in the following experiments.

It is known that rearranged Ig light chain locus of the DT40 cell line is constitutively diversified by gene conversion [122]. Hence the artificial evolution of the transgene knocked into the *IgL* locus by hypermutation could be combined with gene conversion remodeling if sequences homologous to the transgene would be used as donor pseudo-genes [292]. For this purpose a *Spe*I site was inserted upstream of the *RSV* promoter of the *pHypermut2* for the cloning of donor sequences if gene conversion diversification of the transgene would be desirable (Figure 12).

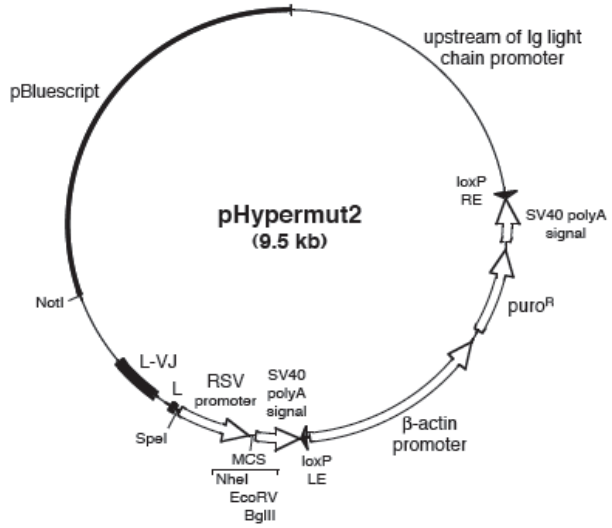

Figure 12. A map of the *pHypermut2*. Target genes for artificial evolution can be cloned into *Nhe*I, *Eco*RV or *Bgl*II sites.

The main advantage of the *pHypermut2* was that the direction of the transgene transcription was the opposite to that of the *IgL* locus after the targeted integration (Figure 13). This prevented the undesirable side-effect of the previous system caused by mutations of the splice signal sites.

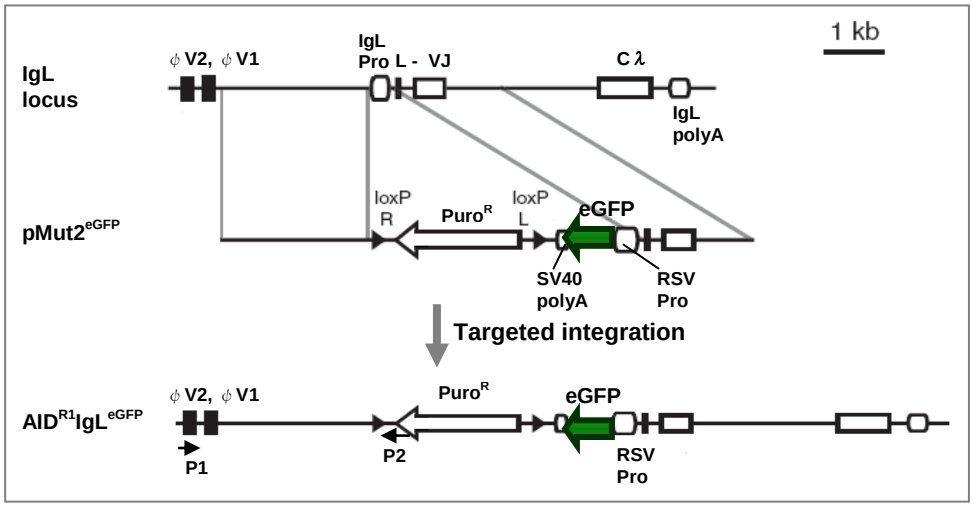

Figure 13. A scheme of the rearranged *IgL* locus, targeting construct *pMut2*^{eGFP} carrying the *GFP2* reporter and targeting arms for replacement of the *IgL* promoter after targeted integration of the *pMut2*^{eGFP}. Transcriptional orientation of the reporter cassette is opposite to that one of the *IgL* locus (the primers for the targeting screening are indicated as P1 and P2).

In order to test the suitability of *pHypermut2* for the artificial evolution system, the *eGFP* gene was cloned into the multiple cloning site of this vector. For this *Avr*II sites were added to the cDNA of the gene by amplification with Pfu Ultra Hotstart polymerase ("Materials", I.3, "Enzymes") using primers P3 and P4 (" Materials " I.9, " Oligonucleotides ") and the resulted amplicon was cloned into the *Nhe*I site of the *pHypermut2*. (Primer pair P3/P4 was used further for the amplification of all the *GFP* variants in order to clone them into this vector). *PHypermut2,* carrying the *eGFP* reporter gene, was named *pMut2*^{eGFP}. Following transfection of this vector into the *ψV*-knockout AID^{R1} cell line, puromycin resistant clones were expanded and targeted integration was checked by PCR screening with Expand Long Template PCR system ("Materials", I.3, "Enzymes") using one primer annealing at the remaining *ψV2*-gene, and another to the *polyA* signal of the *puroR* gene of the *pHypermut2* (primers P1 and P2, respectively; see " Materials ", I.9, " Oligonucleatides " and Figure 13). The frequency of the targeted integrations after transfections of the *pHypermut2* was about 50 - 70% (Figure 14).

After insertion of the reporter into the *IgL* locus, it was important to test whether the vector was correctly integrated into the chromosome carrying the rearranged *IgL* locus. This is essential in order to achieve the high mutation rate desired for the transgene. This could be confirmed by a PCR for checking the presence of the intervening sequence inside of a fragment between *V* and *J* (using primers VJi1 and VJi2 ("Materials", I.9, "Oligonucleotides"), which is normally excised during the process of rearrangement. Since *LVJ* was used as one of the targeting arms, the successful amplification of the described fragment after targeting means, by exclusion, that the construct was inserted into the rearranged allele of the *IgL* locus (Figure 14).

A positive clone, ψV^{-}AID^{R1}IgL^{eGFP}, (indicated in the Figure 13 as AID^{R1}IgL^{eGFP}) was subcloned by limited dilution, and 24 subclones were analyzed by FACS after 14 days of culture. The average percentage of the cells with the decreased fluorescence of GFP (GFP^{low} population) was 10.9%. This result suggested that the *pHypermut2* can be used for efficient diversification of the transgene by the hypermutation for the artificial evolution. In the project for improvement of the GFP protein, *pHypermut2* was used for confirmation of the brighter variants developed earlier using *pHypermut1*. For validation of the suitability of the system *in*

situ, *pHypermut2* was applied to a red fluorescent protein ("Results", I.2).

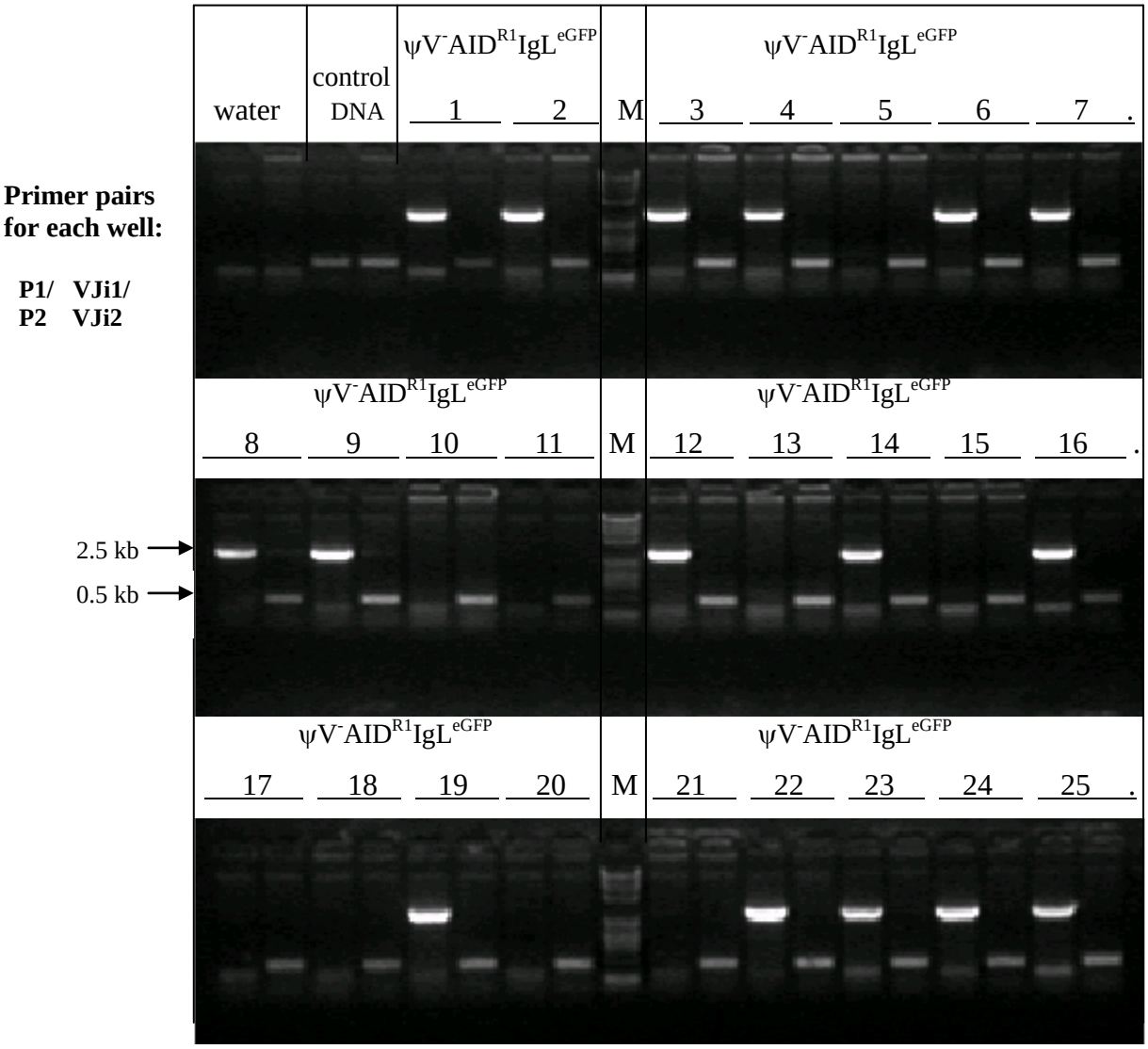

Figure 14. Targeting screening after integration of the *pMut2*^{eGFP} to the ψV^{-}AID^{R1} cell line. Crude extract of the ψV^{-}AID^{R1}IgL^{eGFP} cells was used as a template. Different clones are shown by numbers above lines. DNA size marker is indicated by "M". For each clone two pairs of primers were used: outside and inside targeting primers P1 and P2 allowed a check of the proper integration of the vector (in case of successful targeting the length of the PCR product was ~2.5 kb); a pair of primers VJi1 and VJi2 were used to test whether the integration took place into the rearranged allele of the *IgL* locus (this is indicated by the appearance of the PCR product of length 0.5 kb). Purified genomic DNA of the AID$^{-/-}$ψV$^{r\text{-}E}$ clone of DT40 was used as a positive control for primers VJi1 and VJi2 and PCR mix without template was used as a negative control. 16 correctly targeted clones were identified from 25 screened clones (65%).

I.1.c. Confirmation of the new GFP phenotypes

In order to confirm the phenotypes of the developed GFP variants, their coding sequences were cloned into the *pHypermut2* and transfected to the AID $^{-/-}$ cell line which does not have the hypermutation activity. *EGFP* and *GFP* variant *Emerald* [278] were cloned into *pHypermut2* and transfected into the same cell line as a control for the measurement of the brightness increase. Following transfection into the AID$^{-/-}$ cell line, puromycin resistant clones containing targeted integration of the vectors were identified by PCR screening using primers described in Figure 14. More than 50% of all stable transfectants had integrated the constructs into the rearranged *IgL* locus and these clones were named according to the inserted transgene (AID$^{-/-}$IgL^{eGFP}, AID$^{-/-}$IgL^{Emerald}, AID$^{-/-}$IgL^{GFPv1}, AID$^{-/-}$IgL^{GFPv2} etc.).

Two independent clones from each cell line were analyzed by FACS (Figure 15). The brightness of two clones of the same cell lines showed slight variation (Table 3). This was possibly due to an epigenetic effect as the FACS machine was calibrated every time prior the experiment. The comparison of the transfectants revealed that the fluorescent intensity of the AID$^{-/-}$IgL^{Emerald} clone was 1.2 times higher than of the AID$^{-/-}$IgL^{eGFP} clone. Among nine *GFP* variant knock-in cell lines, four (AID$^{-/-}$IgL^{GFPv2}, AID$^{-/-}$IgL^{GFPv5}, AID$^{-/-}$IgL^{GFPv6} and AID$^{-/-}$IgL^{GFPv8}) were brighter than the control AID$^{-/-}$IgL^{eGFP} clone, and the fluorescent intensity of three clones (AID$^{-/-}$IgL^{GFPv5}, AID$^{-/-}$IgL^{GFPv6} and AID$^{-/-}$IgL^{GFPv8}) even exceeded the intensity of the AID$^{-/-}$IgL^{Emerald}.

Among the analyzed GFP variants, the AID$^{-/-}$IgL^{GFPv6} possessed the highest fluorescent intensity (2.5-fold higher than of AID$^{-/-}$IgL^{eGFP} clone) and the AID$^{-/-}$IgL^{GFPv5} clone was the second brightest (2.0-fold brighter than the AID$^{-/-}$IgL^{eGFP}) (Figure 15, Table 3).

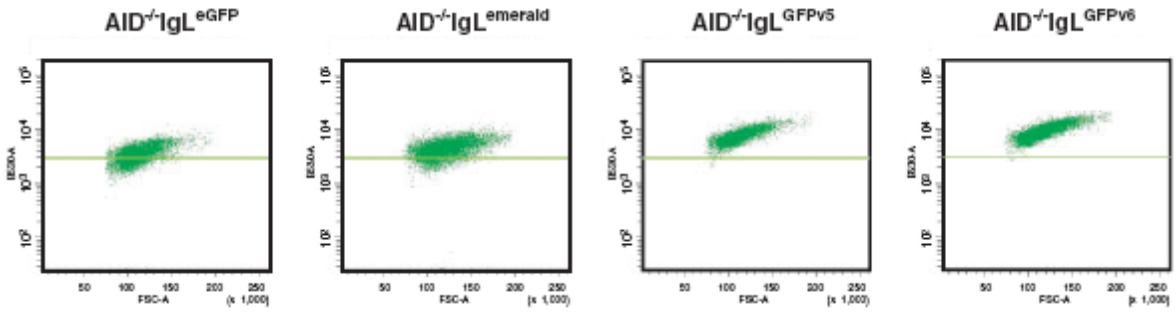

Figure 15. FACS analysis for comparison of the fluorescence intensity among the transfectants containing different *GFP* variants. The brightness of AID$^{-/-}$IgL^{eGFP} is shown at each dot plot by green guideline. Quantitative FACS data is shown in Table 3.

GFP variant	Amino acid changes	Number of sequences	Subclone	Relative brightness[a]
eGFP	Change from wild-type GFP 1aG, F64L, S65T, H231L, 239S Change from eGFP	–	–	1.0±0.1
GFPv1	Q80E	28	1, 2, 3	0.7±0.0
GFPv2	Q80E, Q184E, A206T	19	1	**1.2±0.0**
GFPv3	Q80E, E124D, L141V, Y237stop	11	3	0.3±0.0
GFPv4	Q80E, S202T	4	1, 2	0.9±0.1
GFPv5	Q80E, V163A	4	1	**2.0±0.0**
GFPv6	Q80E, Y145F, S202T	3	2	**2.5±0.0**
GFPv7	Q80E, S208T	2	3	0.7±0.1
GFPv8	Q80E, L221V	2	3	**1.5±0.3**
GFPv9	Q80E, L141V, S202I	5	3	**1.0±0.1**
GFPv10	Q80E, Y145F, V163A, S202T	–	–	**3.0±0.1**
GFPv11 (GFPnovo1)	Y145F, V163A, S202T	–	–	**3.2±0.0**
GFPv12 (GFPnovo2)	Y145F, V163A, S202T, L221V	–	–	**3.3±0.0**
GFPv13	L141V, Y145F, V163A, Q184E, S202T, A206T, L221V	–	–	**2.9±0.1**
Emerald	Change from wild-type GFP S65T, S72A, N149K, M153T, I167T	–	–	1.2

Table 3. Amino acids changes of the GFP variants and their relative to the eGFP brightness. [a]Relative brightness was estimated based on the analysis of the two clones of each transfectant.

I.1.d. Development of chimeric *GFP* variants for an additional increase of brightness

Since not all beneficial nucleotide changes were shared among the *GFP* variants (Table 3), it was decided to combine the obtained mutations by site-directed mutagenesis into a single sequence in order to achieve brighter GFP variants. Nucleotide substitutions corresponding to the amino acid changes of *GFPv6, v5, v8, v2* and *v9* were chosen for this (Table 3 and Figure 16). This also served to validate the observed nucleotide changes indeed influence function.

In order to combine the codon changes found in different *eGFP* variants, primers P6–P17 were designed ("Materials", I.9, "Oligonucleotides") which included the described mutations in the center of the primer sequence for a specific codon change. As a first step, parts of the *eGFP* gene were amplified by PCR using at least one mutation-containing primer. In the second step PCR fragments containing mutations were mixed with other PCR fragments to cover the full *eGFP* coding sequence. This mixture served as a template for chimeric PCR using the primer pair of P3/P4 for cloning the final amplicon into the *Nhe*I site of the *pHypermut2*. The orientation and the sequence of the mutant *eGFPs* within the *pHypermut2* were confirmed by sequencing using primer pair P4/P5.

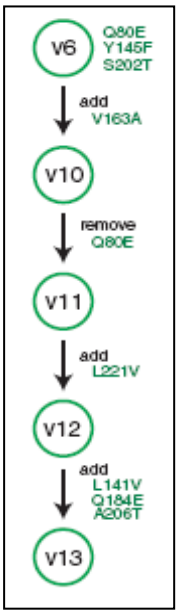

Using the technique of chimeric PCR, at first Y145F and S202T amino acid changes of the GFPv6 were combined with V163A (GFPv5) to generate GFPv10. Because GFPv1 containing Q80E showed less brightness than eGFP, we subtracted Q80E from GFPv10 and generated GFPv11. We also added L221V of GFPv8 to GFPv11, and generated GFPv12. Finally we added Q184E and A206T of GFPv2 and L141V of GFPv9 to produce GFPv13. All the chimeric *GFP* PCR products were cloned into *pHypermut2*, and inserted into the rearranged *IgL* locus of $AID^{-/-}$ cells for confirmation of the new phenotypes.

Figure 16. Subsequent introduction of the amino acids changes during site-directed mutagenesis. Generations of the variants GFPv10-13.

Using FACS two clones of each of the new cell lines were analyzed (Figure 17). All of these new clones showed higher fluorescent intensity than the $AID^{-/-}IgL^{GFPv6}$ clone. The $AID^{-/-}IgL^{GFPv10}$ was 3.0-fold brighter than the $AID^{-/-}IgL^{eGFP}$ clone (Figure 17). The $AID^{-/-}IgL^{GFPv11}$ and the $AID^{-/-}IgL^{GFPv12}$ clones were even brighter, showing 3.2- and 3.3- fold more brightness than the $AID^{-/-}IgL^{eGFP}$, respectively. The $AID^{-/-}IgL^{GFPv13}$ did not show higher brightness than other chimeric GFP-expressing clones (Figure 17). The second brightest GFP chimera, GFPv11 was named as "GFPnovo1" and the brightest one, GFPv12, as "GFPnovo2".

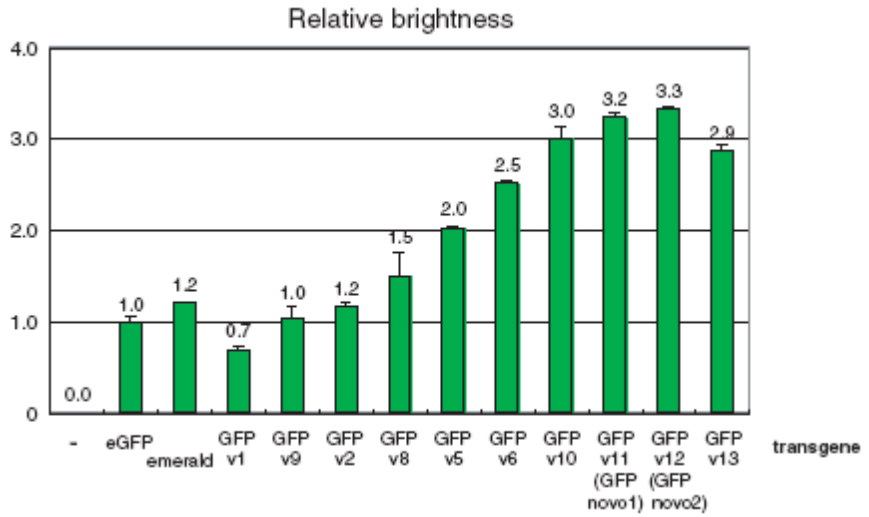

Figure 17. Relative fluorescence of the transfectants normalized to the fluorescence of $AID^{-/-}IgL^{eGFP}$.

I.1.e. Spectral properties of the brightest GFP variants

EGFP has its excitation maximum at 488 nm and emission maximum at 509 nm [277]. In order to characterize the spectral profiles of the new GFP variants, clones AID$^{-/-}$IgL^{Emerald}, the AID$^{-/-}$IgL^{GFPv5}, the AID$^{-/-}$IgL^{GFPv6}, the AID$^{-/-}$IgL^{GFPnovo1} and the AID$^{-/-}$IgL^{GFPnovo2} were analyzed by a luminescence scanning spectrometer (Figure 18A). AID$^{-/-}$IgL^{eEGFP} was used as a control. Excitation spectra were scanned using fixed emission 540nm and emission spectra were measured using excitation at 460nm. This analysis showed that the fluorescent intensity, not the excitation and emission spectra, had been changed in the transfectants expressing variant GFPs. All the analyzed GFP variants possessed almost the same excitation and emission spectrum with the eGFP of the AID$^{-/-}$IgL^{eGFP} clone. The lack of shift of the excitation or emission maxima was most likely due to our selection strategy which only enriched for cells with an increased brightness, not for shifts in spectra.

We also analyzed AID$^{-/-}$IgL^{eGFP}, AID$^{-/-}$IgL^{Emerald}, AID$^{-/-}$IgL^{GFPv5}, AID$^{-/-}$IgL^{GFPv6}, AID$^{-/-}$IgL^{GFPnovo1} and AID$^{-/-}$IgL^{GFPnovo2} by fluorescence microscopy (Figure 18B). Consistent with the FACS and spectral analysis the GFPv5, v6, GFPnovo1 and GFPnovo2 variants showed the same color as eGFP, with increased brightness. Especially the brightness of AID$^{-/-}$IgL^{GFPnovo1} and the AID$^{-/-}$IgL^{GFPnovo2} clones over the AID$^{-/-}$IgL^{eGFP} clone were confirmed by images of the eukaryotic cells (Figure 18B).

A

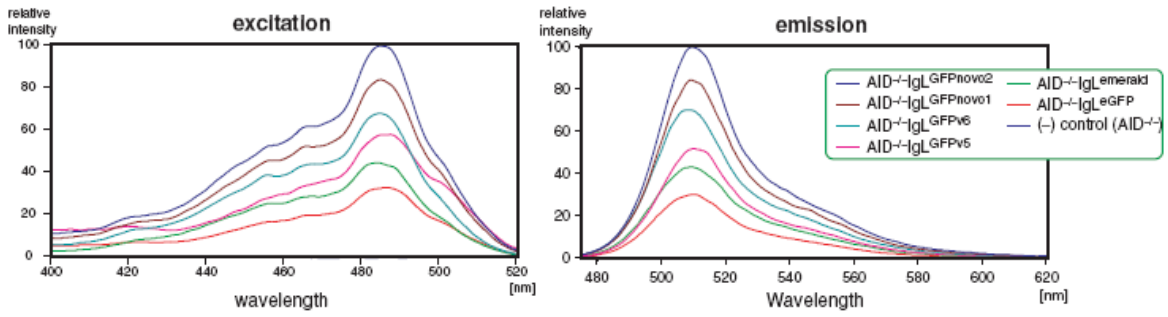

B

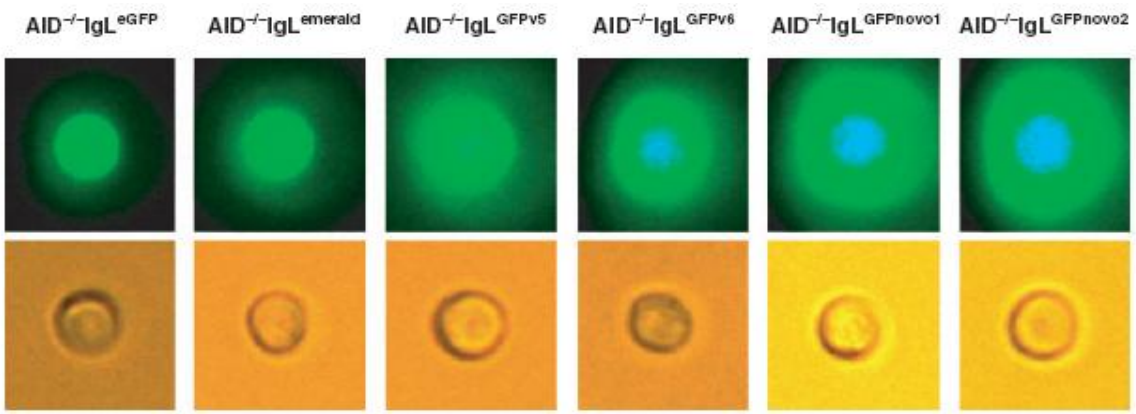

Figure 18. (A) Excitation and emission spectra of the GFP variants. (B) Image of single cells by fluorescence microscopy. The image of the same single cells is shown with fluorescence activation using blue filter with the range of 450-490 nm (upper row) and without fluorescence activation (lower row). No time lack was used between the measurements in order to prevent the photobleaching.

I.2. Application of the advanced artificial evolution system for optimization of the RFP proteins

The described artificial evolution system can theoretically be applied to any gene whose phenotype can be screened in the DT40 cell line. After establishing the method using the GFP protein, we have chosen a red fluorescent protein as the next object for optimization by artificial evolution. We were successful in generating the new variants of this protein with either increased or red shifted emission compared to the starting protein.

I.2.a. EqFP615 and strategy for its improvement by somatic hypermutation

The group of S. Lukyanov provided us with the cDNA of the mutant protein eqFP615, which was one of the intermediates of the eqFP578 *in vitro* mutagenesis, which lead later to the development of the TurboRFP and Katushka ("Introduction, VII.2, Figure 9). The alignment of mentioned proteins together with the eqFP611 revealed that the sequence of the eqFP615 has 8 amino acid changes in comparison with the wild type eqFP578, seven of which share with Katushka and its monomer mKate and 4 – with TurboRFP; the eqFP611 and eqFP615 had 76% identity in amino acid sequence (Figure 19).

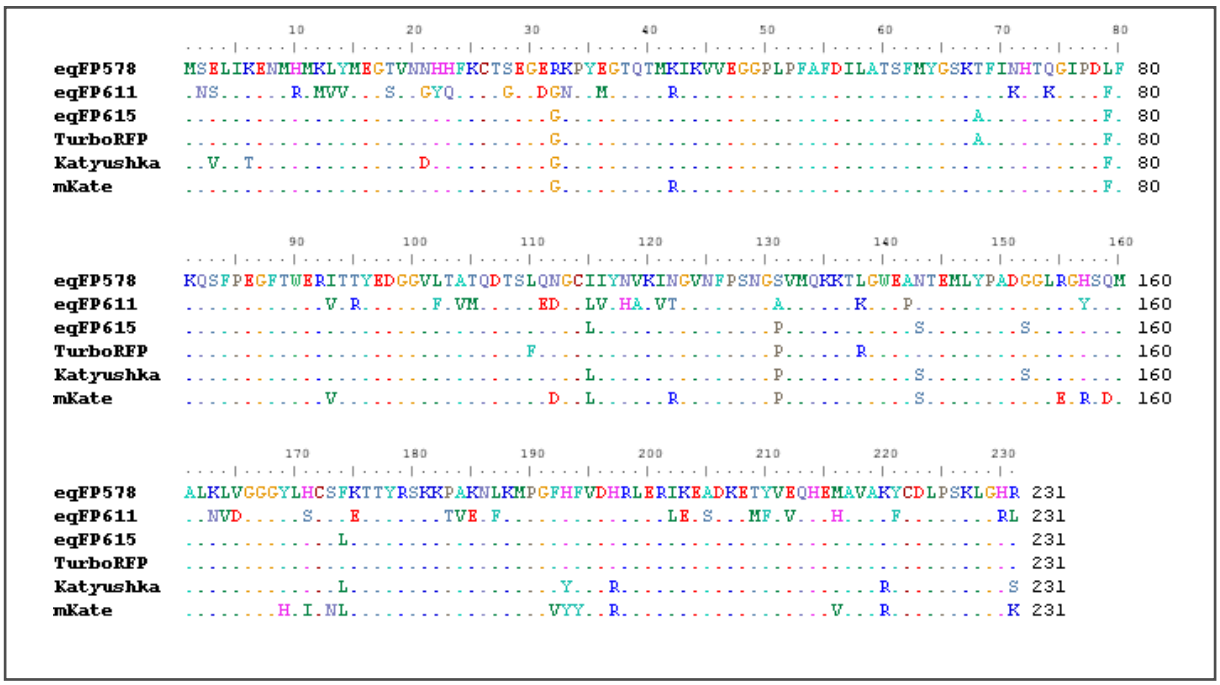

Figure 19. Amino acid sequence alignment of the wild types eqFP578 and eqFP611 and the mutants of the eqFP578: TurboRFP, Katushka and its monomer - mKate.

The eqFP615 protein is less bright than the wild type precursor, but is more red-shifted, with excitation and emission maxima at 559 nm and 615 nm, respectively (unpublished data from the provider). The emission spectrum measurement of the DT40 cells expressing the eqFP615 by the luminescence spectrometer ("Materials and Methods", I.1) confirmed that this protein had a large stock shift and a broad peak of emission (Figure 28 and 29B). Due to these properties of the eqFP615, it was suggested that this protein could be excited by the red laser 633 nm used in the FACS analysis.

We reasoned that two optimizations of this protein, regarding either intensity or spectrum, might be worthwhile.

Optimization strategy A. In order to increase the brightness of the eqFP615 a FACS screening for sorting of mutants with increased fluorescence intensity after excitation by the red laser could be used. Such a protein would be useful in the cell and mouse biology applications because it can be easily visualized.

Optimization strategy B. Development of a variant with an emission maximum shifted, if possible, to the far red spectrum with an emission peak of sufficient intensity at the red laser excitation was of special interest. The fluorescence of such a variant could be easily distinguished from those of other FPs commonly used for FACS because the later have detectable emissions at excitations by lasers of blue or shorter wavelengths. This would allow coexpression and analysis of the new mutant even in the presence of other red fluorescent proteins.

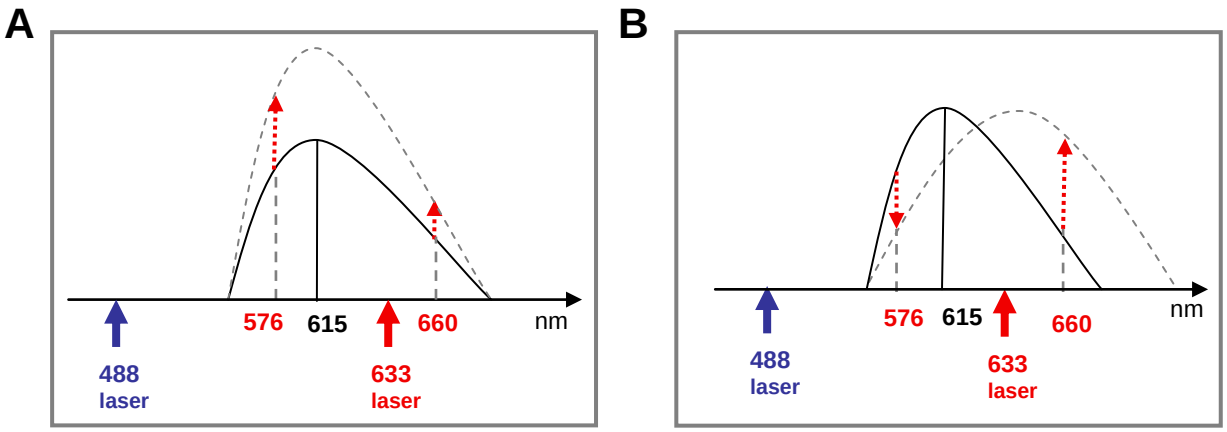

Figure 20. Suggested optimizations for the eqFP615 fluorescent properties. The present spectrum of the eqFP615 protein is indicated by a solid line; the spectrum of the theoretical mutant proteins expected from the defined optimization is drawn by a dashed line. The FACS blue and red lasers excitation wavelengths are indicated by blue and red arrows respectively. Wavelengths corresponding to the FACS red fluorescence detection filters are shown in red. (A) Suggested increase of the excitation/emission intensity. (B) Suggested far- red shift of the spectrum.

I.2.b. Generation of the RFP variants with increased fluorescence and far-red shifted emission spectrum

In order to perform the artificial evolution of the eqFP615, its coding sequence was cloned into the *pHypermut2* vector. To do this the cDNA was firstly amplified using Pfu Ultra Hotstart polymerase ("Materials and Methods", I.3) using primers P18 and P19. The cDNA was then cloned into the *pHypermut*2 vector between the *Nhe*I and *EcoR*V sites (Figure 12). The correct orientation of the cloned gene was checked using primer P3 annealing at the *RSV* promoter of the vector. The resulted plasmid, named $pMut^{eqFP}$, was transfected into the ψV^{-} AID^{R1} cell line (further – AID^{R1}). Targeted integration of the transgene into the *IgL* locus in the $AID^{R1}IgL^{eqFP}$ transfectants was validated by target screened using the primer pair P1/P2. Similar to the integration of the *eGFP* using *pHypermut2*, described in the "Results" I.1, the transcriptional orientation of the *eqFP615* transgene was designed to be opposite to that of the *V* gene of the *IgL* locus (Figure 13).

FACS analysis of the $AID^{R1}IgL^{eqFP}$ revealed that it was possible to excite these cells with both of blue (488 nm) and red (633 nm) lasers; the fluorescence was analyzed at 660/20 nm long pass detection filter (further referred as 660 nm DF) (Figure 21B). FACS analysis of 10000 cells revealed that each clone contained a major cell population with high fluorescence, which most likely represented cells expressing non-mutated *eqFP615,* and a minor population of 5-10 % with a decreased or absent fluorescence, most likely representing cells with deleterious mutations in the *RFP* gene.

In order to generate a reference point for the new RFP variants, $pMut^{eqFP}$ was transfected to the $AID^{-/-}$ clone of the DT40. Almost none of the cells possessing the decreased or vanished fluorescence were observed in the transfectant $AID^{-/-}IgL^{eqFP}$ cells (Figure 25), confirming the AID – dependency of the hypermutation of the *eqFP615* gene.

In order to test whether the $AID^{R1}IgL^{eqFP}$ transfectant produced mutants with characteristics fitting the suggested optimizations, approximately 10^6 of the cells were analyzed by FACS using appropriate detection filters. To determine if intensity increased mutants were excited by the red laser (633 nm) and the fluorescence intensity at 660 nm DF was plotted against FSC as shown on the Figure 21A. A minor population of the cells with increased fluorescent brightness was indeed detected. These cells were further gated and sorted according to the strategy A.

In order to recover the cells expressing the mutated protein according to the optimization B, the fluorescence of the $AID^{R1}IgL^{eqFP}$ cells was analyzed using a dotplot with a combination of two different detection filters: fluorescence intensity at 576/26 nm (further –

"576 nm"; excitation at the 488 nm laser) was plotted against the fluorescence at 660 nm (excitation by the 633 nm red laser) (Figure 21B). There was a minor population of the cells expressing the protein with the desirable properties observed. These had a fluorescence intensity increased at 660 nm and decreased at 576 nm. These were most likely corresponded to the mutant eqFP615, possessing emission with a maximum, shifted to the far red spectrum (Figure 20B).

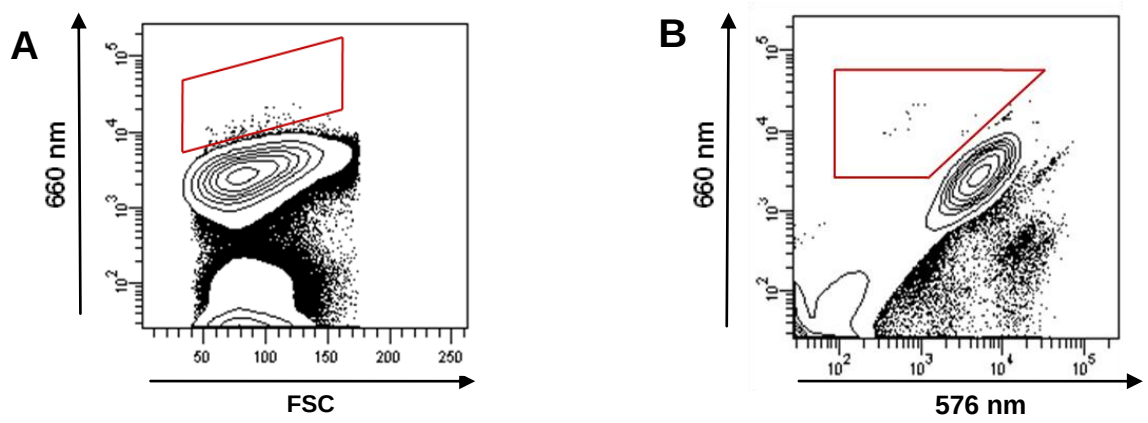

Figure 21. FACS analysis of the $AID^{R1}IgL^{eqFP}$ cells in order to test the suggested sort strategies. (A) Fluorescence intensity at 660 nm detection filter after red laser excitation. (B) Fluorescence intensity at 660 nm detection filter after red laser excitation plotted against intensity at 576 nm DF after blue laser excitation. Gated cells were used for the sorts.

In order to enrich the cell population with an increased fluorescent brightness of the expressed eqFP615, three sequential sorts were done in agreement with the sort strategy A. Each time approximately 0.2% of the cells (shown in blue and violet on the Figure 22) were sorted. After each sort we obtained an enrichment of the cell populations with the increased fluorescence intensity (Figure 22).

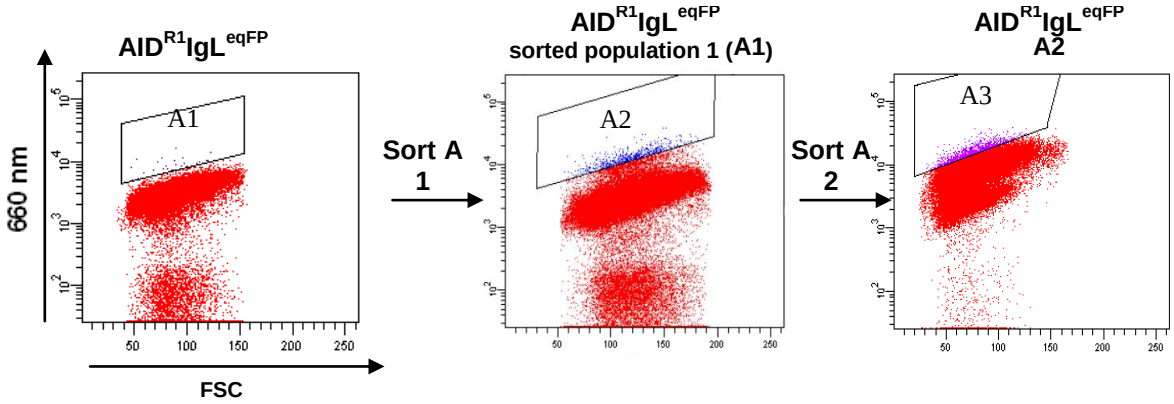

Figure 22. Sorts of the populations with the increase of the fluorescent intensity at the 660 nm DF. (sort strategy A).

FACS analysis after expansion of the sorted cell population by culture according to the strategy B (AID^{R1}IgL^{eqFP} B1), revealed a new population, named β (Figure 23).

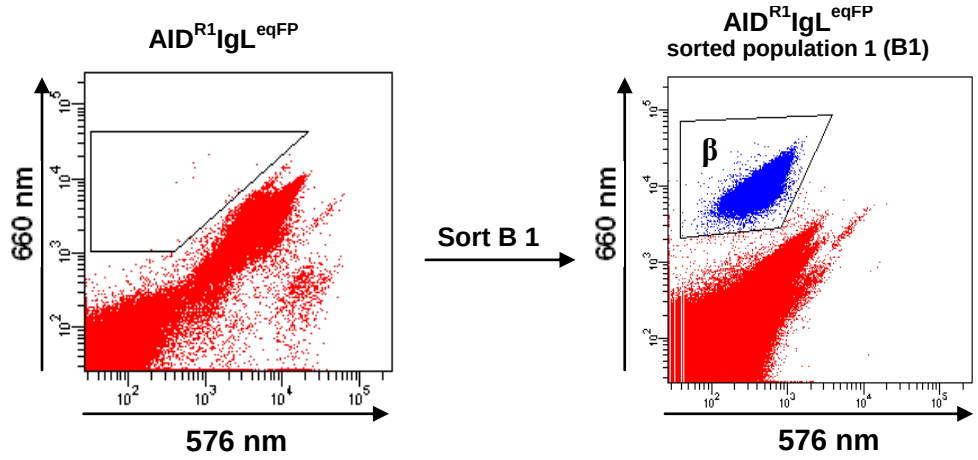

Figure 23. Sort according to the strategy B. The gates set up for enrichment of the cells with the fluorescence, increased at 660 nm DF and reduced at the 576 nm DF. The gates for the next sort of the population β (marked in blue) are shown on the right dotplot.

The population with the increased brightness after sorts A (Figure 22) could also contain cells expressing mutant protein with a spectrum change, because increase of the fluorescence at the 660 nm detection filter could indicate either increase of the emission maximum, but also a the far red shift of the emission peak as well (Figure 20A and 20B). To distinguish between different spectrum changes of the cells after the first sorts A they were analyzed using the combination of detection filters used for the sort B. This analysis revealed that the AID^{R1}IgL^{eqFP} A1, A2 and A3 populations all contained new multiple populations (Figure 24B for A1, Figure 26 (left dotplot) for A3; for A2 data is not shown), which were very uncommon in the initial cells AID^{R1}IgL^{eqFP} (Figure 23A). Interestingly, when the cells from sort A1 were analyzed using the combination of the 660 nm and 576 nm DFs, it appeared that A1 cells contained a population (named α) which was similar in properties to the population β enriched after the sort B1 (Figure 23 (right dotplot) and 24B).

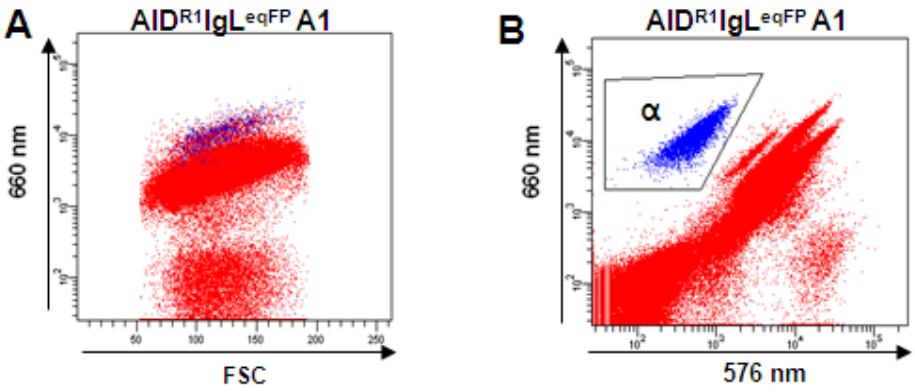

Figure 24. FACS analysis of the cells after the first sort A ($AID^{R1}IgL^{eqFP}$ A1 clone) analyzed using different combinations of filters. (A) A dotplot with the 660 nm on y-axis and FSC on x-axis was used. Cells marked in blue belong to the population α in (B). (B) A dotplot with the 660 nm on y-axis and 576 nm on x-axis was used. The gates for the sort of the population α are shown.

There was a possibility that these populations (named $AID^{R1}IgL^{eqFP}\alpha$ and $AID^{R1}IgL^{eqFP}$ β) contained cells expressing a mutant *eqFP615* with similar or identical sequence changes. In order to check the sequence similarity of the *eqFP* transgenes, each of the *RFP* genes from the sorted populations α and β was PCR-amplified (the sequenced genes were named *Mα1* and *Mβ1* respectively). These coding sequences were re-cloned into the *pHyprmut2* and sequenced using primers P4 and P5 annealing at *RSV* promoter and *polyA* signal. Sequence analysis ("Results", I.2.d) confirmed that both of these genes and hence the two cell clones arising through repeated selection contained identical nucleotide changes (Figure 31).

As the sort strategy A identified more mutated populations than the sort strategy B, and as it delievered the population containing a mutant identical to that obtained with sort B, it was decided to concentrate upon the sort strategy A for future studies.

The brightness increase of the major cell population after the third sort (A3) in comparison with the cells expressing initial eqFP615 was approximately 2 fold (Figure 25).

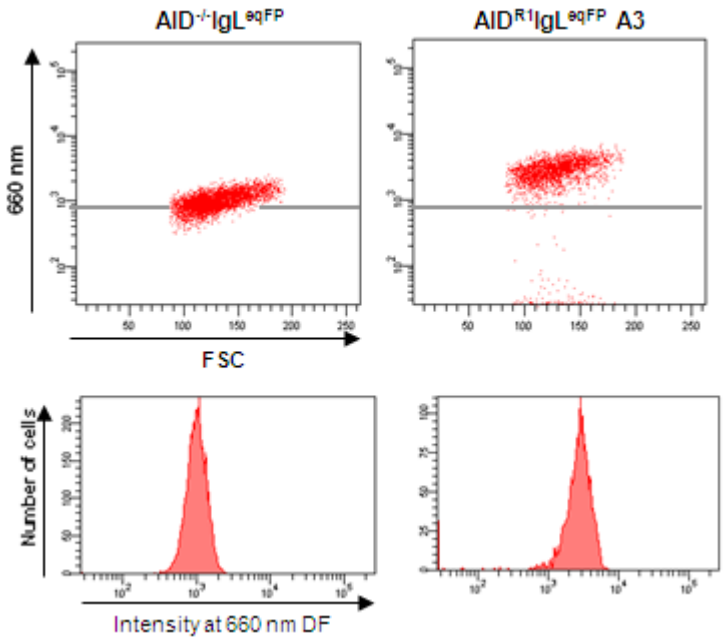

Figure 25. FACS analysis of the $AID^{-/-}IgL^{eqFP}$ clone and $AID^{R1}IgL^{eqFP}$A3 cells after three sort rounds according to the strategy A. Upper panel: the fluorescence at 660 nm DF plotted against FSC (the brightness of $AID^{-/-}IgL^{eqFP}$ is shown at each dot plot by grey guideline); lower panel: the fluorescence at 660 nm (x-axis) plotted against the number of the analyzed cells (y-axis).

After the AID^{R1}IgL^{eqFP}A3 sorted population was expanded, an analysis using the two detection filters (660 nm and 576 nm) was applied again in order to distinguish between the cells expressing proteins with different spectrum changes, as was done for the AID^{R1}IgL^{eqFP}A1 cells. This analysis revealed that A3 cells contained three different populations: P1, P2 and P3 with the percentages 42, 46 and 0.4% respectively (Figure 26). This analysis allowed a clear distinction between populations that had an increase only at 660 nm DF (P1) and those that combined an increase at 660 nm with a reduced fluorescence at 576nm DF (P2 and P3). Due to the low percentage of cells in the population P3 an additional sort for its enrichment was performed. After this sort the percentage of P3 cells increased from 0.4% to 57% (Figure 26).

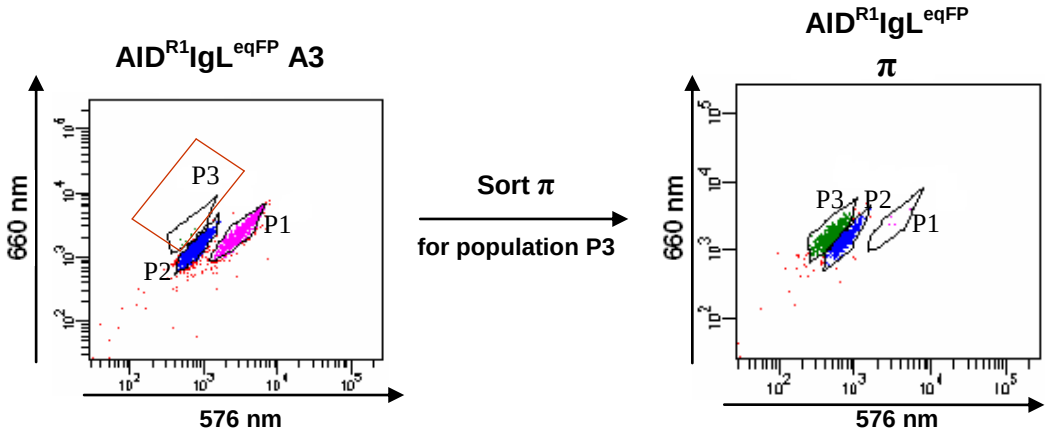

Figure 26. Sort π for enrichment of the P3 population of the AID^{R1}IgL^{eqFP} A3 cells. The gates are shown in red.

In order to analyze the spectrums and sequences of the *eqFP* expressed by the cell populations P1 - P3, we subcloned AID^{R1}IgL^{eqFP}A3 to obtaine monoclonal P1, P2 and P3 cells. In order to prevent the further mutations the *Aid* cassette was excised from the AID^{R1}IgL^{eqFP}A3 and AID^{R1}IgL^{eqFP}π prior to subcloning using tamoxifen induction of Cre recombinase ("Methods", II.18). Figure 27 shows the FACS profiles of the subclones, AID$^{-/-}$IgL^{eqFP} P1, AID$^{-/-}$IgL^{eqFP} P2 and AID$^{-/-}$IgL^{eqFP} P3 in comparison with the AID$^{-/-}$IgL^{eqFP} cells analyzed using dotplots with the combination of the 660 nm and 576 nm DFs.

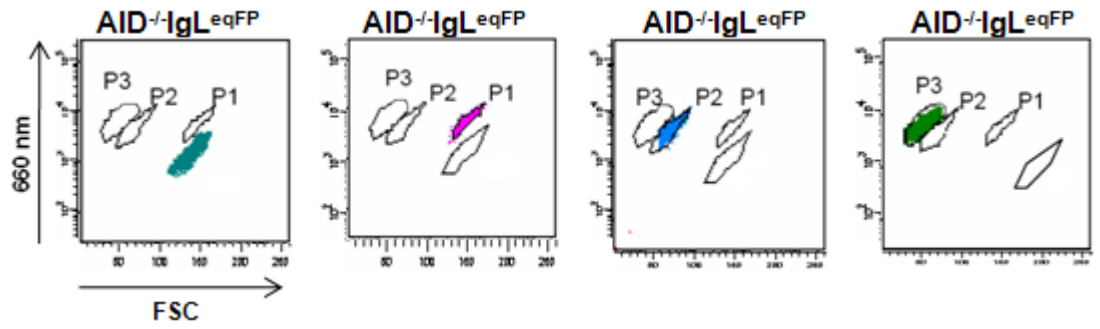

Figure 27. FACS analysis of the AID$^{-/-}$IgL^{eqFP} transfectant and the subclones AID$^{-/-}$IgL^{eqFP} P1, AID$^{-/-}$IgL^{eqFP} P2 and AID$^{-/-}$IgL^{eqFP} P3 on the dotplot with the combination of the 660 nm and 576 nm DFs. On each dotplots the positions of the other clones are shown by their respective gates.

I.2.c. Spectral characteristics of the new RFP variants

Excitation and emission spectra of the RFP variants were analyzed by the luminescence spectrometry. The background luminescence of the non-transfected DT40 cells was subtracted from the obtained spectrums of the monoclonal populations. Excitation was scanned for 670 nm of emission (Figure 28), and emission spectra were obtained using excitation at 550 nm (close to the maximum of the excitation peak for parental eqFP615) as well as at wavelengths corresponding to the blue (488nm) and red (633nm) lasers of the FACS machine (Figure 29).

Compared to the cells expressing the initial eqFP615 protein, the excitation and emission spectra of the cells from all three analyzed clones were improved as predicted under the optimization strategies. As discussed below, the spectral changes were consistent with the differences observed for the FACS profile of the populations P1-P3, except for the case of the excitation at 633 nm (Figure 29C). The probable reason for this is the lower sensitivity of the spectrometer compared to that of the FACS machine, which prevented us from distinguishing between the clones after excitation at 633 nm.

P1 population. The excitation spectrum of the AID$^{-/-}$IgL^{eqFP}P1 cells had approximately twice the intensity compared to the AID$^{-/-}$IgL^{eqFP} cells (Figure 28). Accordingly, there was an increase observed in the emission spectrum maximum of the P1 clone at all three used excitation wavelengths (Figure 29). This result was consistent with the FACS data, demonstrating that this population was brighter than the AID$^{-/-}$IgL^{eqFP} cells at both 660 nm and 576 nm DFs (Figure 27). The increase at 576 nm in the FACS analysis was less than at 660 nm. This is explained by the emission spectrum at 488 nm excitation on Figure 29A: the curves of the AID$^{-/-}$IgL^{eqFP} and AID$^{-/-}$IgL^{eqFP} P1 almost interfuse at 576 nm which complicates the distinguishing of the fluorescence at this DF. Comparing P1 cells to those expressing wild type eqFP615, the emission peak of the P1 cells exhibited a very minor shift to the far red wavelengths. Therefore, the population AID$^{-/-}$IgL^{eqFP} P1 expressed a mutant protein which was improved in intensity but nit wavelength, according to optimization A.

P2 and P3 populations. The cells from the clones AID$^{-/-}$IgL^{eqFP} P2 and P3 possessed excitation spectra with a reduced background at wavelengths shorter than 550 nm, and at the same time a new peak that was considerably shifted into the far-red spectrum compared to the cells expressing eqFP615. This result was consistent with the FACS analysis of these clones

(Figure 27), demonstrating that the P2 and P3 clones were excited more efficiently by the red laser and less efficiently by the blue laser compared to the clone expressing parental eqFP615. According to the excitation spectra changes, the emission spectra maximums of the P2 and P3 clones were far-red shifted (new emission maximum accounted for approximately 640nm) (Figure 29B). The shift of the excitation spectrum also explains why it was not possible to obtain a clear emission spectrum of the P2 and P3 clones at 488 nm excitation (Figure 29A) as this wavelength is now out of the range of the excitation peak of these cells.

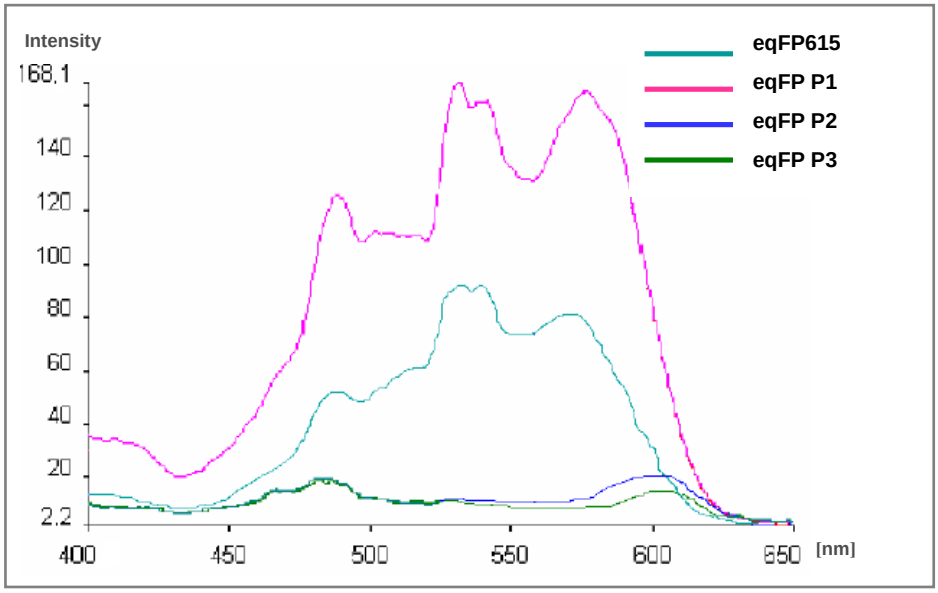

Figure 28. Excitation spectrum scan. Emission fixed at 670 nm.

Therefore, the proteins expressed by the cells of the P2 and P3 clones corresponded to the suggested optimization B. As they had a considerably reduced fluorescence at 488 nm excitation and increased fluorescence intensity at 633 nm excitation, it could be possible to coexpress and analyze them in parallel with many other known RFPs, most of which are excited efficiently at 488 nm but are not excited by the 633 nm red laser. However, compared to the AID$^{-/-}$IgL^{eqFP} and AID$^{-/-}$IgL^{eqFP} P1cells, the fluorescence intensity of these dropped, due to the reduction of the intensity of their excitation peaks maximums.

I.2.d. Analysis of the mutations responsible for the RFP improvement

In order to analyze the nucleotide and amino acid changes of the obtained eqFP variants, the coding sequence of the *eqFP* transgene was amplified from the cell extracts using the primers P4 and P5 annealing at the *RSV* promoter and the *polyA* signal of the *pHypermut2* reporter cassette; respectively. The amplicons were digested with *Nhe*I and *Bgl*II and cloned back into the *pHypermut2* vector. For sequencing the same primer pair P4/P5 was used for detection of mutations outside of the coding sequence. The sequence analysis revealed amino acid changes in the coding sequences of all three mutants.

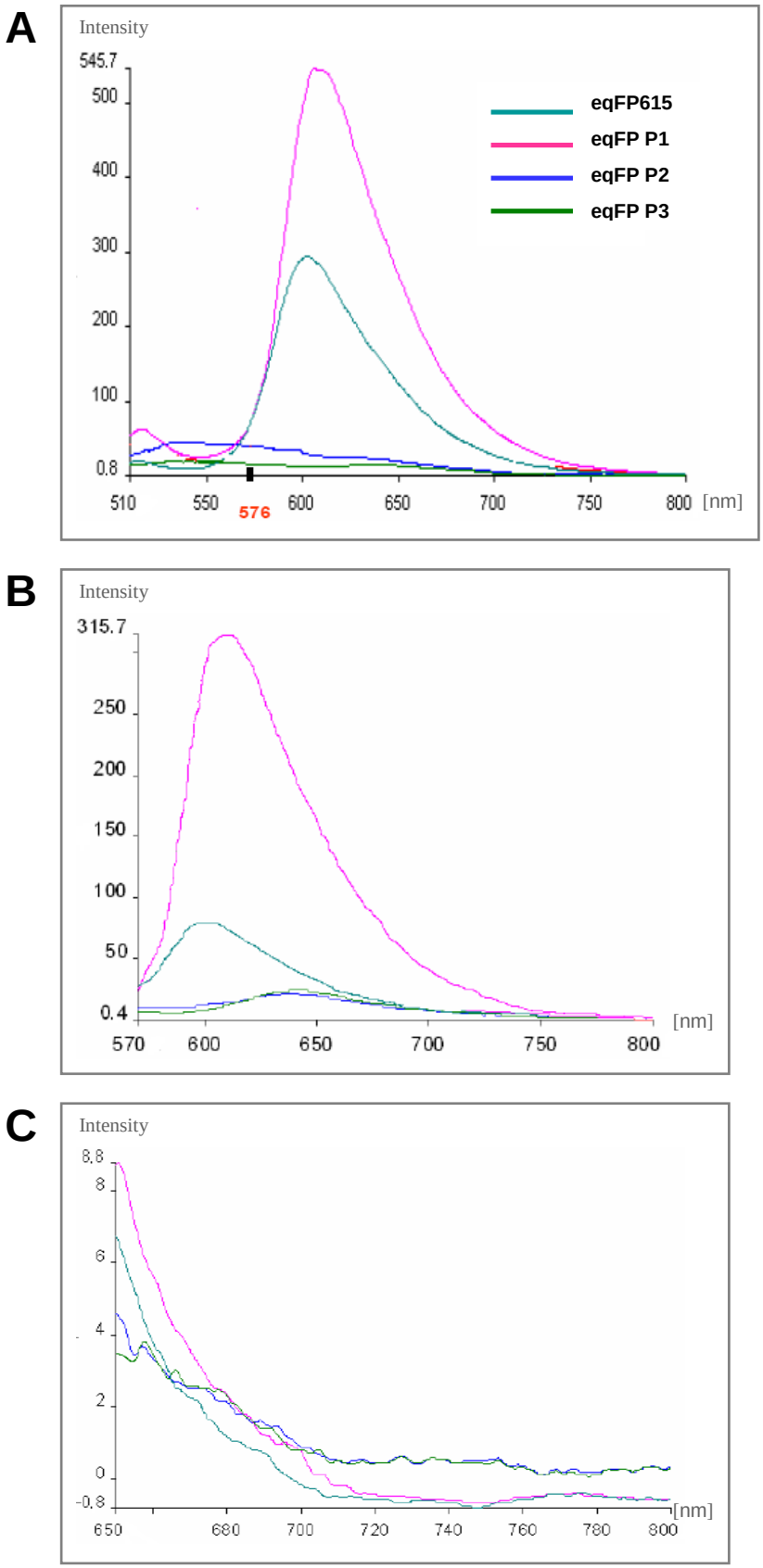

Figure 29. Emission spectra of the AID$^{-/-}$ cells expressing *eqFP615* and its mutants *eqFP M1, M2* and *M*3. (A). Excitation of the FACS blue laser, 488 nm, was used. Wavelength corresponding to the 576 nm DF is marked in red. (B) Excitation 550 nm was used. (C) Excitation of the FACS red laser, 633

nm, was used. Negative values appear due to the subtraction of the values of the background, which appeared to be higher than intensity of the cells due to the low sensitivity of the spectrophotometer at these wavelengths.

At first, the sequences of the *eqFP* mutants amplified from the cell populations α and β (named *Mα* and *Mβ*), sorted from the cells AID$^{-/-}$IgL^{eqFP}A1 and AID$^{-/-}$IgL^{eqFP}B1, respectively, were analyzed. The alignment of these two sequences to the initial *eqFP615* revealed that both *Mα* and *Mβ* carried identical nucleotide substitution, C589T which corresponds to the amino acid change H197Y.

Later the *RFP* sequences of the obtained subclones AID$^{-/-}$IgL^{eqFP}, AID$^{-/-}$IgL^{eqFP}P1, AID$^{-/-}$IgL^{eqFP} P2 and AID$^{-/-}$IgL^{eqFP} P3 were analyzed.

Gene *M1* amplified from the AID$^{-/-}$IgL^{eqFP} P1 clone contained a nucleotide substitution C439A which corresponds to the amino acid change L147M.

Genes *M2* and *M3* from the AID$^{-/-}$IgL^{eqFP} P2 and AID$^{-/-}$IgL^{eqFP} P3 clones shared one common mutation C589T which corresponds to the amino acid change H197Y (the mutation of earlier observed *Mα* and *Mβ*).

The gene *M3* contained an additional mutation G243C which corresponds to the amino acid substitution K81N (Figure 31).

I.2.e. Confirmation of the new RFP phenotypes

In order to confirm the phenotypes of the *eqFP615* variants, the vectors *pMut*^{eqFPM1}, *pMut*^{eqFPM2} and *pMut*^{eqFPM3}, used for sequencing, were transfected into the AID$^{-/-}$ cells. Figure 30 demonstrates the FACS analysis of one of the clones (AID$^{-/-}$IgL^{eqFPM2}) compared to the AID^{R1}IgL^{eqFP}A3 cells. Population P2 of the AID^{R1}IgL^{eqFP}A3 cells and AID$^{-/-}$IgL ^{eqFPM2} fall into the same gate (Figure 30).

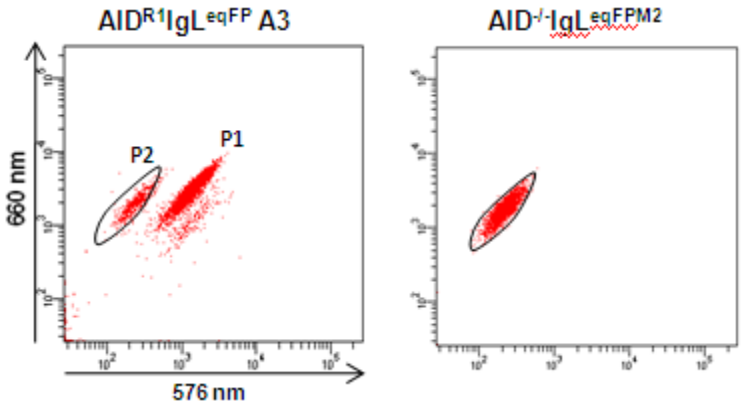

Figure 30. FACS analysis of the transfectant after integration of the *eqFPM2* to the AID$^{-/-}$ clone of the DT40 (right dotplot) compared to the AID^{R1}IgL^{eqFP}A3 cells (left dotplot).

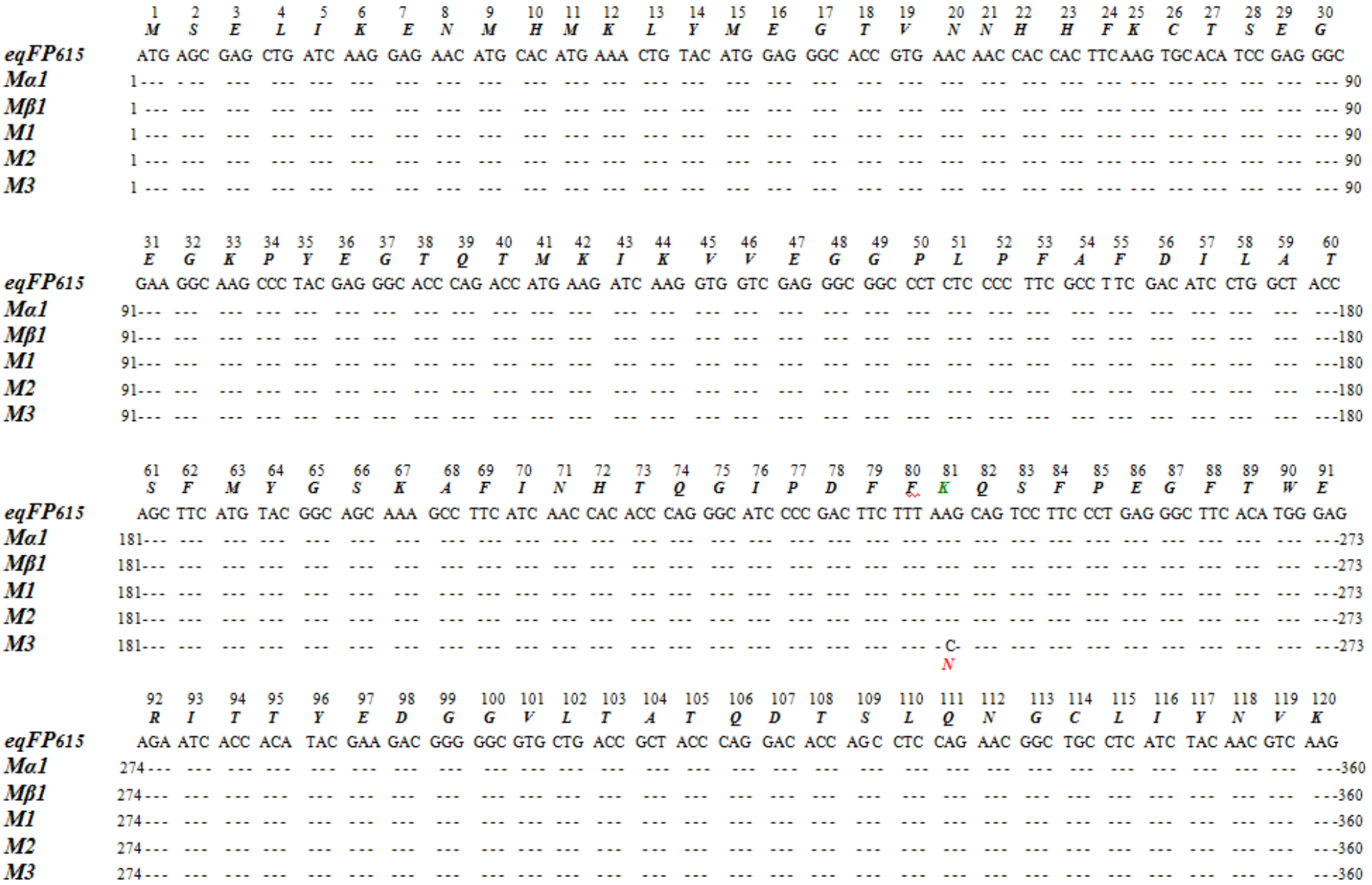
1 2 3 4 5 6 7 8 9 10 11 12 13 14 15 16 17 18 19 20 21 22 23 24 25 26 27 28 29 30
M S E L I K E N M H M K L Y M E G T V N N H H F K C T S E G
eqFP615 ATG AGC GAG CTG ATC AAG GAG AAC ATG CAC ATG AAA CTG TAC ATG GAG GGC ACC GTG AAC AAC CAC CAC TTC AAG TGC ACA TCC GAG GGC
Mα1 1--- 90
Mβ1 1--- 90
M1 1--- 90
M2 1--- 90
M3 1--- 90
31 32 33 34 35 36 37 38 39 40 41 42 43 44 45 46 47 48 49 50 51 52 53 54 55 56 57 58 59 60
E G K P Y E G T Q T M K I K V V E G G P L P F A F D I L A T
eqFP615 GAA GGC AAG CCC TAC GAG GGC ACC CAG ACC ATG AAG ATC AAG GTG GTC GAG GGC GGC CCT CTC CCC TTC GCC TTC GAC ATC CTG GCT ACC
Mα1 91--- ---180
Mβ1 91--- ---180
M1 91--- ---180
M2 91--- ---180
M3 91--- ---180
61 62 63 64 65 66 67 68 69 70 71 72 73 74 75 76 77 78 79 80 81 82 83 84 85 86 87 88 89 90 91
S F M Y G S K A F I N H T Q G I P D F F K Q S F P E G F T W E
eqFP615 AGC TTC ATG TAC GGC AGC AAA GCC TTC ATC AAC CAC ACC CAG GGC ATC CCC GAC TTC TTT AAG CAG TCC TTC CCT GAG GGC TTC ACA TGG GAG
Mα1 181--- ---273
Mβ1 181--- ---273
M1 181--- ---273
M2 181--- ---273
M3 181--- C- --- --- --- --- --- --- --- --- --- ---273
N
92 93 94 95 96 97 98 99 100 101 102 103 104 105 106 107 108 109 110 111 112 113 114 115 116 117 118 119 120
R I T T Y E D G G V L T A T Q D T S L Q N G C L I Y N V K
eqFP615 AGA ATC ACC ACA TAC GAA GAC GGG GGC GTG CTG ACC GCT ACC CAG GAC ACC AGC CTC CAG AAC GGC TGC CTC ATC TAC AAC GTC AAG
Mα1 274--- ---360
Mβ1 274--- ---360
M1 274--- ---360
M2 274--- ---360
M3 274--- ---360

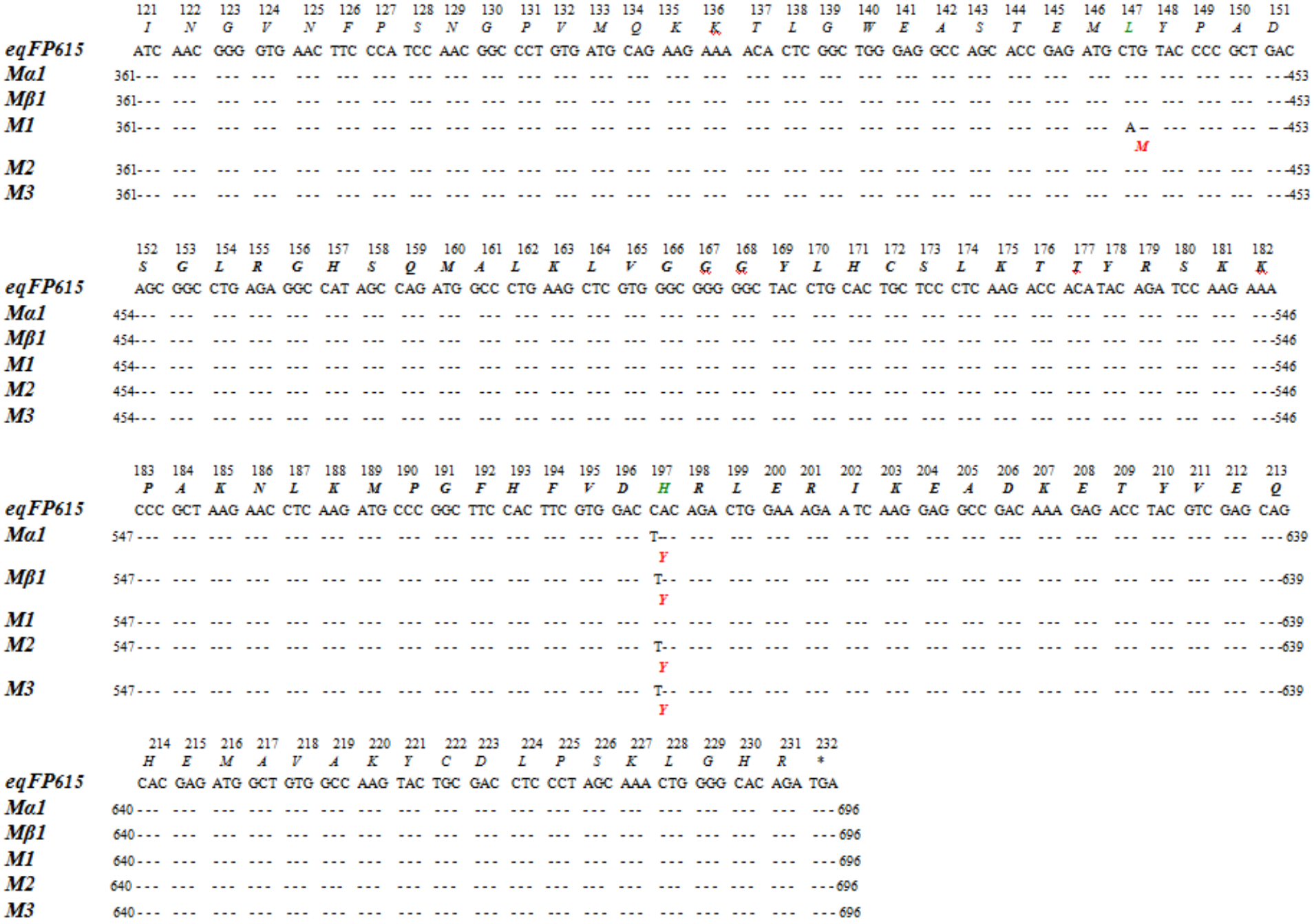

Figure. 31. Codon and amino acid changes in the mutants *Mα1* and *Mβ1* of the *eqFP* gene of the populations AID^{R1}IgL^{eqFP}_A1 and AID^{R1}IgL^{eqFP}_B1 respectively.

II. Identification and characterization of a *cis*-acting diversification activator necessary for the AID mediated hypermutation

Based on the concept of the *pHypermut2* described in Section I.1 of the ” Results", a new reporter construct *pGFP2* was developed, which was suitable for the analysis of the activation and regulation of the somatic hypermutation. This reporter construct was used to perform deletion analysis of the *IgL* locus, which revealed that a 9.8 kb sequence (*DIVAC* for the diversification activator), extending from the *IgL* transcription start site to the border with the neighboring downstream carbonic anhydrase gene, is required for the induction and regulation of hypermutation.

II.1. Construction of a *GFP2* - reporter for somatic hypermutation activity

A new vector *pGFP2* was designed in order to perform quantification analysis of the mutational activity. We assumed that the percentage of cells with a decreased or absent fluorescence (GFP^{low} population) reflects the hypermutation activity of any particular DT40 clones. The GFP^{high} population was not included to this estimation because of its low percentage (“Results”, I.1). The AID dependency of this process indicated that the changes in the fluorescence are indeed caused by hypermutation rather than silencing of the *GFP* gene. This was confirmed in the present study by the semi- quantitative RT-PCR analysis (“Results”, II.3).

The reporter cassette of the *pGFP2* contained the e*GFP* gene (for the visualization of the hypermutation) and the blasticidin resistance gene (*bsr*) (for the selection of the stable transfectants). In order to avoid the artifacts due to the activity of the *β-actin* promoter used to drive in the *pHypermut2*, these two coding sequences (e*GFP* and *bsr*), spaced by an internal ribosome entry site (*IRES*), were put under the common *RSV* promoter and were followed by the *SV40* polyadenylation signal (Figure 32). Such a reporter cassette is referred further as *GFP2*. Fragments, including the *RSV* promoter and the *GFP* open reading frame were amplified from *pHypermut2*; the *IRES* was amplified from *pAidExpressPuro2* [43], and *pLoxBsr*, developed earlier in our laboratory, was used for amplifications of the *bsr* and the *SV40 polyA* signal. PCR was performed using the primers described in the Section I.9 of the “Materials and Methods”.

All the targeting constructs containing the *GFP2* reporter cassette were made using *pKS* as a backbone. The reporter cassette was designed to be excisable by flanking *Bam*HI restriction sites (Figure 32) as this strategy simplified cloning of most target arms into the targeting vectors. All the target arms, except the ones for replacement of the *IgL* promoter by

GFP2, were prepared in the following way. The DT40 genome was screened for the presence of *Bam*HI or *Bgl*II restriction site located at appropriate distance from the *IgL* locus (Figure 45A). Primers were designed for amplification of ~4 kb fragments containing this restriction site (extending ~1 kb to the 5' and 3 kb to the 3' from the *Bam*HI/*Bgl*II sites). At the first step of cloning this 4 kb fragment, containing both targeting arms, was inserted into the multiple cloning site of *pKS*. In the second step the *GFP2* reporter cassette was cloned into the *Bam*HI (*Bgl*II) site between the 3' and 5' targeting arms.

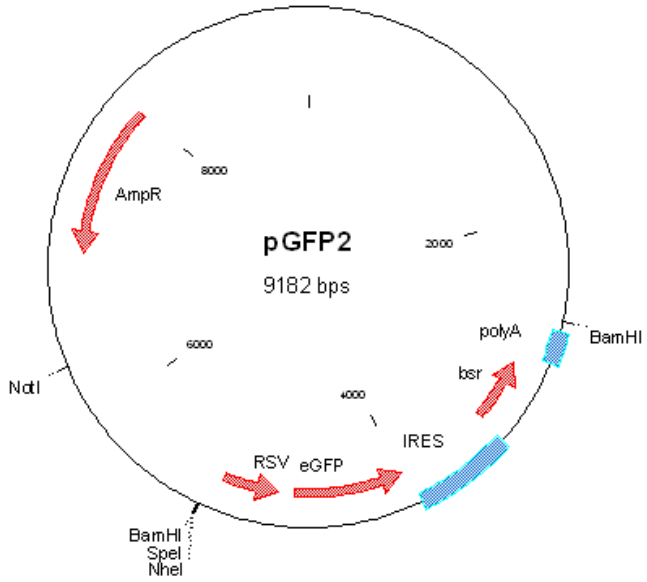

Figure 32. A map of the *pGFP2*. Reporter cassette includes *eGFP* and blasticidin resistance gene (*bsr)* coding sequences, which are spaced by internal ribosome entry site *(IRES)* and driven by the common *RSV* promoter. *GFP2* reporter cassette can be excised by the *Bam*HI restriction sites.

All targeting constructs were named according to the position of the insertion toward *IgL* locus; the *GFP2* reporter cassette was indicated in superscript; upstream and downstream positions were indicated by "+" and "-"(for example, the name p-15IgL^{GFP2} denoted insertion of the *GFP2* reporter cassette 15Kb downstream of the *IgL* locus). In the case of vectors for insertion into the *IgL* locus, the targeting arms of the *pHypermut2* were used ("Results", Section I.1), which allowed cloning of the *GFP2* cassette in a way that the final insertion within the genome would be in the opposite orientation to the *IgL* gene (Figure 33). This avoided mutations in the splice donor sequences for *GFP* transgene (described in the Section I.1 of the "Results"). Such an orientation of the reporter cassette was maintained for the rest of the constructs.

Targeted clones were identified by the PCR screening using one primer annealing at the *polyA* signal of the *GFP2* and another – annealing at a DT40 genome sequence 100-150 bp upstream of the insert ("Materials", I.9, "Oligonucleotides"). In case of vectors for

insertion of the reporter into the *IgL* locus, the targeted integration to the rearranged allele was confirmed by PCR, described in the Section I.1.B of the "Results", using primers VJi1 and VJi2.

II.2. Identification of a *cis*-regulatory element for somatic hypermutation

In order to test the hypothesis for the existence of a *cis*-regulatory element responsible for the activation and regulation of the hypermutation, a deletion analysis was used.

First it was important to determine the rate at which the *GFP2* reporter is normally mutated within the *IgL* locus in AID proficient DT40 cells. The targeting construct *pIgL*^{GFP} for insertion of the *GFP2* reporter into the *IgL* locus contained the target arms of the *pHypermut2*, therefore, the reporter cassette replaced the *IgL* promoter after targeted integration (Figure 33).

A

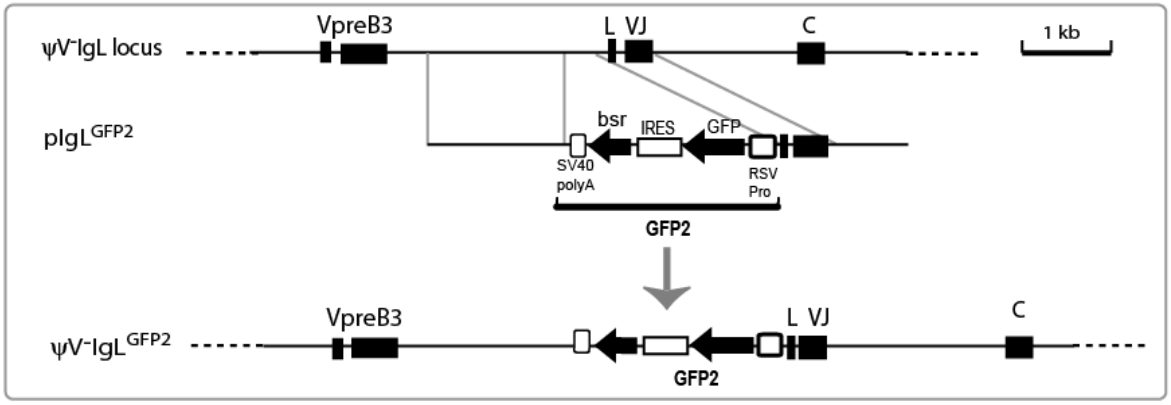

Figure 33. A scheme of the rearranged *IgL* locus with the deletion of the *ψV* locus (ψV$^-$IgL locus), targeting construct *pIgL*^{GFP2} and the locus after targeted integration (ψV$^-$IgL^{GFP2}).

The resulted transfectants were called ψV$^-$IgL^{GFP2}. Two independent primary transfectants were chosen for subcloning by limited dilution. 14 days after this procedure twenty four subclones of each transfectant were analysed by FACS. Median values of decreased green fluorescence for individual subclones from the two independent ψV$^-$IgL^{GFP2} – transfectants were 5.2% and 7.5% (Figure 36A and 36B). This result confirmed previous data of this study on *pHypermut2,* indicating that the *GFP* transgene is mutated at the same high rate within the rearranged *IgL* locus, and that the cell populations with decreased green fluorescence can be used for quantification of the hypermutation activity.

A fragment extending for 9.8 kb from the *IgL* transcription start site until the border with the carbonic anhydrase gene was chosen as a candidate of the sequence containing a *cis*-regulatory element for hypermutation. As we planned to perform a deletion of this fragment, a new recipient cell line with the deletion of the whole *IgL* locus was generated. This clone of

DT40 was named ψV$^-$IgL$^-$; its rearranged *IgL* locus was replaced by the puromycin resistance gene (Figure 34). The targeting construct was named *pIgL$^{-,GFP}$* (minus indicated the excision of the *IgL* locus after its targeted integration). The 3‘ targeting arm of the *pIgL$^{-,GFP}$* contained part of the carbonic anhydrase gene; the 5‘ targeting arm was amplified from the sequence downstream of the pseudo genes locus. After targeted integration, the *GFP2* cassette replaced the puromycin resistance gene at the position of the deleted *IgL* locus (Figure 34).

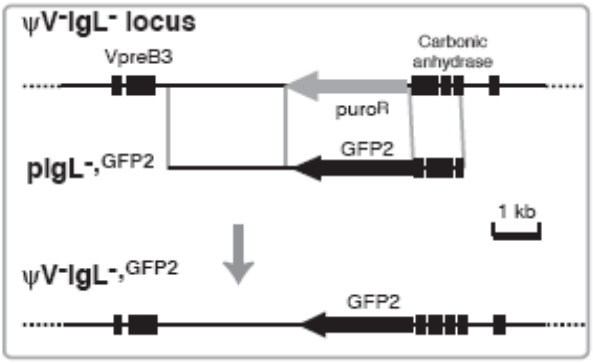

Figure 34. A scheme of the deleted rearranged *IgL* locus of the recipienT-cell line ψV$^-$IgL$^-$, targeting construct *pIgL$^{-,GFP2}$* and the insertion of the *GFP2* after targeted integration at the position of the deleted *IgL* locus (ψV$^-$IgL$^{-,GFP2}$).

Therefore, the successful insertion of the reporter into the rearranged allele could be confirmed by either a test on sensitivity to puromycin, or by the targeting PCR described in the Section I.1 of the “Results” using primers VJi1 and VJi2. The resulted transfectants were named ψV$^-$IgL$^{-,GFP2}$. The FACS analysis of two sublclones revealed median fluorescent intensity decrease of only 0.01% and 0.02%, which was more than 100-fold lower than the medians of the ψV$^-$IgL^{GFP2} subclones (Figure 36A and 36B).

This was the first conclusive evidence that the 9.8 kb fragment, - absent in ψV$^-$IgL$^{-,GFP2}$ but present in ψV$^-$IgL^{GFP2} , was required for hypermutation of the *GFP2* transgene and, therefore, possessed the properties of the predicted *cis*-regulatory element for hypermutation. For convenience this sequence was subsequently referred to the '*W*' fragment.

Later in our laboratory, in collaboration with S. Schmidl, H. Arakawa, R. Caldwell and A. Blagodatski, and the '*W*' fragment was reconstituted. This restored the hypermutation activity back to the levels obtained for the ψV$^-$IgL^{GFP2} subclones. This was shown by the transfection of a targeting construct containing the *GFP2* transgene and the '*W*' fragment (pIgL^{GFP,W}) into the ψV$^-$IgL$^-$ cells (Figure 35). This result confirms the data obtained in the present study, because it demonstrated that the '*W*' fragment was not only necessary, but is also sufficient, for the full level of hypermutation of the reporter gene.

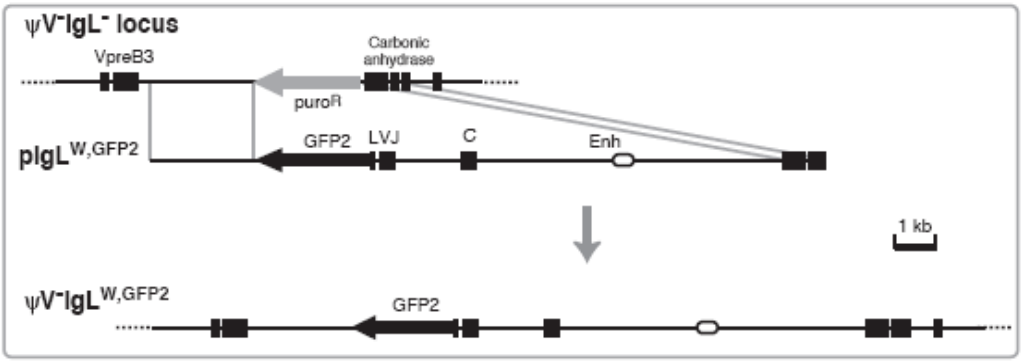

Figure 35. A scheme of the deleted rearranged *IgL* locus ($\psi V^{-}IgL^{-}$ locus), targeting construct including the *GFP2* reporter together with the '*W*' fragment ($pIgL^{W,GFP2}$) and the *GFP2* integration together with the reconstituted *IgL* locus ($\psi V^{-}IgL^{W,GFP2}$).

Three different controls were made to confirm that the decrease in green fluorescence was indeed due to the somatic hypermutation process inactivating the *GFP* protein by mutation.

In order to test the AID dependency of the mutations an $AID^{-/-}$ cell line was used. As described above, targeted integration of the *GFP2* reporter replaced the *IgL* promoter, in this case in the $AID^{-/-}$ cell line. The transfectants were named $\psi V^{-}IgL^{GFP2}AID^{-/-}$. As expected FACS analysis of the subclones of two independent transfectants revealed that almost none of the cells exhibited a decreased green fluorescence; the medians for the analysis of the subclones were not higher than 0.001% (Figure 36A and 36B). The absence of the cells with decreased fluorescence in AID null cells allowed us to conclude that appearance of such cells is due to the process of the hypermutation.

In Figure 36 the FACS analysis dot plots for all four transfections that were used to define the *DIVAC* are shown. Panel B shows the fluctuation analysis of the variability in number of cells with decreased fluorescence of subclones of two representative transfectants.

As the green fluorescence levels in the main populations did not vary considerably within a single transfection, the gates for separation of the main population cells from those that showed decreased or lost green fluorescence, were adapted accordingly in each case. At least 5000 events falling into the gate for the live cell were collected for each primary transfectant or subclone. Subclones in which more than 50% of the live cell events fell into the gates for decreased or lost green fluorescence were excluded from the analysis as they might represent the expansion of a single cell already expressing a mutated *GFP2* transgene at the time of subcloning.

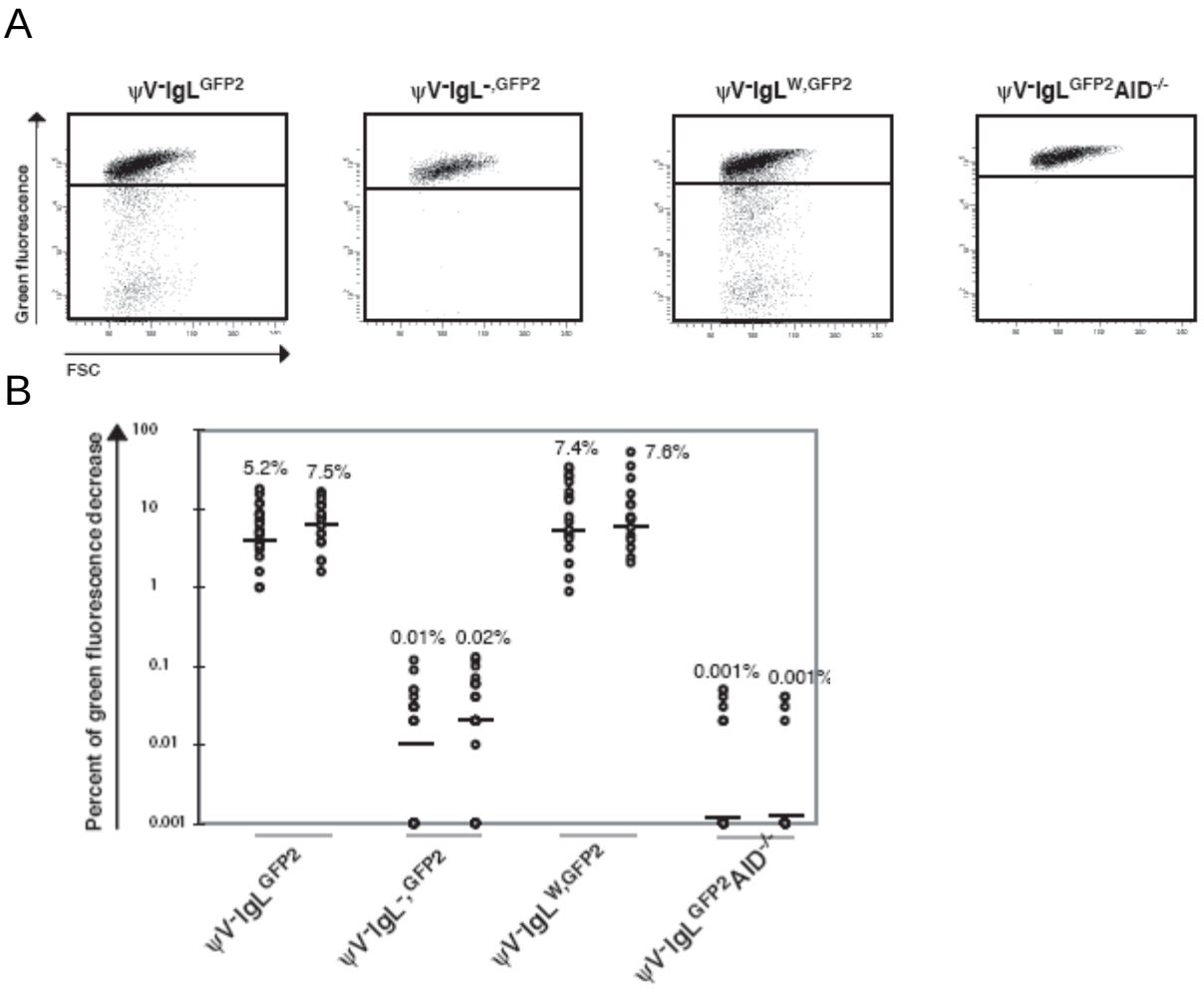

Figure 36. (A) FACS analysis profiles of the primary transfectants. First three dot plots correspond to the transfections based on the schemes in Figures 33-35, respectively; the last dot plot shows the analysis of the transfection of the *GFP2* to the $AID^{-/-}$ cell line. (B) Variation of the subclones corresponding to the transfectants in (A). Each dot represents the analysis of a single subclone and the median of all subclones from the same primary transfectants is indicated by a bar.

Although the AID dependency seen in Figure 36 was a convincing argument for the pesence of hypermutation, there was a possibility that some of the cells with decreased fluorescence appeared due to non-mutational silencing of the *GFP* gene. In order to demonstrate that the decrease in fluorescence was indeed caused exclusively by inactivating AID-mediated mutations due to the hypermutation process, *GFP* gene expression was analyzed by semi-quantitative RT-PCR. For this purpose a bright green fluorescence population (GFP^{high}) and a population with decreased green fluorescence (GFP^{low}) were sorted from the $\psi V^{-}IgL^{GFP2}$ cells (Figure 37A). The *Ef1α* gene was used as a control; its expression was analyzed in parallel with *GFP*, amplified from cells of all three populations. RT-PCR revealed that the cDNA product of both GFP and *Ef1α* could be visualized by the 25^{th} cycle

of the PCR in the case of all three populations, and after 25th cycle its quantity increased proportionally (Figure 37B). This result indicated that the expression levels of the *GFP* gene in both GFP^{high} and GFP^{low} populations were indeed similar, in spite of a more than 100-fold difference in the brightness of these populations. This data conclusively confirmed that the changes in the green fluorescence after insertion of the *GFP2* reporter into the *IgL* locus are not caused by gene silencing. Therefore, they appear most likely to be mutations within the *GFP* coding sequence.

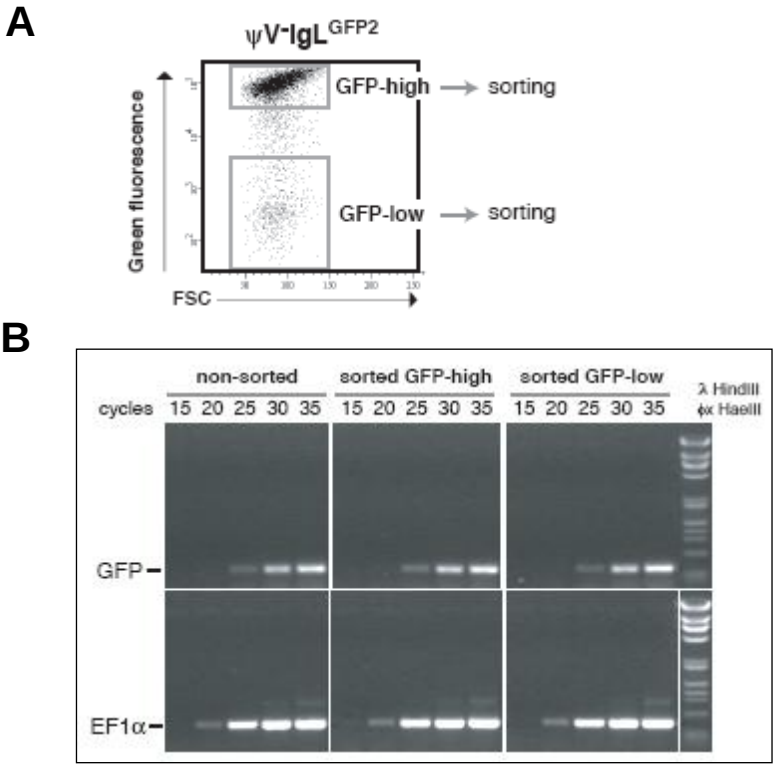

Figure 37. (A) FACS sorting of GFP-high and GFP-low populations from the ψV$^-$IgL^{GFP2} cells.
(B) Electrophoresis of the semi-quantitative RT-PCR of *GFP* and *Ef1α* genes from non-sorted (left raw) and sorted cells (middle and right raw).

Sequence analysis was applied to identify and confirm presence of AID-induced mutations in the reporter gene from the two cell lines: ψV$^-$IgL^{GFP2} and ψV$^-$IgL$^{-,GFP2}$, which have the *IgL* locus present and deleted, respectively. The sequencing was performed on cells grown for six weeks after subcloning. 250 individual clones of the ψV$^-$IgL^{GFP2} cells were analyzed. The sequencing analysis revealed that 224 of them contained *GFP* with nucleotide substitutions, which on average had 0.9 mutations per sequence (Figure 38A). For the 273 bp reading frame of the e*GFP* gene it could be estimated that 0.9 mutations/723 bp = 1.3 x 10^{-3} mutations per 1 bp. It is known that the doubling time of the DT40 cell line is 10 h. As the sequencing was performed 6 weeks after subcloning, it means that the sequences analysis was done after 100 generations. The actual mutation rate in the ψV$^-$IgL^{GFP2} cells can thus be represented as 1.3x10^{-5} mutation per bp per cell generation. Such a mutational rate was relatively high when compared to that obtained for the Ramos cell line, which mutates its *V*

gene at a frequency of $2.2x10^{-5}$ mutation per bp per cell generation [295]. Qualitative analysis of the mutations revealed that the predominant nucleotide substitutions were *C* to *G* and *G* to *C* transversions (Figure 38A). A similar mutation profile was observed for hypermutation of the *IgL VJ* segments from the cell line with the deleted *ψV* locus [67].

The sequence analysis was applied also to the $\psi V^{-}IgL^{-,GFP2}$ cell line. As expected, there was almost no nucleotide substitutions detected within the *GFP* coding sequence. Very few of the mutations that were found (15 per 258 sequenced subclones, i.e. 0.06 mutations per sequence) most likely represent polymerase chain reaction artifacts (Figure 38B).

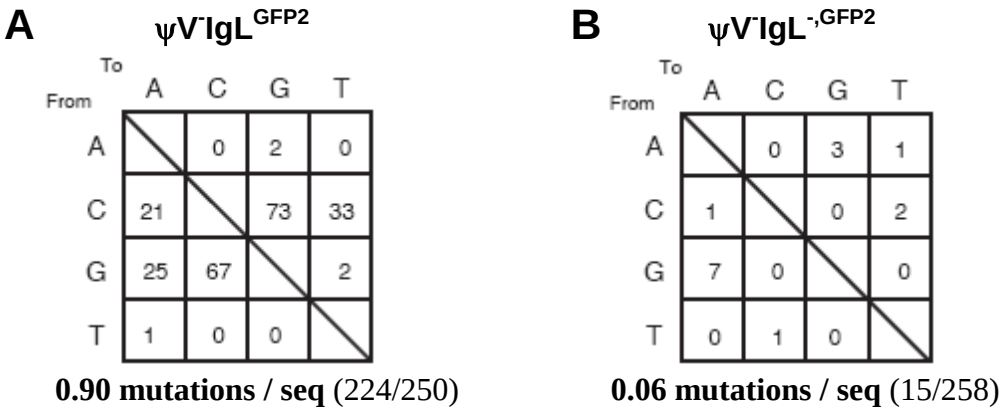

Figure 38. Mutational profile of the *GFP* reporter of the $\psi V^{-}IgL^{GFP2}$ and $\psi V^{-}IgL^{-,GFP2}$ cell lines. The number of the particular nucleotide substitutions within the *GFP* open reading frame are shown.

II.3. Distance of the bidirectional effect of the *cis*-regulatory element for hypermutation

In order to characterise the putative *DIVAC* ("Results", II.2), it was decided to check the physical distance over which it exerts its activity. In order to measure the precise distances in this experiment a cell line which contained the native full length *ψV* locus instead of the cells with the deleted pseudo-gene locus was used. For this we used *ψV* - positive *Aid* conditional knockout DT40 clone AID^{R2}, which was generated earlier in our laboratory from the $AID^{-/-}$ ("Results", I.1.A) by transfection of a construct which targeted an *Aid* cDNA expression cassette into one of the deleted *Aid* loci.

Hypermutation within the IgL locus. It was important to check the hypermutation activity within the *IgL* locus of the new cell line. For this purpose the plasmid $pIgL^{GFP2}$ was transfected into the AID^{R2} cell line. The resulted transfectants were named IgL^{GFP2} (Figure 39A). Targeted integration was confirmed using the primer pair P1/P2 ("Materials", I.9, "Oligonucleotides"). A total of 13 correctly targeted primary transfectants were obtained and analysed by FACS about three weeks after transfection (Table 4). Median values of decreased green fluorescence for a subclone series of the IgL^{GFP2} transfectants were 12.8% and 14.5%

(Figure 45B). The activity of the hypermutation that was previously seen in the presence of the *ψV* genes was only twice that of the *ψV* negative transfectants *ψV*IgL^{GFP2} (Figure 36). As a one-fold difference in the green fluorescence decrease is within the experimental variation due to the different AID expression levels in the AID^{R2} and ψV^{-}AID^{R1} precursors, the conclusion was that the *ψV* locus did not contain a *cis*-regulatory element for hypermutation.

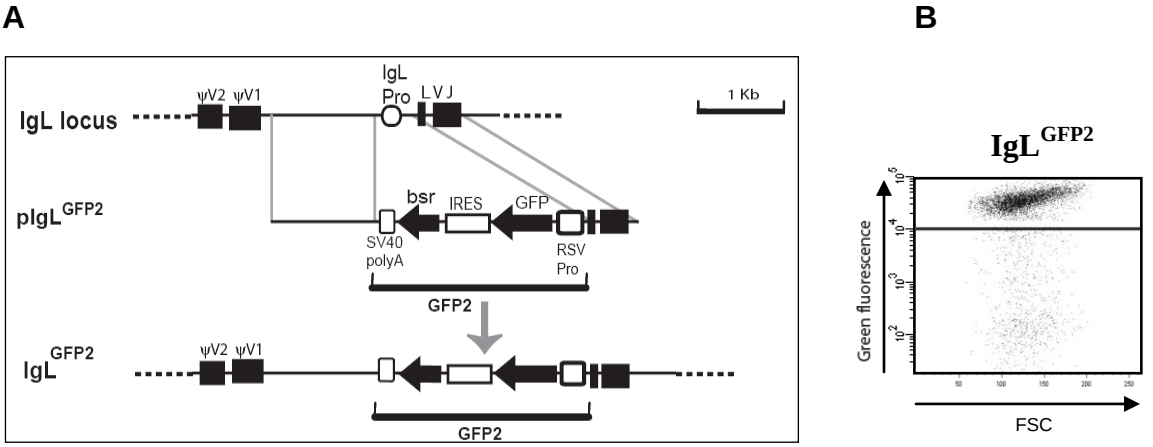

Figure 39. (A) A scheme of the rearranged *IgL* locus, targeting construct *pIgL*^{GFP2} carrying the *GFP2* reporter and targeting arms for replacement of the *IgL* promoter and *IgL* locus after targeted insertion of the reporter. (B) FACS analysis of the primary transfectant after integration of the *GFP2* reporter to the *IgL* locus of the AID^{R2} clone.

Hypermutation in the vicinity of the IgL locus. It was important to check if the *DIVAC* sequence could activate hypermutation outside the *IgL* locus, and whether this activity was bidirectional. To test this, *GFP2* was inserted into the neighboring to the *IgL* locus genes. The targeting constructs were named according to the distance of the insertion from the transcriptional start point of the *V* gene: *p+26KbIgL*^{GFP2} for insertion into the *VpreB3* gene and *p-15KbIgL*^{GFP2} for insertion into the carbonic anhydrase gene (26 kb upstream and 15 kb downstream of the *V* gene respectively) of the AID^{R2} clone (Figure 40 and 41).

Targeting the reporter upstream of the putative DIVAC. After targeted integration into one of the alleles of the carbonic anhydrase gene, the transfectants were named +26KbIgL^{GFP2} (Figure 40).

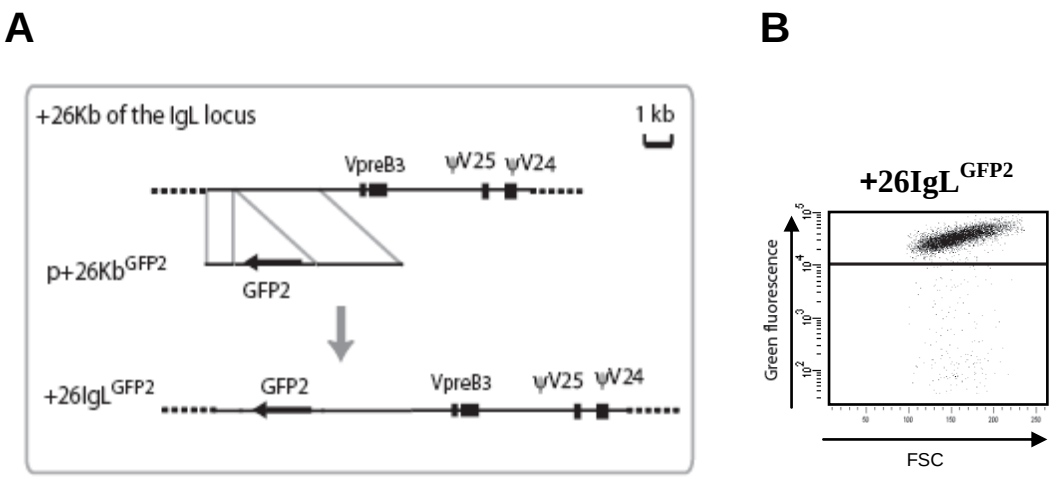

Figure 40. (A) Targeting strategy of the *GFP2* reporter 26 kb upstream of the *IgL* locus and the (B) FACS analysis of the primary transfectant +26IgL^{GFP2}.

Targeting reporter downstream of putative DIVAC. After targeted integration into one of the alleles of the *VpreB3* gene, the transfectants were named -15KbIgL^{GFP2} (Figure 41).

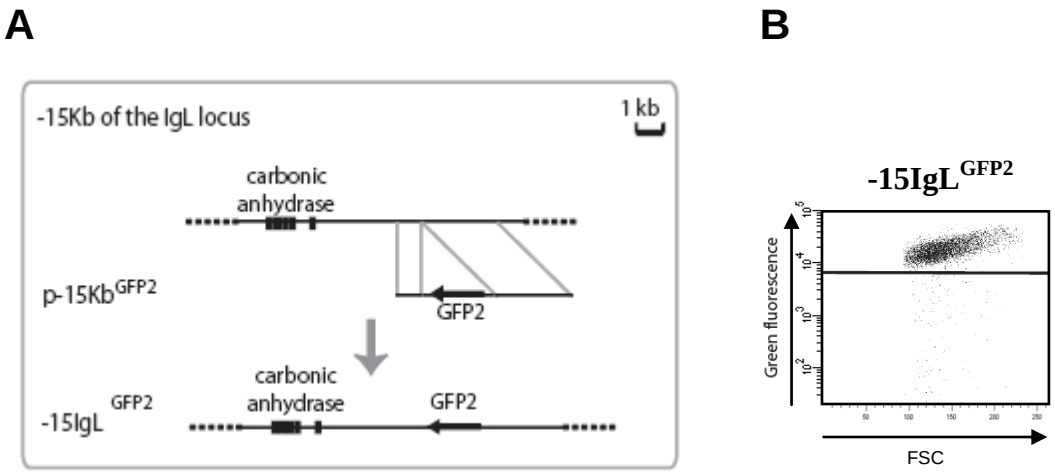

Figure 41. (A) Targeting strategy of the *GFP2* reporter 15 kb downstream of the *IgL* locus and the (B) FACS analysis of the primary transfectant -15IgL^{GFP2}.

After confirmation of the targeted integration, hypermutation activity was measured as before. FACS analysis of the primary transfectants (Figure 40 and 41, Table 4) and their subclones (Figure 45B) revealed that the hypermutation activity decreased, but did not disappear, within these genes when compared to the IgL^{GFP2} cells. Compared to the IgL^{GFP2} the medians of the cell number with decreased green fluorescence fell to about 3% at both the +26 kb and -15 kb positions.

The fact that the hypermutation rate was reduced, but did not disappear when the reporter was inserted into the flanking genes of the *IgL* locus, raised the question of how large

is the range of the hypermutation activity. For this purpose targeting constructs were designed for insertions of the *GFP2* into sites even more distant from the *IgL* locus. Following the strategy described in II.1, we amplified the fragments for the targeting arms which corresponded to the insertions at the +52 kb and -135 kb positions. The insertion 52 kb upstream of the *IgL* locus was between the coding sequences of the genes *VpreB3* and *Mmp11* (Figure 42A). Subclones for primary +52IgL^{GFP2} transfectants revealed 0.5% of the cells to have the decreased green fluorescence (Figure 42B and 45B).

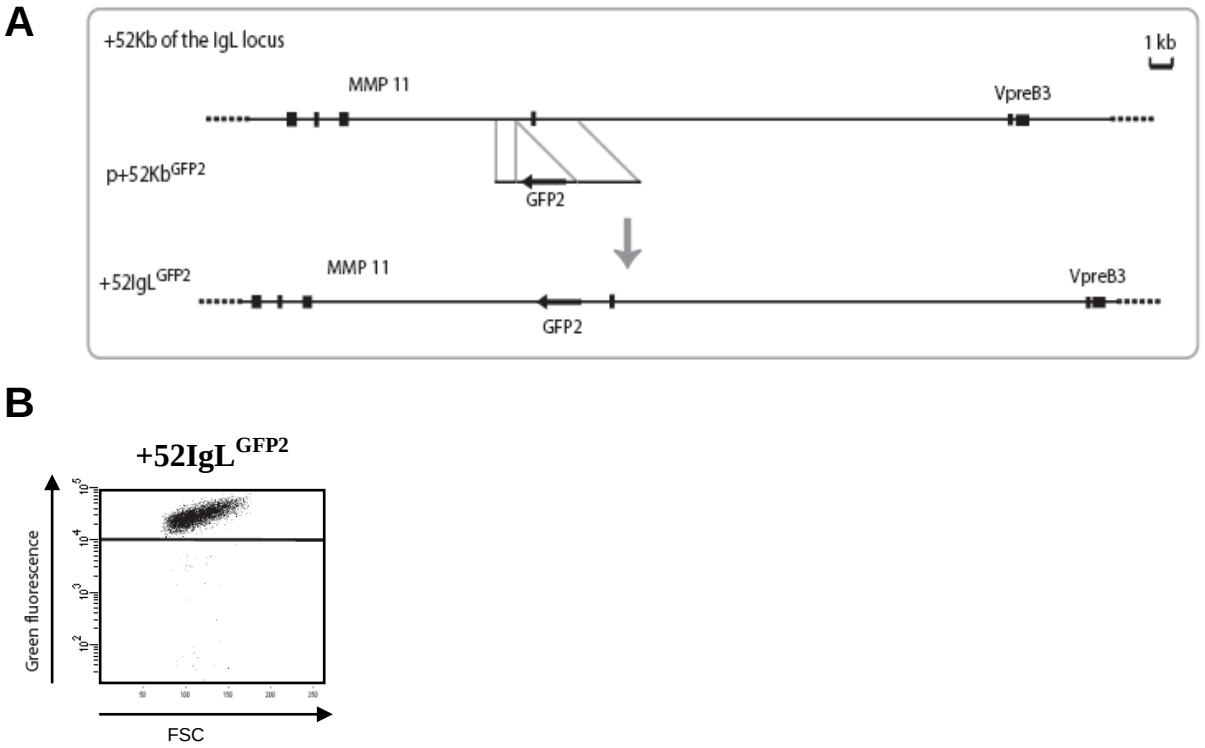

Figure 42. (A) Targeting strategy of the *GFP2* reporter 52 kb upstream of the *IgL* locus. (B) FACS analysis of the primary transfectant +52IgL^{GFP2}.

For insertion of the *GFP2* 135 kb downstream of the *IgL* locus, the targeting construct was integrated into a position between the genes *Kremen1* and *Znrf3* (Figure 43A).

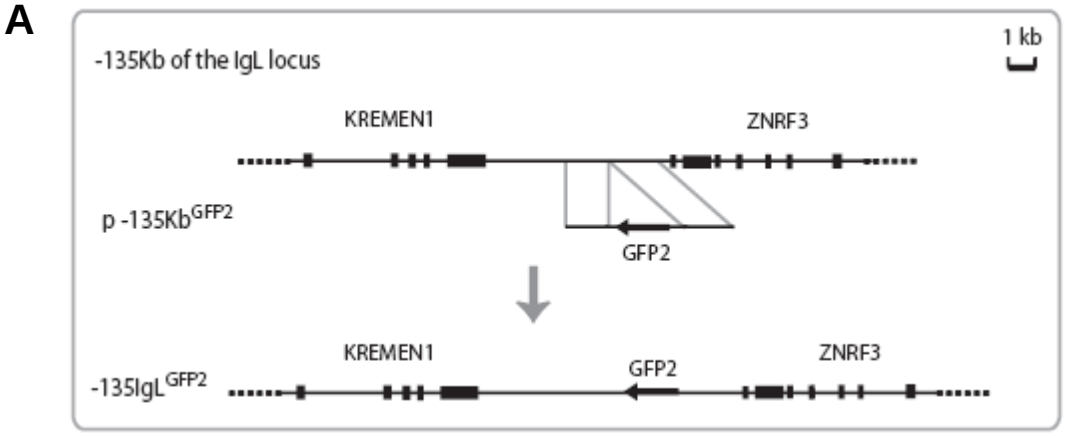

B

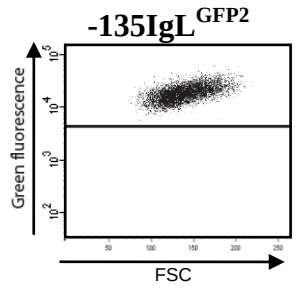

Figure 43. (A) Targeting strategy of the *GFP2* reporter 135 kb downstream of the *IgL* locus. (B) FACS analysis of the primary transfectant -135IgL^{GFP2}.

The medians of the cells possessing decreased green fluorescence for the subclones of the two transfectants -135IgL^{GFP2} fell to 0.05% and 0.07% of the total population (Figure 43B and 45B).

To confirm whether the hypermutation in the vicinity of the *IgL* locus was still dependent on AID, the cell line AID$^{-/-}$ was also used for transfections of the targeting constructs corresponding to the +52, +26 and –135 kb insertions of the *GFP2* reporter (Figure 44, Table 4). As expected, the medians number of cells with decreased green fluorescence for all three insertions were not higher than 0.001% (Figure 44 and 45B). This result demonstrated that the hypermutation of the *GFP2* reporter in the vicinity of the *IgL* locus still had its typical dependency on the functionality of the *Aid* gene.

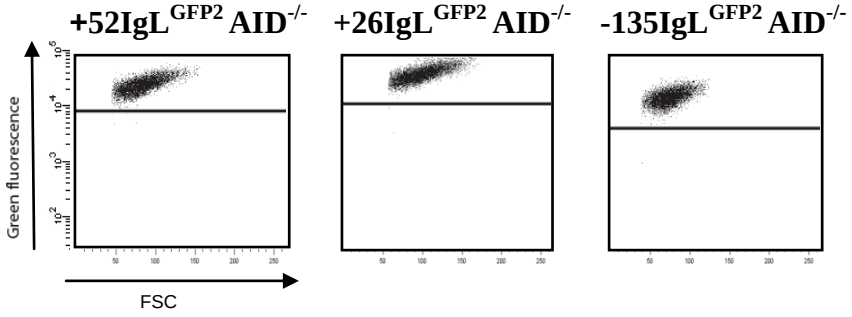

Figure 44. FACS analysis profiles of the primary transfectants after integration of the *GFP2* reporter to three different positions on the chromosome 15 of the AID$^{-/-}$ clone.

The insertions outside of the *IgL* locus may target either the rearranged or unrearranged allele of the 15th chromosome. For each transfection we obtained FACS measurements for several independent primary clones (Table 4), which allowed us to claim that obtained results were representative.

Cell Line	+52IgL^{GFP2}	+26IgL^{GFP2}	IgL^{GFP2}	-15IgL^{GFP2}	-135IgL^{GFP2}	+52IgL^{GFP2} AID$^{-/-}$	+26IgL^{GFP2} AID$^{-/-}$	-135IgL^{GFP2} AID$^{-/-}$
Number of cells with decreased green fluorescence of individual primary transfectants, %	0.50	4.40	18.90	2.50	0.03	0.06	0.018	0.03
	0.30	4.60	27.00	2.30	0.01	0.015	0.016	0.000
	0.80	4.90	40.60	3.40	0.14	0.000	0.000	
	0.20	3.70	12.60	0.40	0.02		0.03	
	1.00	1.50	12.50	2.30	0.08		0.000	
	0.50	11.30	8.60	2.60	0.10		0.000	
	0.30	6.80	23.90		0.00		0.000	
	0.30	4.30	12.80		0.08		0.000	
	0.20	6.30	13.00		0.10			
	1.20		16.90		0.10			
	0.40		7.40		0.02			
	0.20		21.10		0.12			
			14.90					

Table 4. Green fluorescence decrease of individual primary transfectants. *GFP2* reporter is integrated either into the *IgL* locus (IgL^{GFP2}) or in the vicinity of the *IgL* locus (+52IgL^{GFP2}, +26IgL^{GFP2}, -15IgL^{GFP2}). AID$^{-/-}$ indicates transfections to the cell line without *Aid*.

In Figure 45 positions of all five insertions of the *GFP2* within the chromosome 15 of the AID^{R2} clone are shown. The subcloning data for all corresponding transfections is summarized in one graph (Figure 45B).

It is important to emphasize that the decrease of the hypermutation activity in the vicinity of the *IgL* locus was not caused by changes in the transcription activity of the *GFP* gene. For this purpose transcriptional levels of the *GFP* and the decrease of the hypermutation activity were compared for the insertions at different distances from the *IgL* locus. The *GFP* transcription is reflected by the levels of green fluorescence in the major cell population in FACS profile, which most likely expresses un-mutated *GFP*. There was only a slight fluctuation in the transcriptional levels of the major cell populations of the primary transfectants of different *GFP2* insertions (Figure 33-35, 44), which could be explained by a chromosomal position effect. At the same time, the hypermutation activity levels among these transfectants varied considerably. A pair of transfectants IgL^{GFP2} and +52IgL^{GFP2} was quite representative in this respect: the fluorescence level for the major cell populations of these clones (therefore, transcriptional levels) were almost similar, while the medians of the florescence decrease varied more than 20-fold. This comparison conclusively demonstrated that the regulation of hypermutation activity has a distance effect, with a decline in activity relative to the distance from the *IgL* locus; this is independent of the changes in the transcription of the reporter gene.

A

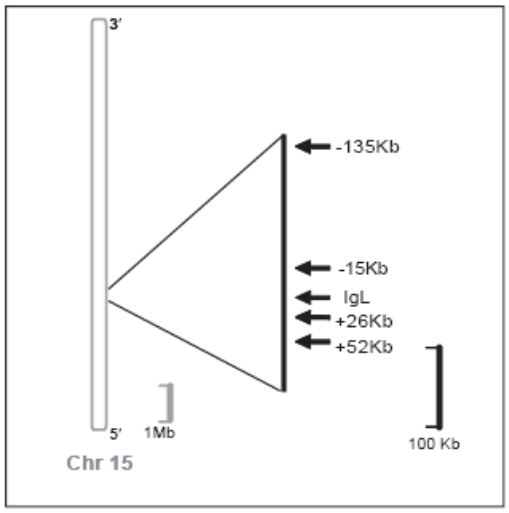

B

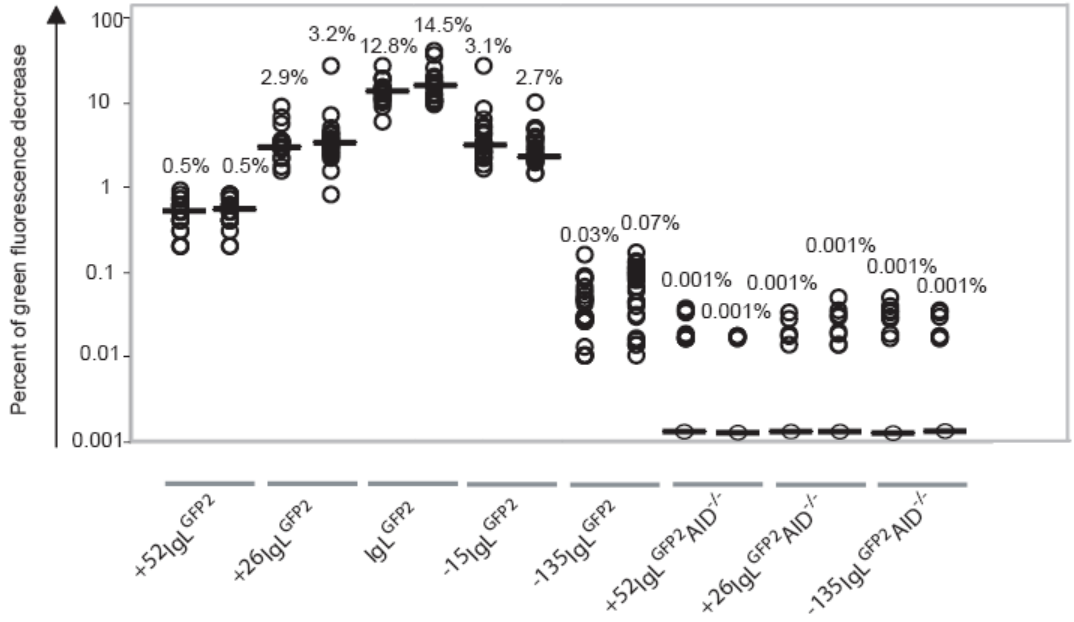

Figure 45. (A) Positions of the *GFP2* insertions on chromosome 15 at different distances from the *IgL* locus. (B) Fluctuation analysis of the subclones. The names of the respective transfections are indicated below the graph.

DISCUSSION

The main goals of the present study were: 1) to develop an improved artificial protein evolution system and to validate it by the analysis of new GFP phenotypes, 2) to apply the new system to the optimization of the red fluorescent protein; 3) to find and characterize a *cis*-DNA-element responsible for activation and regulation of the somatic hypermutation within the *IgL* locus of the DT40 cell line.

I. Application of the somatic hypermutation for artificial protein evolution

The generation of the new vector *pHypermut2* described in the present study allows *in vivo* diversification of transgenes inserted into the *IgL* locus of the DT40 cell line. This reaction is specific and efficient and results in an artificial evolution system that improves upon that created earlier in our laboratory ("Introduction", VII.2).

The use of the *pHypermut2* in conjunction with a clone of the DT40 cell line with deleted pseudo-genes and *Aid*-conditional knockout results in a high ratio of targeted integration. The new system allowed standardization of the artificial protein evolution process (Figure 46). The evolution of a selected protein in this system includes the following steps: 1) cloning of the gene template to be modified by artificial evolution into the *pHypermut2* vector followed by transfection of the final construct into the $\psi V^{-}AID^{R1}$ cell line; 2) target screening PCR for the identification of the clones with transgene inserted into the *IgL* locus; 3) selection and expansion of the cells expressing the protein with the desired new properties introduced by hypermutation (expansion can be repeated until the final mutant has acquired the desired properties); 4) isolation of the clonal cell population expressing this mutant, followed by switching off further hypermutation by excision of the AID-expression cassette; 5) subcloning, PCR - amplification of the transgene and cloning of it back to the *pHypermut2* vector; 6) after analysis of the mutations responsible for the optimization of the protein, the new phenotype can be confirmed by insertion of the mutant sequence into the *IgL* locus of DT40 cells lacking AID.

Using *pHypermut2* we created and analyzed the phenotypes of a range of new eGFP variants of enhanced brightness. Alignment of the gene sequences found in those mutants with AID-induced substitutions observed in previous studies revealed that several of the amino acid changes in the GFP structure increasing fluorescence have already been reported (discussed below). The fact that some of the found amino acid changes were previously reported for GFP mutants validated the strategy of artificial evolution, and gave hints of the

process by which GFP variants developed in the present study were improved. Combination of the nucleotide substitutions observed in different enhanced fluorescence-variants into a single sequence by site-directed mutagenesis allowed the production of GFP proteins with an even stronger increase in brightness.

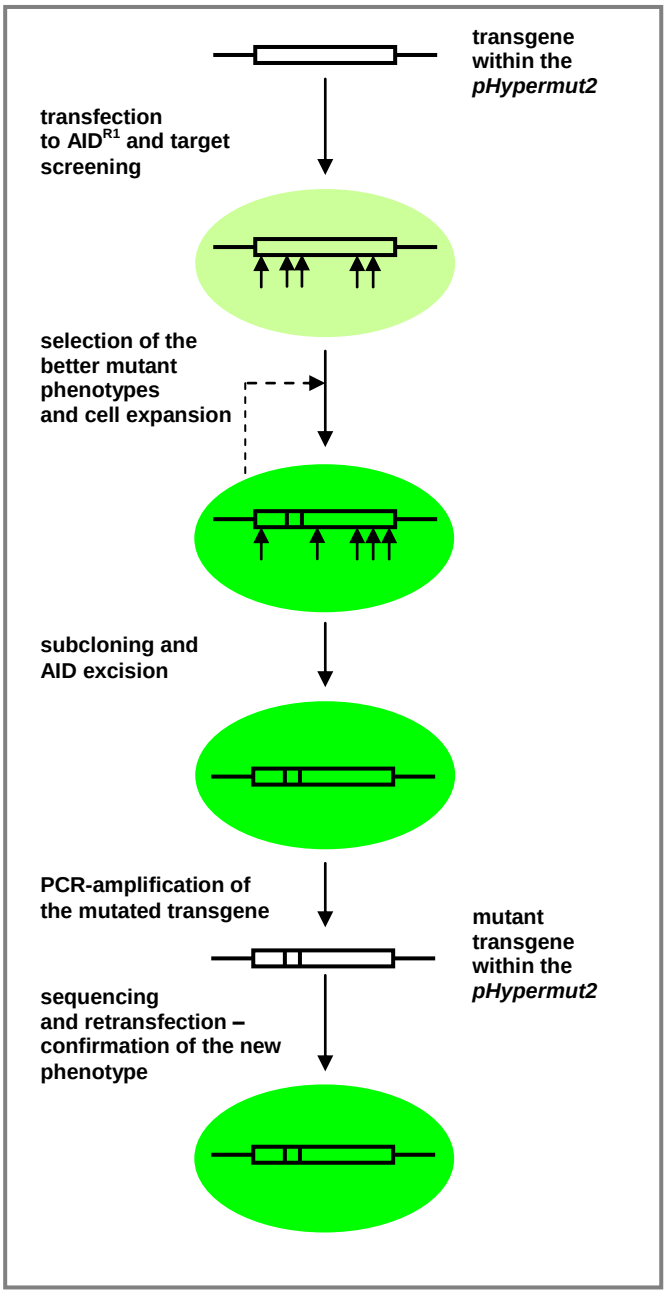

Figure 46. Artificial protein evolution in the DT40 cell line.

Amino acid changes found in the enhanced GFP clones v6, v5, v8, v2 and v9 ("Results", Figure 17 and Table 3) are candidates for the substitutions responsible for the observed improvement in GFP brightness. These amino acids did not locate close to each other, and were dispersed through the protein (Figure 47). The V163A change, which plays a pivotal role in folding of the GFP protein [296], was previously seen in the GFP variants

Cycle3 [297], T-Sapphire [298], Venus [299, 300], eCFP and W1C [278]. The Y145F change responsible for the increase of the protein brightness [301] was reported in GFP variants of Sapphire [292], p4-3 [278, 301] and eBFP [277, 278]. The V163A substitution is suggested to support correct protein folding of GFP, most likely increasing the yield of a properly matured protein.

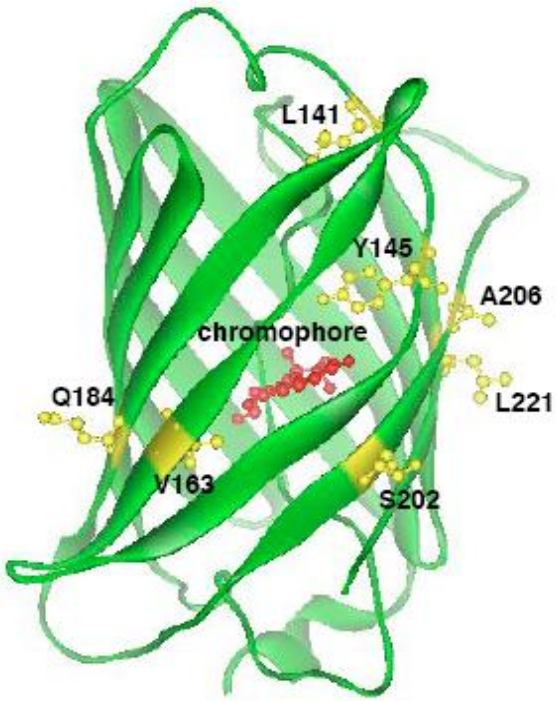

Figure 47. Amino acids involved in increase of the brightness of eGFP variants. The positions of amino acids (in yellow), which are identified in the brighter GFP variants (GFPv6, v5, v8, v2 and v9) are mapped on the crystal structure of GFP. Chromophore is highlighted in red. Made using Swiss PDB Viewer program in collaboration with H. Kudo.

The other amino acid changes associated with improvement in the properties of GFP are newly identified in this study. Because amino acids A206 and L221 can play a role in dimerization of GFP, A206T and L221V may act to stabilize the GFP dimer, leading to higher fluorescence intensity. The Q80E change did not contribute to GFP brightness although interestingly, this mutation was shared among all the GFP variants. This apparently neutral mutation might be selected for as the result of a high frequency of hypermutation at this site, because this amino acid may be located in the hotspot motif of the hypermutation.

The combination of the Y145F, V163A and S202T amino acid changes into a single peptide further increased GFP brightness, generating the “GFPnovo1” variant. The addition of the L221V mutation to GFPnovo1 resulted in the slightly brighter GFPnovo2 variant (Figure 6 and 7). The novo1/2 GFP variants might have advantageous applications in imaging

biology. The GFPnovo1 might be also recommended for constructing fusion protein reporters because this variant is probably less likely to dimerize due to the lack of the L221V mutation.

In the process of generating chimeric GFP molecules, their brightness could not be predicted simply as the additive or multiplicative effects of individual amino acid changes. Some of the individual amino acid changes observed may have the same effect on protein structure and, therefore, may not show any synergy. As seen in GFPv13, some of the amino acid changes might in fact interfere with each other and thus, decrease overall brightness (Figure 16 and 17, Table 3).

Although the crystal structure of GFP is determined [302], the role of all individual amino acid substitutions in the increase of the fluorescence of variant GFP proteins is not clear. As the residues of the changed amino acids are not predicted to locate in the direct proximity of the chromophore, the most likely reason for the increase of the brightness is enhanced protein maturation, improved folding or stability.

Compared to other techniques of protein mutagenesis ("Intorduction", VII), the creation of an artificial evolution system in hypermutating DT40 cell line has an important advantage. The selection of the optimized phenotypes takes place from an almost infinite pool of mutant proteins within living vertebrate cells. This is extremely important as the folding and properties of many proteins are affected by intra-cellular parameters such as pH and salt concentration, post-translational modifications and interactions with other proteins that are not presented in *in vitro* systems. In conventional *ex-vivo* systems protein degradation after the expression of the *in vitro* developed mutants may be encountered. Moreover, the proteins encoded by such mutants may prove to be toxic to cells. These issues are automatically avoided in the *in vivo* DT40 system created in the present study. Although optimization of proteins has been previously reported in hypermutating mammalian B-cell lines such as Ramos [285] or 18–81 [279], DT40 offers considerable advantages, such as insertion of only a single copy of the transgene into the *IgL* locus, specific and efficient mutation of the transgene and the possibility to stop mutation via the inducible deletion of the AID expression. Diversification of a target protein in DT40 may even be facilitated by a combination of hypermutation and gene conversion if homologous conversion donor sequences are inserted upstream of the transgene. Recently it was demonstrated that gene conversion on its own can be a useful strategy for the diversification of transgenes [292].

As the artificial evolution system is based on *IgL* hypermutation, the mutations are supposed to be restricted to the 1 kb region at the 5' end of the transcribed sequence. Therefore, this system is more suitable for the evolution of small gene targets within 1 kb.

Different rates of hypermutation may be suitable for different artificial evolution goals. Hypermutation at a very low frequency cannot diversify the transgene efficiently, and may make it difficult to achieve the desired variants in a limited time period. On the other hand, hypermutation at too high frequency may mask or even remove a desired mutation after its generation unless AID is switched off. The hypermutation rate of our $AID^{R1}IgL^{eGFP}$ cell line fell into the appropriate range to achieve efficient and speedy *in situ* engineering of the *eGFP* transgene. When targeted to the *IgL* locus of the $\psi V^{-}AID^{R1}$ cell line, the GFP transgene is mutated at a rate $4.7x10^{-6}$ mutations per bp per cell generation within the *pHypermut2* cassette [303] and $1.3x10^{-5}$ mutations/bp/generation within the *pGFP2* cassette. This mutation frequency is slightly lower than the mutation rate observed for the rearranged *VJ* segment in the pseudo-gene deleted $\psi V^{-}AID^{R}$ cell line, which showed $2.2x10^{-5}$ mutations/bp/generation [67]. This reduction could be a reflection of a difference in promoter strength, transcriptional orientation, and lower numbers of hypermutation hotspots within the *eGFP* sequence in comparison with the *V* gene. In general, the mutation rate in our system has a similar mutating rate compared to that seen in the mammalian cell line Ramos used for the alternative artificial protein evolution (average rate $2.2x10^{-5}$ mutations/bp/generation [295]). If needed, a higher frequency of hypermutation may be achieved in our system by creating stronger over-expression of AID, the additional use of an UNG knockout [172] or histone deacetylase inhibitors treatment [253, 290] (corresponding effects are described in "Introduction", V.2.a and VI.3, respectively).

The artificial evolution system might be applied to optimization of any coding or non-coding sequences whose phenotype can be screened in DT40 cells, including enzymes, pharmaceutical drugs, *cis*-regulatory elements, sensors etc. As FACS analysis is convenient for the screening for the new variant phenotypes, fluorescent proteins are ideal objects for the artificial evolution.

Therefore, the created system of artificial protein evolution was applied for the optimization of the red fluorescent protein eqFP615 derived from the sea anemone *Entacmaea quadricolor*. The different screening strategies led to the generation of variants with increased brightness and a red-shift of the emission spectrum. In total, three new mutations were selected for study, that alone or in combination, lead to changes to the starting protein phenotype. Compared to the initial eqFP615 template, the variant eqFP_M1 possessed a 2.5-fold higher fluorescent brightness, whilst the other two variants, eqFP_M2 and eqFP_M3, had the emission peak shifted approximately 25 nm into the far-red spectrum (Figure 29B). Sequence analysis of each of these improved variants of wild type eqFP578, combined with

data on the resolved crystal structure of the two eqFP615-realated proteins, eqFP611 and mKate, allowed a prediction of the role of the new mutations on the defined changes of the fluorescent properties of the variants.

First it was considered whether the increase of the brightness of the cells expressing mutant eqFP_M1 was caused by the oligomerization of the starting protein. The sequence and structural comparison analysis revealed that the substitution L147M found in the sequence of the eqFP_M1 was not included in the list of mutations responsible for the formation of the monomer TagRFP [281] and the monomer-forming substitutions predicted after resolution of the crystal structure of the mKate (both monomers originated from the wild type eqFP578). This observation allowed suggesting that the brightness increase of the eqFP_M1 was not caused by a tetramerization of the initial dimer form of the eqFP615. The residue L147 is listed as a structurally important amino acid forming part of one of the strands of the eqFP beta-barrel [286]. Therefore, it is likely that the increase in brightness is due to an increased stability of the protein structure.

The two mutants, eqFP_M2 and eqFP_M3, possessing a red-shift of their emission spectra, shared the mutation H197Y. Following the determination of the eqFP611 crystal structure in 2002 it was reported that residues H197, N143 and F174 surround the chromophore and have a significant impact on its conformation and its spectral properties. In particular, the hydroxyphenyl group of the T64 residue of the chromophore is sandwiched between H197 and F174 (Figure 48). The π-stack between T64 and H197 is claimed to be a candidate for the red-shift in the fluorescent spectrum of the eqFP611 as the highly polarizable aromatic ring of H197 stabilizes the excited state of the chromophore [288].

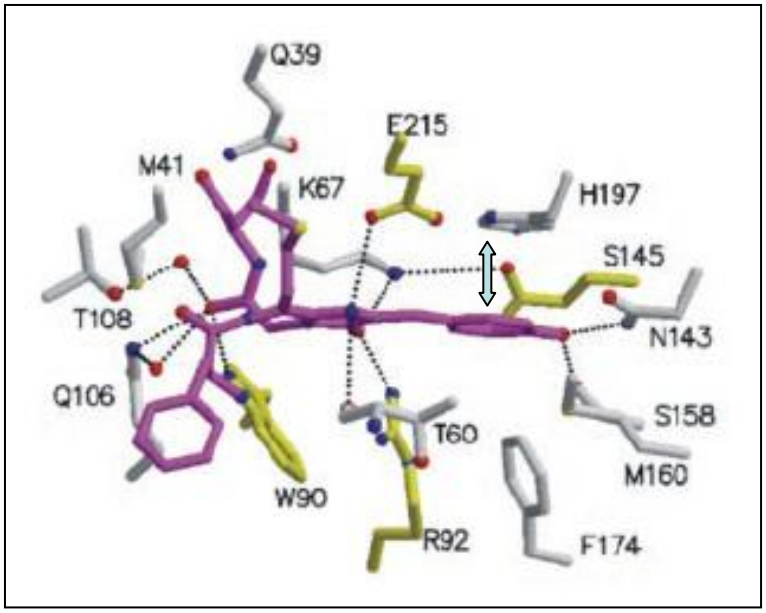

Figure 48. Residues surrounding the chromophore of the eqFP611. The hydroxyphenyl group of the chromophore-forming Y64 is sandwiched between H197 and F174. Stacking of the hydroxyphenil group of the Y64 and heterocycle ring of the H197 is shown by blue arrow. Taken from [288].

Later in 2008, the report of the analysis of the mKate crystal structure [289] revealed that the red-shift of its fluorescent spectrum is due to substitutions at three key residues; all of which were identified in the eqFP611 crystal structure analysis: H197, N143 and F174. Sequence alignment with mKate revealed that eqFP615 initially had two of these key "far-red-shifting" substitutions, N143S and F174L (Figure 19). The third substitution, crucial for the red shift in case of the mutants eqFP_M2 and eqFP_M3, was at the residue H197, but in contrast to Kate which has changed histidine to arginine (H197R), eqFP_M2 and M3 had it changed to the tyrosine (H197Y).

It is known that the electron density of the phenyl ring of tyrosine is higher than that of the two-nitrogen heterocycle of the histidine. Therefore, it is possible to speculate that in the eqFP_M2 and eqFP_M3 proteins, having H197 substituted by Tyrosine, the stacking with the chromophore is more powerful which leads to the stronger stabilization of the excited state of the chromophore.

The residue R197 of mKate is also noted in the list of amino acids forming the backbone of the pore of the β-barrel that is suggested to be essential for maturating of the chromophore by providing access for molecular oxygen [289, 304]. We cannot exclude the possibility that the spectrum of the mutants eqFP_M2 and eqFP_M3 is red-shifted due to the influence of the H197Y substitution on the improvement of this mechanism.

Compared to eqFP_M2, the eqFP_M3 mutant contained an additional substitution K81N. As this mutant possessed a slightly greater red shift in emission than that of eqFP_M2, it is possible that the mutation K81N was responsible. The residue K81 is located in the alpha-helix mentioned as one of the structurally important regions of the β-barrel of the wild type eqFP578 [286]. Therefore, the additional red shift of the eqFP_M3 spectrum may be caused by an additional stabilization of the protein structure due to the K81N substitution.

The generation of the optimized variants of eqFP615 validated our artificial evolution system. The analyzed mutations demonstrated two new phenotypes, both of which are relevant improvements for imaging biology. The variant with increased brightness is advantageous for bio-imaging in living cells, while the far-red shifted variants are of high value for methods based on FRET and imaging in living tissues due to penetration of red light into tissues. The mutants developed in this study are not superior to the best proteins currently available on the market, such as Katushka and others, as none of the single mutations could

satisfy all of the spectral requirements necessary to compete with the commercial products. For example the emission peak of the bright eqFP_M1 is not shifted as far as that of Katushka; mutants eqFP_M2 and eqFP_M3, having emission maximum further than of Katushka, are not sufficiently bright.

The developed mutants may be further improved using different approaches. Firstly, it is reasonable to combine the single mutations, responsible for different changes in phenotype, into one common sequence as shown for GFP above. Secondly, it should be possible to further improve the phenotype of the obtained variants by additional FACS sorts. For example, the detection of the shift of emission analyzed with a 660 nm detection filter would be possible until the emission maximum would reach 660 nm (after that we would detect the decrease of the fluorescent intensity (Figure 20)). This could be solved by switching to the more far-red detection filter.

II. Identification of a *cis*-acting diversification activator both necessary and sufficient for the AID mediated hypermutation

The idea of the artificial evolution system was based on the observation that a transgene inserted into the chicken *IgL* locus undergoes hypermutation at a high rate. Based on the idea of the *pHypermut2* a new vector, *pGFP2*, was generated. Using this reporter gene construct a deletion analysis of the *IgL* locus was performed. This allowed identification of a *cis*-regulatory element responsible for activation of the somatic hypermutation. This *cis*-acting diversification activator (*DIVAC*), extending for 9.8 kb from the *IgL* transcription start site towards the next downstream gene, carbonic anhydrase, activated the hypermutation more than 100-fold above the background level.

As somatic hypermutation is commonly used to diversify *Ig* in most vertebrates species (“Introduction”, I), *DIVAC* may be conserved during the evolution of vertebrates. Consistent with this hypothesis, it was reported that the hypermutation in mice is recruited and controlled by the sequences included into and surrounding sequences of the *Ig* enhancers [71, 72, 305, 306]. The functional characteristics of these mammalian regions appear to be similar to chicken *DIVAC* sequence obtained in the present study. The difficulty to find an exact sequence match between the sequences of chicken and murine *cis*-regulatory element can be explained by large size of the murine *Ig* loci compared to that of the chicken Ig loci and the assumption that these diversification activators seem to be composed of multiple interacting regions.

As the rearranged *IgL* locus of the B-lymphocytes is constitutively diversified by gene

conversion in the bursa Fabricius [107] and DT40 [122] using *ψV* genes, *DIVAC* may also activate gene conversion. This is supported by a recent publication showing that a deletion of the rearranged *IgL* locus downstream of the *C* region stopped *IgL* gene diversification in *ψV* positive DT40 [46].

The experiments on insertion of the *pGFP2* reporter upstream and downstream of the *IgL* locus revealed that the reporter transgene was subjected to AID-dependent hypermutation outside the normal boundaries of the *IgL* locus, with the degree of the decrease in the mutation activity proportional to the distance from the *IgL* locus. This result allowed us to characterize the *DIVAC* as an element with a bidirectional action with a wide range of activity. The assumption that this effect also affects the endogenous *IgL* locus requires additional experiments, including sequence analysis of the endogenous genes present alongside the insertions.

Sequence analysis of the region neighboring the *IgL* locus genes was performed recently by S. Fugmann's group [222]. They used a different experiment system and their results partially contradict the data obtained in the present study. Based on the sequence analysis, the researches claim that sequences flanking the *IgL* locus genes, namely the *VpreB3* and carbonic anhydrase, do not undergo hypermutation in DT40. In the case of carbonic anhydrase the lack of hypermutation is completely expected, as this gene is not transcribed in this cell line [222]. As hypermutation is tied to transcription, after insertion of the *GFP2* cassette with its own promoter, thus transcribed, into this gene, we could observe the hypermutation. In contrast to carbonic anhydrase, the *VpreB3* gene is transcribed in DT40 [222]. Sequence analysis in Fugmann's study revealed only a single A to G point mutation in a total of 84 sequences of *VpreB3*, while in the present study the *GFP2* reporter inserted into the *VpreB3* undergoes hypermutation although the medians of the green fluorescent decrease dropped to 3.1% and 2.7% compared to the hypermutation within the *IgL* locus (12.8% and 14.5%). The explanation for these contradictory results can be found in the difference of the experimental approaches. One possible reason is using of the transgene instead of the endogenous *VpreB3.* In this case different promoter and transcription orientation of the reporter, presence of the SHM hotspots within the *GFP*, epigenetic changes after integration might separately or together allow the hypermutation of the transgene. Also S. Fugmann's group tested too low number of the gene sequences that together with possible sequencing artifacts, was probably not enough sensitive method to detect the decreased hypermutation, whilst FACS analysis used in the present study allowed testing the green fluorescent decrease

in 10^4 of cells for each transfection that significantly increased chances to detect the mutations.

The ability of the *GFP2* reporter to undergo hypermutation when inserted into different positions on chromosome 15 of the chicken genome may be interpreted as an indication of the ability of AID to act outside the *IgL* locus. This correlates with the recent observation of D. Schatz's group showing a broad action of the murine AID on the genome [70]. This result suggested that, while this enzyme deaminates uracils of transcribed genes throughout the genome, it is not the targeting of AID itself but targeting of the error-prone DNA repair which makes hypermutation specific for the *IgL* locus.

As switch recombination is accompanied by hypermutation of the switch regions [307] and chicken *IgL DIVAC* can activate hypermutation in both directions over large distances, we can speculate that a single *DIVAC* may regulate both somatic hypermutation and class switch recombination in the heavy chain loci.

One of the hints to the mechanism of *DIVAC* action, which in general remains unclear, is the fact that it not only contains the *IgL* transcriptional enhancer but also functions in the manner characteristic for typical enhancers, i.e. acting in both directions and over large distances. Concerning the enhancer function of *DIVAC,* and the dependency of the somatic hypermutation on transcription [62, 63, 307], one can assume that this *cis*-regulatory element plays a role in regulation of the B-cell specificity of SHM [308] and the targeting of this process to the *Ig* loci [39, 50-52] via involvement with the protein transcription factory [309]. In respect of the targeting of the hypermutation to the *IgL* locus, the hypothesis for *DIVAC* functioning would assume that this element contains DNA motifs essential for the binding of cofactors of the transcription machinery and for proteins of the error-prone DNA-repair pathway.

Therefore the present study allowed identification of the *cis*-regulatory element necessary for the activation of the hypermutation targeted to the *IgL* locus and also provided a hint to the mechanism of the action of this element.

REFERENCES

1. Medzhitov, R. and C. Janeway, Jr., *Innate immune recognition: mechanisms and pathways.* Immunol Rev, 2000. 173: p. 89-97.
2. Medzhitov, R. and C.A. Janeway, Jr., *An ancient system of host defense.* Curr Opin Immunol, 1998. 10(1): p. 12-5.
3. Janeway, C.A., Jr., *How the immune system protects the host from infection.* Microbes Infect, 2001. 3(13): p. 1167-71.
4. Hozumi, N. and S. Tonegawa, *Evidence for somatic rearrangement of immunoglobulin genes coding for variable and constant regions.* Proc Natl Acad Sci U S A, 1976. 73(10): p. 3628-32.
5. Tonegawa, S., *Somatic generation of antibody diversity.* Nature, 1983. 302(5909): p. 575-81.
6. Papavasiliou, F., et al., *V(D)J recombination in mature B-cells: a mechanism for altering antibody responses.* Science, 1997. 278(5336): p. 298-301.
7. Longerich, S., et al., *Brca1 in immunoglobulin gene conversion and somatic hypermutation.* DNA Repair (Amst), 2008. 7(2): p. 253-66.
8. Schatz, D.G., M.A. Oettinger, and D. Baltimore, *The V(D)J recombination activating gene, RAG-1.* Cell, 1989. 59(6): p. 1035-48.
9. Oettinger, M.A., et al., *RAG-1 and RAG-2, adjacent genes that synergistically activate V(D)J recombination.* Science, 1990. 248(4962): p. 1517-23.
10. Cannon, J.P., R.N. Haire, and G.W. Litman, *Identification of diversified genes that contain immunoglobulin-like variable regions in a protochordate.* Nat Immunol, 2002. 3(12): p. 1200-7.
11. Rast, J.P. and G.W. Litman, *Towards understanding the evolutionary origins and early diversification of rearranging antigen receptors.* Immunol Rev, 1998. 166: p. 79-86.
12. Agrawal, A., Q.M. Eastman, and D.G. Schatz, *Transposition mediated by RAG1 and RAG2 and its implications for the evolution of the immune system.* Nature, 1998. 394(6695): p. 744-51.
13. Hiom, K., M. Melek, and M. Gellert, *DNA transposition by the RAG1 and RAG2 proteins: a possible source of oncogenic translocations.* Cell, 1998. 94(4): p. 463-70.
14. Fugmann, S.D., et al., *An ancient evolutionary origin of the Rag1/2 gene locus.* Proc Natl Acad Sci U S A, 2006. 103(10): p. 3728-33.
15. Eason, D.D., et al., *Mechanisms of antigen receptor evolution.* Semin Immunol, 2004. 16(4): p. 215-26.
16. Cannon, J.P., et al., *The phylogenetic origins of the antigen-binding receptors and somatic diversification mechanisms.* Immunol Rev, 2004. 200: p. 12-22.
17. Litman, G.W., M.K. Anderson, and J.P. Rast, *Evolution of antigen binding receptors.* Annu Rev Immunol, 1999. 17: p. 109-47.
18. Schatz, D.G., *Antigen receptor genes and the evolution of a recombinase.* Semin Immunol, 2004. 16(4): p. 245-56.
19. Pancer, Z., et al., *Somatic diversification of variable lymphocyte receptors in the agnathan sea lamprey.* Nature, 2004. 430(6996): p. 174-80.
20. Pancer, Z. and M.D. Cooper, *The evolution of adaptive immunity.* Annu Rev Immunol, 2006. 24: p. 497-518.
21. Greenberg, A.S., et al., *A new antigen receptor gene family that undergoes rearrangement and extensive somatic diversification in sharks.* Nature, 1995. 374(6518): p. 168-73.

22. Diaz, M., et al., *Mutational pattern of the nurse shark antigen receptor gene (NAR) is similar to that of mammalian Ig genes and to spontaneous mutations in evolution: the translesion synthesis model of somatic hypermutation.* Int Immunol, 1999. 11(5): p. 825-33.
23. Lee, S.S., et al., *Hypermutation in shark immunoglobulin light chain genes results in contiguous substitutions.* Immunity, 2002. 16(4): p. 571-82.
24. Ota, T., et al., *Lineage-restricted retention of a primitive immunoglobulin heavy chain isotype within the Dipnoi reveals an evolutionary paradox.* Proc Natl Acad Sci U S A, 2003. 100(5): p. 2501-6.
25. Mussmann, R., et al., *Microsites for immunoglobulin switch recombination breakpoints from Xenopus to mammals.* Eur J Immunol, 1997. 27(10): p. 2610-9.
26. Conticello, S.G., et al., *Evolution of the AID/APOBEC family of polynucleotide (deoxy)cytidine deaminases.* Mol Biol Evol, 2005. 22(2): p. 367-77.
27. Grawunder, U., R.B. West, and M.R. Lieber, *Antigen receptor gene rearrangement.* Curr Opin Immunol, 1998. 10(2): p. 172-80.
28. Lieber, M.R., et al., *The mechanism of vertebrate nonhomologous DNA end joining and its role in V(D)J recombination.* DNA Repair (Amst), 2004. 3(8-9): p. 817-26.
29. Di Noia, J.M. and M.S. Neuberger, *Molecular mechanisms of antibody somatic hypermutation.* Annu Rev Biochem, 2007. 76: p. 1-22.
30. Knight, K.L. and M.A. Crane, *Generating the antibody repertoire in rabbit.* Adv Immunol, 1994. 56: p. 179-218.
31. Reynaud, C.A., et al., *A single rearrangement event generates most of the chicken immunoglobulin light chain diversity.* Cell, 1985. 40(2): p. 283-91.
32. Butler, J.E., *Immunoglobulin diversity, B-cell and antibody repertoire development in large farm animals.* Rev Sci Tech, 1998. 17(1): p. 43-70.
33. Arakawa, H. and J.M. Buerstedde, *Immunoglobulin gene conversion: insights from bursal B-cells and the DT40 cell line.* Dev Dyn, 2004. 229(3): p. 458-64.
34. McCormack, W.T. and C.B. Thompson, *Chicken IgL variable region gene conversions display pseudogene donor preference and 5' to 3' polarity.* Genes Dev, 1990. 4(4): p. 548-58.
35. Meyer, A., et al., *Immunoglobulin gene diversification in cattle.* Int Rev Immunol, 1997. 15(3-4): p. 165-83.
36. Parng, C.L., et al., *Gene conversion contributes to Ig light chain diversity in cattle.* J Immunol, 1996. 157(12): p. 5478-86.
37. Reynaud, C.A., et al., *Formation of the chicken B-cell repertoire: ontogenesis, regulation of Ig gene rearrangement, and diversification by gene conversion.* Adv Immunol, 1994. 57: p. 353-78.
38. Reynaud, C.A., et al., *A hyperconversion mechanism generates the chicken light chain preimmune repertoire.* Cell, 1987. 48(3): p. 379-88.
39. Thompson, C.B. and P.E. Neiman, *Somatic diversification of the chicken immunoglobulin light chain gene is limited to the rearranged variable gene segment.* Cell, 1987. 48(3): p. 369-78.
40. Carlson, L.M., et al., *Templated insertions in the rearranged chicken IgL V gene segment arise by intrachromosomal gene conversion.* Genes Dev, 1990. 4(4): p. 536-47.
41. Reynaud, C.A., et al., *Somatic hyperconversion diversifies the single Vh gene of the chicken with a high incidence in the D region.* Cell, 1989. 59(1): p. 171-83.
42. Reynaud, C.A., et al., *Somatic generation of diversity in a mammalian primary lymphoid organ: the sheep ileal Peyer's patches.* Cell, 1991. 64(5): p. 995-1005.

43. Arakawa, H., J. Hauschild, and J.M. Buerstedde, *Requirement of the activation-induced deaminase (AID) gene for immunoglobulin gene conversion.* Science, 2002. 295(5558): p. 1301-6.
44. Harris, R.S., et al., *AID is essential for immunoglobulin V gene conversion in a cultured B-cell line.* Curr Biol, 2002. 12(5): p. 435-8.
45. Conlon, T.M. and K.B. Meyer, *The chicken Ig light chain 3'-enhancer is essential for gene expression and regulates gene conversion via the transcription factor E2A.* Eur J Immunol, 2006. 36(1): p. 139-48.
46. Kothapalli, N., D.D. Norton, and S.D. Fugmann, *Cutting edge: a cis-acting DNA element targets AID-mediated sequence diversification to the chicken Ig light chain gene locus.* J Immunol, 2008. 180(4): p. 2019-23.
47. Rajewsky, K., I. Forster, and A. Cumano, *Evolutionary and somatic selection of the antibody repertoire in the mouse.* Science, 1987. 238(4830): p. 1088-94.
48. Peled, J.U., et al., *The biochemistry of somatic hypermutation.* Annu Rev Immunol, 2008. 26: p. 481-511.
49. Siskind, G.W. and B. Benacerraf, *Cell selection by antigen in the immune response.* Adv Immunol, 1969. 10: p. 1-50.
50. Sharpe, M.J., et al., *Somatic hypermutation of immunoglobulin kappa may depend on sequences 3' of C kappa and occurs on passenger transgenes.* EMBO J, 1991. 10(8): p. 2139-45.
51. Lebecque, S.G. and P.J. Gearhart, *Boundaries of somatic mutation in rearranged immunoglobulin genes: 5' boundary is near the promoter, and 3' boundary is approximately 1 kb from V(D)J gene.* J Exp Med, 1990. 172(6): p. 1717-27.
52. Both, G.W., et al., *Distribution of mutations around rearranged heavy-chain antibody variable-region genes.* Mol Cell Biol, 1990. 10(10): p. 5187-96.
53. Rada, C. and C. Milstein, *The intrinsic hypermutability of antibody heavy and light chain genes decays exponentially.* EMBO J, 2001. 20(16): p. 4570-6.
54. Longerich, S., et al., *The very 5' end and the constant region of Ig genes are spared from somatic mutation because AID does not access these regions.* J Exp Med, 2005. 202(10): p. 1443-54.
55. Betz, A.G., et al., *Passenger transgenes reveal intrinsic specificity of the antibody hypermutation mechanism: clustering, polarity, and specific hot spots.* Proc Natl Acad Sci U S A, 1993. 90(6): p. 2385-8.
56. Gonzalez-Fernandez, A., et al., *Somatic mutation of immunoglobulin lambda chains: a segment of the major intron hypermutates as much as the complementarity-determining regions.* Proc Natl Acad Sci U S A, 1994. 91(26): p. 12614-8.
57. Diaz, M., M.F. Flajnik, and N. Klinman, *Evolution and the molecular basis of somatic hypermutation of antigen receptor genes.* Philos Trans R Soc Lond B Biol Sci, 2001. 356(1405): p. 67-72.
58. Rogozin, I.B. and M. Diaz, *Cutting edge: DGYW/WRCH is a better predictor of mutability at G:C bases in Ig hypermutation than the widely accepted RGYW/WRCY motif and probably reflects a two-step activation-induced cytidine deaminase-triggered process.* J Immunol, 2004. 172(6): p. 3382-4.
59. Kinoshita, K. and T. Honjo, *Linking class-switch recombination with somatic hypermutation.* Nat Rev Mol Cell Biol, 2001. 2(7): p. 493-503.
60. Martin, A., et al., *Activation-induced cytidine deaminase turns on somatic hypermutation in hybridomas.* Nature, 2002. 415(6873): p. 802-6.
61. Golding, G.B., P.J. Gearhart, and B.W. Glickman, *Patterns of somatic mutations in immunoglobulin variable genes.* Genetics, 1987. 115(1): p. 169-76.
62. Fukita, Y., H. Jacobs, and K. Rajewsky, *Somatic hypermutation in the heavy chain locus correlates with transcription.* Immunity, 1998. 9(1): p. 105-14.

63. Peters, A. and U. Storb, *Somatic hypermutation of immunoglobulin genes is linked to transcription initiation.* Immunity, 1996. 4(1): p. 57-65.
64. Yoshikawa, K., et al., *AID enzyme-induced hypermutation in an actively transcribed gene in fibroblasts.* Science, 2002. 296(5575): p. 2033-6.
65. Muramatsu, M., et al., *Class switch recombination and hypermutation require activation-induced cytidine deaminase (AID), a potential RNA editing enzyme.* Cell, 2000. 102(5): p. 553-63.
66. Revy, P., et al., *Activation-induced cytidine deaminase (AID) deficiency causes the autosomal recessive form of the Hyper-IgM syndrome (HIGM2).* Cell, 2000. 102(5): p. 565-75.
67. Arakawa, H., H. Saribasak, and J.M. Buerstedde, *Activation-induced cytidine deaminase initiates immunoglobulin gene conversion and hypermutation by a common intermediate.* PLoS Biol, 2004. 2(7): p. E179.
68. Shen, H.M., et al., *Mutation of BCL-6 gene in normal B-cells by the process of somatic hypermutation of Ig genes.* Science, 1998. 280(5370): p. 1750-2.
69. Storb, U., et al., *Molecular aspects of somatic hypermutation of immunoglobulin genes.* Cold Spring Harb Symp Quant Biol, 1999. 64: p. 227-34.
70. Liu, M., et al., *Two levels of protection for the B-cell genome during somatic hypermutation.* Nature, 2008. 451(7180): p. 841-5.
71. Betz, A.G., et al., *Elements regulating somatic hypermutation of an immunoglobulin kappa gene: critical role for the intron enhancer/matrix attachment region.* Cell, 1994. 77(2): p. 239-48.
72. Klix, N., et al., *Multiple sequences from downstream of the J kappa cluster can combine to recruit somatic hypermutation to a heterologous, upstream mutation domain.* Eur J Immunol, 1998. 28(1): p. 317-26.
73. Michael, N., et al., *The E box motif CAGGTG enhances somatic hypermutation without enhancing transcription.* Immunity, 2003. 19(2): p. 235-42.
74. Kong, Q. and N. Maizels, *DNA breaks in hypermutating immunoglobulin genes: evidence for a break-and-repair pathway of somatic hypermutation.* Genetics, 2001. 158(1): p. 369-78.
75. Bross, L., et al., *DNA double-strand breaks in immunoglobulin genes undergoing somatic hypermutation.* Immunity, 2000. 13(5): p. 589-97.
76. Papavasiliou, F.N. and D.G. Schatz, *Cell-cycle-regulated DNA double-stranded breaks in somatic hypermutation of immunoglobulin genes.* Nature, 2000. 408(6809): p. 216-21.
77. Zan, H., et al., *AID-dependent generation of resected double-strand DNA breaks and recruitment of Rad52/Rad51 in somatic hypermutation.* Immunity, 2003. 18(6): p. 727-38.
78. Sale, J.E. and M.S. Neuberger, *TdT-accessible breaks are scattered over the immunoglobulin V domain in a constitutively hypermutating B-cell line.* Immunity, 1998. 9(6): p. 859-69.
79. Chua, K.F., F.W. Alt, and J.P. Manis, *The function of AID in somatic mutation and class switch recombination: upstream or downstream of DNA breaks.* J Exp Med, 2002. 195(9): p. F37-41.
80. Dunnick, W., et al., *DNA sequences at immunoglobulin switch region recombination sites.* Nucleic Acids Res, 1993. 21(3): p. 365-72.
81. Honjo, T., K. Kinoshita, and M. Muramatsu, *Molecular mechanism of class switch recombination: linkage with somatic hypermutation.* Annu Rev Immunol, 2002. 20: p. 165-96.

82. Stavnezer-Nordgren, J. and S. Sirlin, *Specificity of immunoglobulin heavy chain switch correlates with activity of germline heavy chain genes prior to switching.* EMBO J, 1986. 5(1): p. 95-102.
83. Rolink, A., F. Melchers, and J. Andersson, *The SCID but not the RAG-2 gene product is required for S mu-S epsilon heavy chain class switching.* Immunity, 1996. 5(4): p. 319-30.
84. Longerich, S., et al., *AID in somatic hypermutation and class switch recombination.* Curr Opin Immunol, 2006. 18(2): p. 164-74.
85. Okazaki, I.M., et al., *The AID enzyme induces class switch recombination in fibroblasts.* Nature, 2002. 416(6878): p. 340-5.
86. Manis, J.P., M. Tian, and F.W. Alt, *Mechanism and control of class-switch recombination.* Trends Immunol, 2002. 23(1): p. 31-9.
87. Chaudhuri, J., et al., *Transcription-targeted DNA deamination by the AID antibody diversification enzyme.* Nature, 2003. 422(6933): p. 726-30.
88. Chaudhuri, J. and F.W. Alt, *Class-switch recombination: interplay of transcription, DNA deamination and DNA repair.* Nat Rev Immunol, 2004. 4(7): p. 541-52.
89. Casellas, R., et al., *Ku80 is required for immunoglobulin isotype switching.* EMBO J, 1998. 17(8): p. 2404-11.
90. Stavnezer, J., J.E. Guikema, and C.E. Schrader, *Mechanism and regulation of class switch recombination.* Annu Rev Immunol, 2008. 26: p. 261-92.
91. Akashi, K., et al., *Lymphoid development from stem cells and the common lymphocyte progenitors.* Cold Spring Harb Symp Quant Biol, 1999. 64: p. 1-12.
92. ten Boekel, E., F. Melchers, and A. Rolink, *The status of Ig loci rearrangements in single cells from different stages of B-cell development.* Int Immunol, 1995. 7(6): p. 1013-9.
93. Casellas, R., et al., *Contribution of receptor editing to the antibody repertoire.* Science, 2001. 291(5508): p. 1541-4.
94. Hardy, R.R. and K. Hayakawa, *B-cell development pathways.* Annu Rev Immunol, 2001. 19: p. 595-621.
95. Berek, C., A. Berger, and M. Apel, *Maturation of the immune response in germinal centers.* Cell, 1991. 67(6): p. 1121-9.
96. Ziegner, M., G. Steinhauser, and C. Berek, *Development of antibody diversity in single germinal centers: selective expansion of high-affinity variants.* Eur J Immunol, 1994. 24(10): p. 2393-400.
97. Jacob, J., et al., *Intraclonal generation of antibody mutants in germinal centres.* Nature, 1991. 354(6352): p. 389-92.
98. Honjo, T. and T. Kataoka, *Organization of immunoglobulin heavy chain genes and allelic deletion model.* Proc Natl Acad Sci U S A, 1978. 75(5): p. 2140-4.
99. Rajewsky, K., *Clonal selection and learning in the antibody system.* Nature, 1996. 381(6585): p. 751-8.
100. Cunningham, A.F., et al., *Salmonella induces a switched antibody response without germinal centers that impedes the extracellular spread of infection.* J Immunol, 2007. 178(10): p. 6200-7.
101. Pape, K.A., et al., *Visualization of the genesis and fate of isotype-switched B-cells during a primary immune response.* J Exp Med, 2003. 197(12): p. 1677-87.
102. Brenner, S. and C. Milstein, *Origin of antibody variation.* Nature, 1966. 211(5046): p. 242-3.
103. Kuppers, R., et al., *Tracing B-cell development in human germinal centres by molecular analysis of single cells picked from histological sections.* EMBO J, 1993. 12(13): p. 4955-67.

104. Reynaud, C.A., et al., *Hypermutation generating the sheep immunoglobulin repertoire is an antigen-independent process.* Cell, 1995. 80(1): p. 115-25.
105. Jenne, C.N., L.J. Kennedy, and J.D. Reynolds, *Antibody repertoire development in the sheep.* Dev Comp Immunol, 2006. 30(1-2): p. 165-74.
106. Becker, R.S. and K.L. Knight, *Somatic diversification of immunoglobulin heavy chain VDJ genes: evidence for somatic gene conversion in rabbits.* Cell, 1990. 63(5): p. 987-97.
107. Weill, J.C. and C.A. Reynaud, *The chicken B-cell compartment.* Science, 1987. 238(4830): p. 1094-8.
108. Reynaud, C.A., et al., *Emergence of committed B lymphoid progenitors in the developing chicken embryo.* EMBO J, 1992. 11(12): p. 4349-58.
109. Kohonen, P., K.P. Nera, and O. Lassila, *Avian model for B-cell immunology--new genomes and phylotranscriptomics.* Scand J Immunol, 2007. 66(2-3): p. 113-21.
110. Pink, J.R., O. Vainio, and A.M. Rijnbeek, *Clones of B lymphocytes in individual follicles of the bursa of Fabricius.* Eur J Immunol, 1985. 15(1): p. 83-7.
111. Weill, J.C., S. Weller, and C.A. Reynaud, *A bird's eye view on human B-cells.* Semin Immunol, 2004. 16(4): p. 277-81.
112. Mansikka, A., et al., *Rearrangement of immunoglobulin light chain genes in the chicken occurs prior to colonization of the embryonic bursa of Fabricius.* Proc Natl Acad Sci U S A, 1990. 87(23): p. 9416-20.
113. Arakawa, H., et al., *Effect of environmental antigens on the Ig diversification and the selection of productive V-J joints in the bursa.* J Immunol, 2002. 169(2): p. 818-28.
114. Arakawa, H., et al., *Immunoglobulin gene hyperconversion ongoing in chicken splenic germinal centers.* EMBO J, 1996. 15(10): p. 2540-6.
115. Arakawa, H., et al., *Oligoclonal development of B-cells bearing discrete Ig chains in chicken single germinal centers.* J Immunol, 1998. 160(9): p. 4232-41.
116. Baba, T.W., B.P. Giroir, and E.H. Humphries, *Cell lines derived from avian lymphomas exhibit two distinct phenotypes.* Virology, 1985. 144(1): p. 139-51.
117. Hayward, W.S., B.G. Neel, and S.M. Astrin, *Activation of a cellular onc gene by promoter insertion in ALV-induced lymphoid leukosis.* Nature, 1981. 290(5806): p. 475-80.
118. Kim, S., et al., *Ongoing diversification of the rearranged immunoglobulin light-chain gene in a bursal lymphoma cell line.* Mol Cell Biol, 1990. 10(6): p. 3224-31.
119. Sale, J.E., *Immunoglobulin diversification in DT40: a model for vertebrate DNA damage tolerance.* DNA Repair (Amst), 2004. 3(7): p. 693-702.
120. Schubach, W. and M. Groudine, *Alteration of c-myc chromatin structure by avian leukosis virus integration.* Nature, 1984. 307(5953): p. 702-8.
121. Yamazoe, M., et al., *Reverse genetic studies of the DNA damage response in the chicken B lymphocyte line DT40.* DNA Repair (Amst), 2004. 3(8-9): p. 1175-85.
122. Buerstedde, J.M., et al., *Light chain gene conversion continues at high rate in an ALV-induced cell line.* EMBO J, 1990. 9(3): p. 921-7.
123. Smithies, O., et al., *Insertion of DNA sequences into the human chromosomal beta-globin locus by homologous recombination.* Nature, 1985. 317(6034): p. 230-4.
124. Thomas, K.R., K.R. Folger, and M.R. Capecchi, *High frequency targeting of genes to specific sites in the mammalian genome.* Cell, 1986. 44(3): p. 419-28.
125. Buerstedde, J.M. and S. Takeda, *Increased ratio of targeted to random integration after transfection of chicken B-cell lines.* Cell, 1991. 67(1): p. 179-88.
126. Takeda, S., et al., *RAG-2 expression is not essential for chicken immunoglobulin gene conversion.* Proc Natl Acad Sci U S A, 1992. 89(9): p. 4023-7.
127. Winding, P. and M.W. Berchtold, *The chicken B-cell line DT40: a novel tool for gene disruption experiments.* J Immunol Methods, 2001. 249(1-2): p. 1-16.

128. Arakawa, H. and J.M. Buerstedde, *Review. Activation-induced cytidine deaminase-mediated hypermutation in the DT40 cell line.* Philos Trans R Soc Lond B Biol Sci, 2008.
129. Sonoda, E., et al., *Reverse genetic studies of homologous DNA recombination using the chicken B-lymphocyte line, DT40.* Philos Trans R Soc Lond B Biol Sci, 2001. 356(1405): p. 111-7.
130. West, S.C., *Molecular views of recombination proteins and their control.* Nat Rev Mol Cell Biol, 2003. 4(6): p. 435-45.
131. Jasin, M., *Homologous repair of DNA damage and tumorigenesis: the BRCA connection.* Oncogene, 2002. 21(58): p. 8981-93.
132. Hatanaka, A., et al., *Similar effects of Brca2 truncation and Rad51 paralog deficiency on immunoglobulin V gene diversification in DT40 cells support an early role for Rad51 paralogs in homologous recombination.* Mol Cell Biol, 2005. 25(3): p. 1124-34.
133. Solinger, J.A., K. Kiianitsa, and W.D. Heyer, *Rad54, a Swi2/Snf2-like recombinational repair protein, disassembles Rad51:dsDNA filaments.* Mol Cell, 2002. 10(5): p. 1175-88.
134. Tauchi, H., et al., *Nbs1 is essential for DNA repair by homologous recombination in higher vertebrate cells.* Nature, 2002. 420(6911): p. 93-8.
135. Bezzubova, O., et al., *Reduced X-ray resistance and homologous recombination frequencies in a RAD54-/- mutant of the chicken DT40 cell line.* Cell, 1997. 89(2): p. 185-93.
136. Takata, M., et al., *Chromosome instability and defective recombinational repair in knockout mutants of the five Rad51 paralogs.* Mol Cell Biol, 2001. 21(8): p. 2858-66.
137. Sale, J.E., et al., *Ablation of XRCC2/3 transforms immunoglobulin V gene conversion into somatic hypermutation.* Nature, 2001. 412(6850): p. 921-6.
138. Bachl, J. and M. Wabl, *An immunoglobulin mutator that targets G.C base pairs.* Proc Natl Acad Sci U S A, 1996. 93(2): p. 851-5.
139. Faili, A., et al., *AID-dependent somatic hypermutation occurs as a DNA single-strand event in the BL2 cell line.* Nat Immunol, 2002. 3(9): p. 815-21.
140. Yamamoto, K., et al., *Fanconi anemia protein FANCD2 promotes immunoglobulin gene conversion and DNA repair through a mechanism related to homologous recombination.* Mol Cell Biol, 2005. 25(1): p. 34-43.
141. Muramatsu, M., et al., *Specific expression of activation-induced cytidine deaminase (AID), a novel member of the RNA-editing deaminase family in germinal center B-cells.* J Biol Chem, 1999. 274(26): p. 18470-6.
142. Muramatsu, M., et al., *Discovery of activation-induced cytidine deaminase, the engraver of antibody memory.* Adv Immunol, 2007. 94: p. 1-36.
143. Petersen-Mahrt, S.K., R.S. Harris, and M.S. Neuberger, *AID mutates E. coli suggesting a DNA deamination mechanism for antibody diversification.* Nature, 2002. 418(6893): p. 99-103.
144. Sohail, A., et al., *Human activation-induced cytidine deaminase causes transcription-dependent, strand-biased C to U deaminations.* Nucleic Acids Res, 2003. 31(12): p. 2990-4.
145. Shen, H.M., S. Ratnam, and U. Storb, *Targeting of the activation-induced cytosine deaminase is strongly influenced by the sequence and structure of the targeted DNA.* Mol Cell Biol, 2005. 25(24): p. 10815-21.
146. Yu, K., F.T. Huang, and M.R. Lieber, *DNA substrate length and surrounding sequence affect the activation-induced deaminase activity at cytidine.* J Biol Chem, 2004. 279(8): p. 6496-500.

147. Di Noia, J. and M.S. Neuberger, *Altering the pathway of immunoglobulin hypermutation by inhibiting uracil-DNA glycosylase.* Nature, 2002. 419(6902): p. 43-8.
148. Neuberger, M.S., et al., *Immunity through DNA deamination.* Trends Biochem Sci, 2003. 28(6): p. 305-12.
149. Bransteitter, R., et al., *Activation-induced cytidine deaminase deaminates deoxycytidine on single-stranded DNA but requires the action of RNase.* Proc Natl Acad Sci U S A, 2003. 100(7): p. 4102-7.
150. Dickerson, S.K., et al., *AID mediates hypermutation by deaminating single stranded DNA.* J Exp Med, 2003. 197(10): p. 1291-6.
151. Besmer, E., E. Market, and F.N. Papavasiliou, *The transcription elongation complex directs activation-induced cytidine deaminase-mediated DNA deamination.* Mol Cell Biol, 2006. 26(11): p. 4378-85.
152. Ramiro, A.R., et al., *Transcription enhances AID-mediated cytidine deamination by exposing single-stranded DNA on the nontemplate strand.* Nat Immunol, 2003. 4(5): p. 452-6.
153. Chaudhuri, J., C. Khuong, and F.W. Alt, *Replication protein A interacts with AID to promote deamination of somatic hypermutation targets.* Nature, 2004. 430(7003): p. 992-8.
154. Basu, U., et al., *The AID antibody diversification enzyme is regulated by protein kinase A phosphorylation.* Nature, 2005. 438(7067): p. 508-11.
155. Pasqualucci, L., et al., *PKA-mediated phosphorylation regulates the function of activation-induced deaminase (AID) in B-cells.* Proc Natl Acad Sci U S A, 2006. 103(2): p. 395-400.
156. Odegard, V.H. and D.G. Schatz, *Targeting of somatic hypermutation.* Nat Rev Immunol, 2006. 6(8): p. 573-83.
157. Okazaki, I.M., et al., *Constitutive expression of AID leads to tumorigenesis.* J Exp Med, 2003. 197(9): p. 1173-81.
158. Barreto, V., et al., *C-terminal deletion of AID uncouples class switch recombination from somatic hypermutation and gene conversion.* Mol Cell, 2003. 12(2): p. 501-8.
159. Shinkura, R., et al., *Separate domains of AID are required for somatic hypermutation and class-switch recombination.* Nat Immunol, 2004. 5(7): p. 707-12.
160. Ta, V.T., et al., *AID mutant analyses indicate requirement for class-switch-specific cofactors.* Nat Immunol, 2003. 4(9): p. 843-8.
161. Brar, S.S., M. Watson, and M. Diaz, *Activation-induced cytosine deaminase (AID) is actively exported out of the nucleus but retained by the induction of DNA breaks.* J Biol Chem, 2004. 279(25): p. 26395-401.
162. Ito, S., et al., *Activation-induced cytidine deaminase shuttles between nucleus and cytoplasm like apolipoprotein B mRNA editing catalytic polypeptide 1.* Proc Natl Acad Sci U S A, 2004. 101(7): p. 1975-80.
163. McBride, K.M., et al., *Somatic hypermutation is limited by CRM1-dependent nuclear export of activation-induced deaminase.* J Exp Med, 2004. 199(9): p. 1235-44.
164. Rada, C., J.M. Jarvis, and C. Milstein, *AID-GFP chimeric protein increases hypermutation of Ig genes with no evidence of nuclear localization.* Proc Natl Acad Sci U S A, 2002. 99(10): p. 7003-8.
165. Lindahl, T., *Suppression of spontaneous mutagenesis in human cells by DNA base excision-repair.* Mutat Res, 2000. 462(2-3): p. 129-35.
166. Nilsen, H., et al., *Nuclear and mitochondrial uracil-DNA glycosylases are generated by alternative splicing and transcription from different positions in the UNG gene.* Nucleic Acids Res, 1997. 25(4): p. 750-5.

167. Pearl, L.H., *Structure and function in the uracil-DNA glycosylase superfamily.* Mutat Res, 2000. 460(3-4): p. 165-81.
168. Martomo, S.A., et al., *Deoxyuridine is generated preferentially in the nontranscribed strand of DNA from cells expressing activation-induced cytidine deaminase.* J Immunol, 2005. 174(12): p. 7787-91.
169. Di Noia, J.M. and M.S. Neuberger, *Immunoglobulin gene conversion in chicken DT40 cells largely proceeds through an abasic site intermediate generated by excision of the uracil produced by AID-mediated deoxycytidine deamination.* Eur J Immunol, 2004. 34(2): p. 504-8.
170. Imai, K., et al., *Human uracil-DNA glycosylase deficiency associated with profoundly impaired immunoglobulin class-switch recombination.* Nat Immunol, 2003. 4(10): p. 1023-8.
171. Rada, C., et al., *Immunoglobulin isotype switching is inhibited and somatic hypermutation perturbed in UNG-deficient mice.* Curr Biol, 2002. 12(20): p. 1748-55.
172. Saribasak, H., et al., *Uracil DNA glycosylase disruption blocks Ig gene conversion and induces transition mutations.* J Immunol, 2006. 176(1): p. 365-71.
173. Bardwell, P.D., et al., *Cutting edge: the G-U mismatch glycosylase methyl-CpG binding domain 4 is dispensable for somatic hypermutation and class switch recombination.* J Immunol, 2003. 170(4): p. 1620-4.
174. Di Noia, J.M., C. Rada, and M.S. Neuberger, *SMUG1 is able to excise uracil from immunoglobulin genes: insight into mutation versus repair.* EMBO J, 2006. 25(3): p. 585-95.
175. Rada, C., J.M. Di Noia, and M.S. Neuberger, *Mismatch recognition and uracil excision provide complementary paths to both Ig switching and the A/T-focused phase of somatic mutation.* Mol Cell, 2004. 16(2): p. 163-71.
176. Pham, P., et al., *Processive AID-catalysed cytosine deamination on single-stranded DNA simulates somatic hypermutation.* Nature, 2003. 424(6944): p. 103-7.
177. Krokan, H.E., F. Drablos, and G. Slupphaug, *Uracil in DNA--occurrence, consequences and repair.* Oncogene, 2002. 21(58): p. 8935-48.
178. Otterlei, M., et al., *Post-replicative base excision repair in replication foci.* EMBO J, 1999. 18(13): p. 3834-44.
179. Jiricny, J., *The multifaceted mismatch-repair system.* Nat Rev Mol Cell Biol, 2006. 7(5): p. 335-46.
180. Nielsen, F.C., et al., *Characterization of human exonuclease 1 in complex with mismatch repair proteins, subcellular localization and association with PCNA.* Oncogene, 2004. 23(7): p. 1457-68.
181. Bardwell, P.D., et al., *Altered somatic hypermutation and reduced class-switch recombination in exonuclease 1-mutant mice.* Nat Immunol, 2004. 5(2): p. 224-9.
182. Neuberger, M.S. and C. Rada, *Somatic hypermutation: activation-induced deaminase for C/G followed by polymerase eta for A/T.* J Exp Med, 2007. 204(1): p. 7-10.
183. Wilson, T.M., et al., *MSH2-MSH6 stimulates DNA polymerase eta, suggesting a role for A:T mutations in antibody genes.* J Exp Med, 2005. 201(4): p. 637-45.
184. Cascalho, M., et al., *Mismatch repair co-opted by hypermutation.* Science, 1998. 279(5354): p. 1207-10.
185. Phung, Q.H., et al., *Increased hypermutation at G and C nucleotides in immunoglobulin variable genes from mice deficient in the MSH2 mismatch repair protein.* J Exp Med, 1998. 187(11): p. 1745-51.
186. Reynaud, C.A., et al., *Mismatch repair and immunoglobulin gene hypermutation: did we learn something?* Immunol Today, 1999. 20(11): p. 522-7.
187. Wiesendanger, M., et al., *Somatic hypermutation in MutS homologue (MSH)3-, MSH6-, and MSH3/MSH6-deficient mice reveals a role for the MSH2-MSH6*

heterodimer in modulating the base substitution pattern. J Exp Med, 2000. 191(3): p. 579-84.
188. Kim, N., et al., *Different mismatch repair deficiencies all have the same effects on somatic hypermutation: intact primary mechanism accompanied by secondary modifications.* J Exp Med, 1999. 190(1): p. 21-30.
189. Martin, A. and M.D. Scharff, *AID and mismatch repair in antibody diversification.* Nat Rev Immunol, 2002. 2(8): p. 605-14.
190. Surtees, J.A., J.L. Argueso, and E. Alani, *Mismatch repair proteins: key regulators of genetic recombination.* Cytogenet Genome Res, 2004. 107(3-4): p. 146-59.
191. Vallur, A.C. and N. Maizels, *Activities of human exonuclease 1 that promote cleavage of transcribed immunoglobulin switch regions.* Proc Natl Acad Sci U S A, 2008. 105(43): p. 16508-12.
192. Shen, H.M., et al., *Somatic hypermutation and class switch recombination in Msh6(-/-)Ung(-/-) double-knockout mice.* J Immunol, 2006. 177(8): p. 5386-92.
193. Martomo, S.A., W.W. Yang, and P.J. Gearhart, *A role for Msh6 but not Msh3 in somatic hypermutation and class switch recombination.* J Exp Med, 2004. 200(1): p. 61-8.
194. Prakash, S., R.E. Johnson, and L. Prakash, *Eukaryotic translesion synthesis DNA polymerases: specificity of structure and function.* Annu Rev Biochem, 2005. 74: p. 317-53.
195. Goodman, M.F., *Error-prone repair DNA polymerases in prokaryotes and eukaryotes.* Annu Rev Biochem, 2002. 71: p. 17-50.
196. Fischhaber, P.L. and E.C. Friedberg, *How are specialized (low-fidelity) eukaryotic polymerases selected and switched with high-fidelity polymerases during translesion DNA synthesis?* DNA Repair (Amst), 2005. 4(2): p. 279-83.
197. Friedberg, E.C., A.R. Lehmann, and R.P. Fuchs, *Trading places: how do DNA polymerases switch during translesion DNA synthesis?* Mol Cell, 2005. 18(5): p. 499-505.
198. Zan, H., et al., *The translesion DNA polymerase zeta plays a major role in Ig and bcl-6 somatic hypermutation.* Immunity, 2001. 14(5): p. 643-53.
199. Zeng, X., et al., *DNA polymerase eta is an A-T mutator in somatic hypermutation of immunoglobulin variable genes.* Nat Immunol, 2001. 2(6): p. 537-41.
200. Delbos, F., et al., *Contribution of DNA polymerase eta to immunoglobulin gene hypermutation in the mouse.* J Exp Med, 2005. 201(8): p. 1191-6.
201. Martomo, S.A., et al., *Different mutation signatures in DNA polymerase eta- and MSH6-deficient mice suggest separate roles in antibody diversification.* Proc Natl Acad Sci U S A, 2005. 102(24): p. 8656-61.
202. McDonald, J.P., et al., *129-derived strains of mice are deficient in DNA polymerase iota and have normal immunoglobulin hypermutation.* J Exp Med, 2003. 198(4): p. 635-43.
203. Martomo, S.A., et al., *Normal hypermutation in antibody genes from congenic mice defective for DNA polymerase iota.* DNA Repair (Amst), 2006. 5(3): p. 392-8.
204. Simpson, L.J. and J.E. Sale, *Rev1 is essential for DNA damage tolerance and non-templated immunoglobulin gene mutation in a vertebrate cell line.* EMBO J, 2003. 22(7): p. 1654-64.
205. Arakawa, H., et al., *A role for PCNA ubiquitination in immunoglobulin hypermutation.* PLoS Biol, 2006. 4(11): p. e366.
206. Jansen, J.G., et al., *Strand-biased defect in C/G transversions in hypermutating immunoglobulin genes in Rev1-deficient mice.* J Exp Med, 2006. 203(2): p. 319-23.
207. Seki, M., et al., *High-efficiency bypass of DNA damage by human DNA polymerase Q.* EMBO J, 2004. 23(22): p. 4484-94.

208. Zan, H., et al., *The translesion DNA polymerase theta plays a dominant role in immunoglobulin gene somatic hypermutation.* EMBO J, 2005. 24(21): p. 3757-69.
209. Casali, P., et al., *DNA repair in antibody somatic hypermutation.* Trends Immunol, 2006. 27(7): p. 313-21.
210. Maga, G. and U. Hubscher, *Proliferating cell nuclear antigen (PCNA): a dancer with many partners.* J Cell Sci, 2003. 116(Pt 15): p. 3051-60.
211. Hoege, C., et al., *RAD6-dependent DNA repair is linked to modification of PCNA by ubiquitin and SUMO.* Nature, 2002. 419(6903): p. 135-41.
212. Kannouche, P.L., J. Wing, and A.R. Lehmann, *Interaction of human DNA polymerase eta with monoubiquitinated PCNA: a possible mechanism for the polymerase switch in response to DNA damage.* Mol Cell, 2004. 14(4): p. 491-500.
213. Garg, P., et al., *Proliferating cell nuclear antigen promotes translesion synthesis by DNA polymerase zeta.* J Biol Chem, 2005. 280(25): p. 23446-50.
214. Garg, P. and P.M. Burgers, *Ubiquitinated proliferating cell nuclear antigen activates translesion DNA polymerases eta and REV1.* Proc Natl Acad Sci U S A, 2005. 102(51): p. 18361-6.
215. Haracska, L., et al., *Interaction with PCNA is essential for yeast DNA polymerase eta function.* Mol Cell, 2001. 8(2): p. 407-15.
216. Langerak, P., et al., *A/T mutagenesis in hypermutated immunoglobulin genes strongly depends on PCNAK164 modification.* J Exp Med, 2007. 204(8): p. 1989-98.
217. Bachl, J., I. Ertongur, and B. Jungnickel, *Involvement of Rad18 in somatic hypermutation.* Proc Natl Acad Sci U S A, 2006. 103(32): p. 12081-6.
218. Clark, A.B., et al., *Functional interaction of proliferating cell nuclear antigen with MSH2-MSH6 and MSH2-MSH3 complexes.* J Biol Chem, 2000. 275(47): p. 36498-501.
219. Flores-Rozas, H., D. Clark, and R.D. Kolodner, *Proliferating cell nuclear antigen and Msh2p-Msh6p interact to form an active mispair recognition complex.* Nat Genet, 2000. 26(3): p. 375-8.
220. Lee, S.D. and E. Alani, *Analysis of interactions between mismatch repair initiation factors and the replication processivity factor PCNA.* J Mol Biol, 2006. 355(2): p. 175-84.
221. Pasqualucci, L., et al., *Hypermutation of multiple proto-oncogenes in B-cell diffuse large-cell lymphomas.* Nature, 2001. 412(6844): p. 341-6.
222. Gopal, A.R. and S.D. Fugmann, *AID-mediated diversification within the IgL locus of chicken DT40 cells is restricted to the transcribed IgL gene.* Mol Immunol, 2008. 45(7): p. 2062-8.
223. Gordon, M.S., et al., *Somatic hypermutation of the B-cell receptor genes B29 (Igbeta, CD79b) and mb1 (Igalpha, CD79a).* Proc Natl Acad Sci U S A, 2003. 100(7): p. 4126-31.
224. Muschen, M., et al., *Somatic mutation of the CD95 gene in human B-cells as a side-effect of the germinal center reaction.* J Exp Med, 2000. 192(12): p. 1833-40.
225. Pasqualucci, L., et al., *BCL-6 mutations in normal germinal center B-cells: evidence of somatic hypermutation acting outside Ig loci.* Proc Natl Acad Sci U S A, 1998. 95(20): p. 11816-21.
226. Parsa, J.Y., et al., *AID mutates a non-immunoglobulin transgene independent of chromosomal position.* Mol Immunol, 2007. 44(4): p. 567-75.
227. Wang, C.L., R.A. Harper, and M. Wabl, *Genome-wide somatic hypermutation.* Proc Natl Acad Sci U S A, 2004. 101(19): p. 7352-6.
228. Warren, J.J., et al., *Structure of the human MutSalpha DNA lesion recognition complex.* Mol Cell, 2007. 26(4): p. 579-92.

229. Yang, S.Y. and D.G. Schatz, *Targeting of AID-mediated sequence diversification by cis-acting determinants.* Adv Immunol, 2007. 94: p. 109-25.
230. Michael, N., et al., *Effects of sequence and structure on the hypermutability of immunoglobulin genes.* Immunity, 2002. 16(1): p. 123-34.
231. Tumas-Brundage, K. and T. Manser, *The transcriptional promoter regulates hypermutation of the antibody heavy chain locus.* J Exp Med, 1997. 185(2): p. 239-50.
232. Bachl, J. and M. Wabl, *Enhancers of hypermutation.* Immunogenetics, 1996. 45(1): p. 59-64.
233. Lin, M.M., et al., *The effects of E mu, 3'alpha (hs 1,2) and 3'kappa enhancers on mutation of an Ig-VDJ-Cgamma2a Ig heavy gene in cultured B-cells.* Int Immunol, 1998. 10(8): p. 1121-9.
234. Goyenechea, B., et al., *Cells strongly expressing Ig(kappa) transgenes show clonal recruitment of hypermutation: a role for both MAR and the enhancers.* EMBO J, 1997. 16(13): p. 3987-94.
235. Inlay, M.A., et al., *Roles of the Ig kappa light chain intronic and 3' enhancers in Igk somatic hypermutation.* J Immunol, 2006. 177(2): p. 1146-51.
236. van der Stoep, N., J.R. Gorman, and F.W. Alt, *Reevaluation of 3'Ekappa function in stage- and lineage-specific rearrangement and somatic hypermutation.* Immunity, 1998. 8(6): p. 743-50.
237. Morvan, C.L., et al., *The immunoglobulin heavy-chain locus hs3b and hs4 3' enhancers are dispensable for VDJ assembly and somatic hypermutation.* Blood, 2003. 102(4): p. 1421-7.
238. Terauchi, A., et al., *A pivotal role for DNase I-sensitive regions 3b and/or 4 in the induction of somatic hypermutation of IgH genes.* J Immunol, 2001. 167(2): p. 811-20.
239. Ronai, D., et al., *Complex regulation of somatic hypermutation by cis-acting sequences in the endogenous IgH gene in hybridoma cells.* Proc Natl Acad Sci U S A, 2005. 102(33): p. 11829-34.
240. Komori, A., et al., *Biased dA/dT somatic hypermutation as regulated by the heavy chain intronic iEmu enhancer and 3'Ealpha enhancers in human lymphoblastoid B-cells.* Mol Immunol, 2006. 43(11): p. 1817-26.
241. Yu, K. and M.R. Lieber, *Nucleic acid structures and enzymes in the immunoglobulin class switch recombination mechanism.* DNA Repair (Amst), 2003. 2(11): p. 1163-74.
242. Duquette, M.L., et al., *AID binds to transcription-induced structures in c-MYC that map to regions associated with translocation and hypermutation.* Oncogene, 2005. 24(38): p. 5791-8.
243. Ronai, D., et al., *Detection of chromatin-associated single-stranded DNA in regions targeted for somatic hypermutation.* J Exp Med, 2007. 204(1): p. 181-90.
244. Schoetz, U., et al., *E2A expression stimulates Ig hypermutation.* J Immunol, 2006. 177(1): p. 395-400.
245. Nambu, Y., et al., *Transcription-coupled events associating with immunoglobulin switch region chromatin.* Science, 2003. 302(5653): p. 2137-40.
246. Storb, U., et al., *Targeting of AID to immunoglobulin genes.* Adv Exp Med Biol, 2007. 596: p. 83-91.
247. Kurdistani, S.K. and M. Grunstein, *Histone acetylation and deacetylation in yeast.* Nat Rev Mol Cell Biol, 2003. 4(4): p. 276-84.
248. Fraenkel, S., et al., *Allelic 'choice' governs somatic hypermutation in vivo at the immunoglobulin kappa-chain locus.* Nat Immunol, 2007. 8(7): p. 715-22.
249. Larijani, M., et al., *Methylation protects cytidines from AID-mediated deamination.* Mol Immunol, 2005. 42(5): p. 599-604.

250. Li, Z., Z. Luo, and M.D. Scharff, *Differential regulation of histone acetylation and generation of mutations in switch regions is associated with Ig class switching.* Proc Natl Acad Sci U S A, 2004. 101(43): p. 15428-33.
251. Wang, L., et al., *AID-dependent histone acetylation is detected in immunoglobulin S-regions.* J Exp Med, 2006. 203(1): p. 215-26.
252. Hesslein, D.G. and D.G. Schatz, *Factors and forces controlling V(D)J recombination.* Adv Immunol, 2001. 78: p. 169-232.
253. Woo, C.J., A. Martin, and M.D. Scharff, *Induction of somatic hypermutation is associated with modifications in immunoglobulin variable region chromatin.* Immunity, 2003. 19(4): p. 479-89.
254. Odegard, V.H., et al., *Histone modifications associated with somatic hypermutation.* Immunity, 2005. 23(1): p. 101-10.
255. Delbos, F., et al., *DNA polymerase eta is the sole contributor of A/T modifications during immunoglobulin gene hypermutation in the mouse.* J Exp Med, 2007. 204(1): p. 17-23.
256. Faili, A., et al., *Induction of somatic hypermutation in immunoglobulin genes is dependent on DNA polymerase iota.* Nature, 2002. 419(6910): p. 944-7.
257. Fernandez-Capetillo, O., C.D. Allis, and A. Nussenzweig, *Phosphorylation of histone H2B at DNA double-strand breaks.* J Exp Med, 2004. 199(12): p. 1671-7.
258. Petersen, S., et al., *AID is required to initiate Nbs1/gamma-H2AX focus formation and mutations at sites of class switching.* Nature, 2001. 414(6864): p. 660-5.
259. Cattoretti, G., et al., *Nuclear and cytoplasmic AID in extrafollicular and germinal center B-cells.* Blood, 2006. 107(10): p. 3967-75.
260. Yang, G., et al., *Activation-induced deaminase cloning, localization, and protein extraction from young VH-mutant rabbit appendix.* Proc Natl Acad Sci U S A, 2005. 102(47): p. 17083-8.
261. Giusti, A.M. and T. Manser, *Hypermutation is observed only in antibody H chain V region transgenes that have recombined with endogenous immunoglobulin H DNA: implications for the location of cis-acting elements required for somatic mutation.* J Exp Med, 1993. 177(3): p. 797-809.
262. Kosak, S.T., et al., *Subnuclear compartmentalization of immunoglobulin loci during lymphocyte development.* Science, 2002. 296(5565): p. 158-62.
263. Osborne, C.S., et al., *Myc dynamically and preferentially relocates to a transcription factory occupied by Igh.* PLoS Biol, 2007. 5(8): p. e192.
264. Minshull, J. and W.P. Stemmer, *Protein evolution by molecular breeding.* Curr Opin Chem Biol, 1999. 3(3): p. 284-90.
265. Petrounia, I.P. and F.H. Arnold, *Designed evolution of enzymatic properties.* Curr Opin Biotechnol, 2000. 11(4): p. 325-30.
266. Matsuura, T. and T. Yomo, *In vitro evolution of proteins.* J Biosci Bioeng, 2006. 101(6): p. 449-56.
267. Dufner, P., L. Jermutus, and R.R. Minter, *Harnessing phage and ribosome display for antibody optimisation.* Trends Biotechnol, 2006. 24(11): p. 523-9.
268. Greener, A., M. Callahan, and B. Jerpseth, *An efficient random mutagenesis technique using an E. coli mutator strain.* Mol Biotechnol, 1997. 7(2): p. 189-95.
269. Chalfie, M., et al., *Green fluorescent protein as a marker for gene expression.* Science, 1994. 263(5148): p. 802-5.
270. Prasher, D.C., et al., *Primary structure of the Aequorea victoria green-fluorescent protein.* Gene, 1992. 111(2): p. 229-33.
271. Shimomura, O., F.H. Johnson, and Y. Saiga, *Extraction, purification and properties of aequorin, a bioluminescent protein from the luminous hydromedusan, Aequorea.* J Cell Comp Physiol, 1962. 59: p. 223-39.

272. Delagrave, S., et al., *Red-shifted excitation mutants of the green fluorescent protein.* Biotechnology (N Y), 1995. 13(2): p. 151-4.
273. Zolotukhin, S., et al., *A "humanized" green fluorescent protein cDNA adapted for high-level expression in mammalian cells.* J Virol, 1996. 70(7): p. 4646-54.
274. Muhlrad, D., R. Hunter, and R. Parker, *A rapid method for localized mutagenesis of yeast genes.* Yeast, 1992. 8(2): p. 79-82.
275. Zacharias, D.A. and R.Y. Tsien, *Molecular biology and mutation of green fluorescent protein.* Methods Biochem Anal, 2006. 47: p. 83-120.
276. Chudakov, D.M., S. Lukyanov, and K.A. Lukyanov, *Fluorescent proteins as a toolkit for in vivo imaging.* Trends Biotechnol, 2005. 23(12): p. 605-13.
277. Patterson, G.H., et al., *Use of the green fluorescent protein and its mutants in quantitative fluorescence microscopy.* Biophys J, 1997. 73(5): p. 2782-90.
278. Cubitt, A.B., L.A. Woollenweber, and R. Heim, *Understanding structure-function relationships in the Aequorea victoria green fluorescent protein.* Methods Cell Biol, 1999. 58: p. 19-30.
279. Wang, C.L., D.C. Yang, and M. Wabl, *Directed molecular evolution by somatic hypermutation.* Protein Eng Des Sel, 2004. 17(9): p. 659-64.
280. Fradkov, A.F., et al., *Far-red fluorescent tag for protein labelling.* Biochem J, 2002. 368(Pt 1): p. 17-21.
281. Shcherbo, D., et al., *Bright far-red fluorescent protein for whole-body imaging.* Nat Methods, 2007. 4(9): p. 741-6.
282. Konig, K., *Multiphoton microscopy in life sciences.* J Microsc, 2000. 200(Pt 2): p. 83-104.
283. Gurskaya, N.G., et al., *GFP-like chromoproteins as a source of far-red fluorescent proteins.* FEBS Lett, 2001. 507(1): p. 16-20.
284. Shkrob, M.A., et al., *Far-red fluorescent proteins evolved from a blue chromoprotein from Actinia equina.* Biochem J, 2005. 392(Pt 3): p. 649-54.
285. Wang, L., et al., *Evolution of new nonantibody proteins via iterative somatic hypermutation.* Proc Natl Acad Sci U S A, 2004. 101(48): p. 16745-9.
286. Merzlyak, E.M., et al., *Bright monomeric red fluorescent protein with an extended fluorescence lifetime.* Nat Methods, 2007. 4(7): p. 555-7.
287. Wiedenmann, J., et al., *A far-red fluorescent protein with fast maturation and reduced oligomerization tendency from Entacmaea quadricolor (Anthozoa, Actinaria).* Proc Natl Acad Sci U S A, 2002. 99(18): p. 11646-51.
288. Petersen, J., et al., *The 2.0-A crystal structure of eqFP611, a far red fluorescent protein from the sea anemone Entacmaea quadricolor.* J Biol Chem, 2003. 278(45): p. 44626-31.
289. Pletnev, S., et al., *A Crystallographic Study of Bright Far-Red Fluorescent Protein mKate Reveals pH-induced cis-trans Isomerization of the Chromophore.* J Biol Chem, 2008. 283(43): p. 28980-7.
290. Seo, H., et al., *Rapid generation of specific antibodies by enhanced homologous recombination.* Nat Biotechnol, 2005. 23(6): p. 731-5.
291. Cumbers, S.J., et al., *Generation and iterative affinity maturation of antibodies in vitro using hypermutating B-cell lines.* Nat Biotechnol, 2002. 20(11): p. 1129-34.
292. Kanayama, N., et al., *Genetic manipulation of an exogenous non-immunoglobulin protein by gene conversion machinery in a chicken B-cell line.* Nucleic Acids Res, 2006. 34(2): p. e10.
293. Cormack, B.P., R.H. Valdivia, and S. Falkow, *FACS-optimized mutants of the green fluorescent protein (GFP).* Gene, 1996. 173(1 Spec No): p. 33-8.
294. Arakawa, H., D. Lodygin, and J.M. Buerstedde, *Mutant loxP vectors for selectable marker recycle and conditional knock-outs.* BMC Biotechnol, 2001. 1: p. 7.

295. Zhang, W., et al., *Clonal instability of V region hypermutation in the Ramos Burkitt's lymphoma cell line.* Int Immunol, 2001. 13(9): p. 1175-84.
296. Tsien, R.Y., *The green fluorescent protein.* Annu Rev Biochem, 1998. 67: p. 509-44.
297. Fukuda, H., M. Arai, and K. Kuwajima, *Folding of green fluorescent protein and the cycle3 mutant.* Biochemistry, 2000. 39(39): p. 12025-32.
298. Zapata-Hommer, O. and O. Griesbeck, *Efficiently folding and circularly permuted variants of the Sapphire mutant of GFP.* BMC Biotechnol, 2003. 3: p. 5.
299. Nagai, T., et al., *A variant of yellow fluorescent protein with fast and efficient maturation for cell-biological applications.* Nat Biotechnol, 2002. 20(1): p. 87-90.
300. Rekas, A., et al., *Crystal structure of venus, a yellow fluorescent protein with improved maturation and reduced environmental sensitivity.* J Biol Chem, 2002. 277(52): p. 50573-8.
301. Heim, R. and R.Y. Tsien, *Engineering green fluorescent protein for improved brightness, longer wavelengths and fluorescence resonance energy transfer.* Curr Biol, 1996. 6(2): p. 178-82.
302. Ormo, M., et al., *Crystal structure of the Aequorea victoria green fluorescent protein.* Science, 1996. 273(5280): p. 1392-5.
303. Arakawa, H., et al., *Protein evolution by hypermutation and selection in the B-cell line DT40.* Nucleic Acids Res, 2008. 36(1): p. e1.
304. Evdokimov, A.G., et al., *Structural basis for the fast maturation of Arthropoda green fluorescent protein.* EMBO Rep, 2006. 7(10): p. 1006-12.
305. Klotz, E.L. and U. Storb, *Somatic hypermutation of a lambda 2 transgene under the control of the lambda enhancer or the heavy chain intron enhancer.* J Immunol, 1996. 157(10): p. 4458-63.
306. Kong, Q., et al., *A lambda 3' enhancer drives active and untemplated somatic hypermutation of a lambda 1 transgene.* J Immunol, 1998. 161(1): p. 294-301.
307. Nagaoka, H., et al., *Activation-induced deaminase (AID)-directed hypermutation in the immunoglobulin Smu region: implication of AID involvement in a common step of class switch recombination and somatic hypermutation.* J Exp Med, 2002. 195(4): p. 529-34.
308. Milstein, C., *Immunoglobulin kappa-chains. Comparative sequences in selected stretches of Bence-Jones proteins.* Biochem J, 1966. 101(2): p. 352-68.
309. Carter, D.R., C. Eskiw, and P.R. Cook, *Transcription factories.* Biochem Soc Trans, 2008. 36(Pt 4): p. 585-9.

PUBLICATION LIST

- **Batrak V, Blagodatski A, Schmidl S, Schoetz U, Caldwell RB, Arakawa H, Buerstedde JM.** 2009. A c*is*-acting diversification activator both necessary and sufficient for AID-mediated hypermutation. *PLoS Genet.* 5(1):e1000332.

- **Arakawa, H, Kudo H, Batrak V, Caldwell RB, Rieger MA, Ellwart JW, and Buerstedde JM.** 2008. Protein evolution by hypermutation and selection in the B-cell line DT40. *Nucleic Acids Res.* 36:e1.

ACKNOWLEDGEMENTS

Einer ist keiner. One cannot conquer alone, PhD thesis particularly. Without a support of many people working in the building #57 of the Helmholtz Centre of Munich, without a care of my family and friends the present thesis would not exist.

First of all I would like to thank Prof. Jean-Marie Buerstedde for inviting me to work on my PhD in his group, for providing me with the main ideas and supervising of my research projects.

Particularly I would like to thank my dear supervisor Dr. Hiroshi Arakawa for his great self-giving teaching, honest patient tutorage, and constant encouraging. It is his supervision which gave me a possibility to become a Doctor of Philosophy in science and life. I am not only grateful for his ideas, support in all of my projects but also for the great friendship.

I thank Prof. Michael Atkinson for "saving a shot" of the first version of my thesis, for careful reading and interesting discussions of my work.

I would like to thank all the present and previous workers of the Institute of Molecular Radiobiology for attention, support and creating a nice working atmosphere. I thank Prof. Horst Zitzelsberger for the help in many organization questions and reading of my thesis. I am grateful to Hiroshi Arakawa, Claire Innerlohinger, Huseyin and Nesibe Saribasak, Ulrike Schötz for help to become familiar with the methods of our research group and familiarization in the laboratory; I thank those people together with Randy Caldwell and Jürgen Bachl for the helpful discussions of my projects. I would like to thank Randy separately for the support concerning organization questions and computers. I also thank him and Petra Fiedler for the contribution to the idea of the vector *pHypermut2*. I am really grateful to all mentioned people and also particularly to Stephan Meding, secretary Sonia Ehrt and posthumously to Britta Klass for helping me in all the aspects of adaptation in Munich. I am also grateful to Sabine Schmidl, Claudia Gärtner, Martina Heim and all temporal secretaries and students of our laboratory for the friendship and support. I also thank Artem Blagodatski for the friendship and help in struggling with the German language.

Separately I would like to thank the "Gray Eminences" of my projects. I thank Michael Rieger from the Institute of Stem Cell Research for the kind exhausting assistance with FACS Aria and interesting discussions. I am indebted to Tom Meindl from the Institute of Toxicology for his responsive ever-lasting help with the FACS machine in the 57th building. I would like to thank our technicians Margot Böttner and Anna Freno for their

constant support and kind friendship. Particular thank to Margot for her sunny everyday “Morgen!”, a great start of a day. I thank also Herbert Braselmann for his kind help with the computers administration.

In addition I would like to thank the organizers of the hikes for PhD students from Helmholtz Centre. These were my brightest impressions of Alps, a great possibility to get know and stay in touch with many students from our research centre.

I would like to thank Dr. K.Lukyanov, Prof. S. Lukyanov and Dr. V. Belousov (Seva) from the Laboratory of the Molecular Technologies in Moscow for the collaboration.

I thank my Diploma thesis supervisor Vera Ruda for keeping a friendship and a post-diploma supervising of my “foreign” life.

A special vielen Dank to Holger Pflicke for the friendship, organization of the Munich International Hiking Club and contribution to the “Zusammenfassung” of the present thesis.

At last I would like to thank my dear family: my parents, grandparents, my sister’s family and my cousin for their enormous care and support. I am very grateful to my kind friends from Moscow who managed to stay very close over a great distance. I also thank all my friends from Munich and Richusha Neville. All these people helped me stay positive and motivated despite any difficulties.

LEBENSLAUF

Vorname & Name: Vera Batrak
Geburstag & -ort: 05.05.1982, Vladimir, Russland
Nationalität: Russisch
Geschlecht: Weiblich
Anschrift: Schwere-Reiter Str. 35, Zi. 430, 80797 München, Deutschland
E-Mail: vera.batrak@googlemail.com

AUSBILDUNG

Promotion: Technische Universität München, Fakultät Wissenschaftszentrum Weihenstephan für Ernährung, Landnutzung und Umwelt; München, Deutschland.

Diplom: Moskauer Staatliche Lomonosov Universität, Fakultät für Biologie, Spezialisierung: Bioorganische Chemie. S*umma cum laude.*

Gymnasium: Gymnasium mit dem Akzent auf Mathematik and Physik, Istra, Moskauer Region, Russland. S*umma cum laude.*

PUBLIKATIONEN:

- **Batrak V, Blagodatski A, Schmidl S, Schoetz U, Caldwell RB, Arakawa H, Buerstedde JM.** 2009. A cis-acting diversification activator both necessary and sufficient for AID-mediated hypermutation. *PLoS Genet.* 5(1):e1000332
- **Arakawa H, Kudo H, Batrak V, Caldwell RB, Rieger MA, Ellwart JW, and Buerstedde JM.** 2008. Protein evolution by hypermutation and selection in the B-cell line DT40. *Nucleic Acids Res*. 36:e1.
- **Akopov SB, Ruda VM, Batrak V, Vetchinova AS, Chernov IP, Nikolaev LG, Bode J, Sverdlov ED.** 2006. Identification, genome mapping, and CTCF binding of potential insulators within the FXYD5-COX7A1 locus of human chromosome 19q13.12. Mamm Genome. 17(10):1042-9.

WISSENSCHAFTLICHE BERUFSERFAHRUNG:

Helmholtz Zentrum München (früher GSF, Forschungszentrum für Umwelt und Gesundheit), Institut für Molekulare Strahlenbiologie (IMS). Nov 2005-Nov 2008; München, Deutschland.

WISSENSCHAFTLICHE PRAKTIKA:

Institute of Bioorganic Chemistry**,** Laboratory of Human Genes Structure and Functions. Oct 2002 – Jul 2005; Moscow, Russia. Research: Identification of insulators within the extended fragments of the human genome DNA. Supervisor: Dr. Sergey Akopov.